creative commons
COMMONS DEED

저작자표시-비영리-변경금지 2.0 대한민국

이용자는 아래의 조건을 따르는 경우에 한하여 자유롭게

- 이 저작물을 복제, 배포, 전송, 전시, 공연 및 방송할 수 있습니다.

다음과 같은 조건을 따라야 합니다:

저작자표시. 귀하는 원저작자를 표시하여야 합니다.

비영리. 귀하는 이 저작물을 영리 목적으로 이용할 수 없습니다.

변경금지. 귀하는 이 저작물을 개작, 변형 또는 가공할 수 없습니다.

- 귀하는, 이 저작물의 재이용이나 배포의 경우, 이 저작물에 적용된 이용허락조건을 명확하게 나타내어야 합니다.
- 저작권자로부터 별도의 허가를 받으면 이러한 조건들은 적용되지 않습니다.

저작권법에 따른 이용자의 권리는 위의 내용에 의하여 영향을 받지 않습니다.

이것은 이용허락규약(Legal Code)을 이해하기 쉽게 요약한 것입니다.

Disclaimer

dCollection

공학석사 학위논문

Improvement of Subchannel Scale Analysis Capability of CUPID with Grid-directed Cross Flow and Fuel Rod Models

CUPID 부수로 해석능력 향상을 위한 지지격자-유도 횡류 모델 및 핵연료봉 열전도 모델 개선

2018년 8월

서울대학교 대학원

에너지시스템공학부

김 슬 빈

Abstract

Improvement of Subchannel Scale Analysis Capability of CUPID with Grid-directed Cross Flow and Fuel Rod Models

Seul-Been Kim
Department of Nuclear Engineering
The Graduate School
Seoul National University

As the recent computing environment increases, the whole core pin-by-pin analysis has been actively performed using coupled subchannel analysis code and neutron transport code. In particular, the revised safety standards, which emphasize realistic consideration of the fuel status in accident analysis including the thermal conductivity degradation, motivate the whole core pin-by-pin analysis to estimate safety margin more accurately.

In order to guarantee accurate prediction of the reactor thermal-hydraulic behaviors using a subchannel analysis, it is necessary to consider the effect of the mixing vane on fluid lateral transfer and therefore, subchannel analysis codes include a model to reproduce the mixing vane directed cross flow. However, the previous study on whole core calculation of APR1400 using CUPID did not consider the effect of mixing vane. For this reason, this study aims to extend the previous study by implementing grid-directed cross flow model as its first

objective. Furthermore, the previous work did not include the fuel rod heat transfer model and it was required to implement the fuel model to make CUPID possess the features necessary for the reactor core subchannel analysis. The second objective of this study is, therefore, to improve the fuel rod conduction model and verify it by solving conceptual problems.

CTF (COBRA-TF) code uses the grid-directed cross flow model in the momentum equation to simulate the fluid transfer induced by the mixing vane of a spacer grid. It uses the staggered grid, which defines lateral velocities on the gaps between two subchannels. Accordingly, CTF could simulate the momentum exchange by a mixing vane directly as the location of the mixing vane is matched with the gap where the velocities are defined while CUPID uses collocated grid system and all velocity components are defined at the center of the subchannels. In this case, the momentum exchange by the mixing vane could not be well reproduced as the two opposing directional momentum caused by the mixing vane is canceled out and eventually, no momentum is added in the subchannel center. Therefore, to compensate the canceled momentum, two modifications were proposed: first, the grid-directed cross flow model was implemented into not only the momentum equation, but also into the scalar equations, mass and energy equations. The turbulent mixing coefficient β was replaced by $\beta_{\mathrm{default}} + \beta'$ to take into account the additional vane-induced turbulent mixing. β' was determined from code-to-code comparison with CUPID and CTF. In addition, the non-uniform effect of the mixing vane directed cross flow in the near of the guide tube and the pressure drop caused by the spacer grid were considered.

Meanwhile, the fuel rod heat conduction equation of CUPID was improved. The rod-centered approach of the default fuel rod model in CUPID was modified

to a cell-centered approach for subchannel scale analysis, and the fuel rod was divided into four sections. Divided fuel rods face the subchannels which have different coolant temperature and velocity, so the cladding surface temperature could be different in a single rod. Thus, circumstantial heat conduction occurs across the interfaces among the quarter rods, and the temperature difference gradually decreased at the center of the rod. In this study, the circumferential heat conduction was considered explicitly in order to avoid solving a system of equations which increases computational time and memory usage. Furthermore, the Biasi correlation and CE-1 correlation were added as a CHF calculation model to observe the DNBR distribution.

After the implementation and improvement of the models, the verification of APR1400 single assembly was conducted. For simulation, the calculation results of nTRACER, a neutron transport code was applied as the volumetric heat source of the heat conduction equation. The implemented power distribution was from an assembly which has the larger volumetric heat source than surrounding. Afterward, the verification of the models was followed. It has been confirmed that grid-directed cross flow model made temperature distribution flattened and the fluid velocity stream line rotate. Furthermore, the transverse velocity increased at the support grid position. The code-to-code comparison between CUPID and CTF was performed and the result showed comparable liquid temperatures and axial velocities at the outlet. Afterwards, the fuel rod heat conduction model was verified. The pellet centerline temperature and the volumetric power had cosign-shape, whereas maximum cladding surface temperature and coolant temperature occurred at the outlet of the test section. In addition, the DNBR distribution using CE-1 correlation shows more conservative minimum DNBR than that obtained

using Biasi correlation.

Then, the APR1400 whole core was simulated using the verified models. The subchannel type was specified for whole core simulation, and the power distribution was implemented from nTRACER as done in the single assembly calculation. For the whole core simulation which requires efficient memory handling scheme, CUPID parallel processing method was improved. Due to the grid-directed cross flow model, the below was observed; the changed coolant temperature distribution, non-uniform lateral velocity in the vicinity of the guide tube, and the increased flow velocity in the water gap which has higher hydraulic diameter. In addition, the fuel rod heat conduction model was activated for the simulation. For the assembly 23 used for the single assembly calculation, the simulation result of single assembly and the whole assembly were compared and possible reason for the discrepancy was discussed.

……...

Keywords: Subchannel scale T/H analysis, Fuel rod heat conduction, Mixing vane, Reactor core T/H analysis, CUPID, APR1400

Student Number: 2016-26072

List of Contents

List of Tables

List of Figures

Chapter 1

Introduction

1.1 Background

Recently, there is an increasing need for high-fidelity multi-physic thermal hydraulic analysis in nuclear reactor. As computing power increases, coupled three-dimensional analysis has been used as an appropriate tool for transient and non-uniform power simulation. In the accident such as MSLB (Main Steam Line Break) or rod ejection, for example, the raised coolant temperature increases cross flow. The subchannel scale analysis could more accurately simulate the fluid transfer between adjacent assemblies. In addition, the fuel rod pin-by-pin analysis is actively used to simulate AOA (Axial Offset Anomaly) caused by boron deposition and changed power distribution.

In this context, the subchannel scale whole core pin-by-pin has been performed as follows. First, in the CASL (Consortium for Advanced Simulation of Light water reactors) project, whole core pin-by-pin analysis used the improved version of COBRA-TF, CTF; the simulation was progressed coupling with thermal hydraulic code CTF, neutronics code MPACT and simple crud modeling (Salko et al., 2015). In addition, it was observed that the subchannel scale analysis could simulate the phenomenon of the chimney effect, which is the cross flow or reverse flow from the surrounding to the accident-induced hot channel as

described in Fig. 1.1 (Sung et al., 2015). Likewise, in the ARCADIA code system in AREVA, COBRA-FLX was used for 3D pin-by-pin whole core analysis (Gensler et al., 2013); and KIT (Karlsruhe Institute of Technology) used inhouse code SUBCHANFLOW for pin-by-pin full core simulation simulator DYNSUB (Daeubler et al., 2015).

In Korea, currently, MATRA code has been used to perform the subchannel scale thermal hydraulic analysis for reactor whole core. MATRA is a subchannel code developed by KAERI (Korea Atomic Energy Research Institute), which is very effective in reactor core design and calculating DNBR (Departure from Nuclear Boiling Ratio) margin (Kwon, 2014). MATRA contains required accuracy and reasonable calculation time, moreover, has been verified against many experiments. MATRA is optimized for PWR (Pressurized Water Reactor) analysis in highly pressurized single-phase flow condition. However, some features of the models and schemes used by MATRA are not optimized for two-phase accident analysis. For example, MATRA uses Homogeneous Equilibrium Model (HEM), which is suitable for PWR operation condition where bubbles are absent or very small size due to high pressure; thus little difference in speed between two-phase. However, it might not be appropriate to take into account the difference in velocity between liquid and gas, which could be occurred after a boiling by sudden pressure drop in accident condition. In addition, the axial spatial marching scheme used by MATRA is effective when the axial coolant flow is dominant, but it is not optimized for simulating cross flow or reverse flow caused by narrowed flow area due to ballooning. As a result, the necessity of the code increased for accident condition two-phase subchannel scale thermal hydraulic analysis.

CUPID (Component Unstructured Program for Interfacial Dynamics) has been

developed by KAERI for multi-dimensional two-phase flow analysis. Since CUPID uses two-fluid model for two-phase flow analysis, the velocity difference between coolant and gas could be simulated; moreover, transverse and reverse flow could be appropriately analyzed by the single pressure correction equation in entire calculation domain. In the previous study, the cross flow and bypassed fluid caused by severe ballooning could be reproduced using CUPID as described in Fig. 1.2 (Yoon et al., 2018).

Meanwhile, for realistic thermal hydraulic calculation about reactor whole cores, it is important to simulate transverse coolant transfer caused by mixing vane which is attached on the specific spacer grid. The vane-induced cross flow has been studied by CFD (Computational fluid dynamics) scale analysis and experiments. By Chang et al. (2014), it was investigated the difference between swirl type and split type mixing vane which changes the pattern of lateral fluid transfer. The swirl type mixing vane causes the rotation of coolant in the channel which increases the internal heat transfer, whereas it has a weak influence on the cross flow between adjacent channels. On the other hand, the split type mixing vane makes the strong cross flow in the gap with a specific direction. Fig. 1.3 shows the difference of swirl type and split type of mixing vane. Li and Gao (2014) compared 5x5 assembly and 17x17 assembly to observe flow pattern caused by mixing vane. Kawahara et al. (2016) confirmed the effect of mixing vane on the two-phase annular flow using mass transfer coefficient. Recently, based on these experiments and CFD scale analysis, the study for simulating vane-induced fluid transfer was progressed using CTF, which is the subchannel scale thermal hydraulic code (Avramova and Salko, 2016). To obtain information for subchannel scale analysis, CFD scale analysis for PSBT 5x5 experiment was performed; the

lateral convection factor, which is the ratio of lateral to axial velocity, the turbulent mixing multiplier, which is a factor for additional turbulence mixing due to mixing vane were evaluated by CFD calculation (Blyth, 2017).

Besides, in order to meet enhanced safety standard, it is required to consider the fuel rod condition such as ballooning or deformation. Recent revision of the ECCS (Emergency Core Cooling System) acceptance criteria requires modeling of cladding oxidation, crud, fuel deformation and relocation (NRC, 2017). In addition, the revision of RIA (Reactivity-Induced Accident) criteria allows some fuel melting at the center of the pellet (NRC, 2015). To deal with the revised safety criteria, the MARS-KS/FRAPTRAN coupled simulation was progressed for verification of coupled thermal hydraulic/fuel code considering the combustion effect (Kim et al., 2016). In this context, the subchannel scale whole core analysis using mixing vane model and fuel rod model is required.

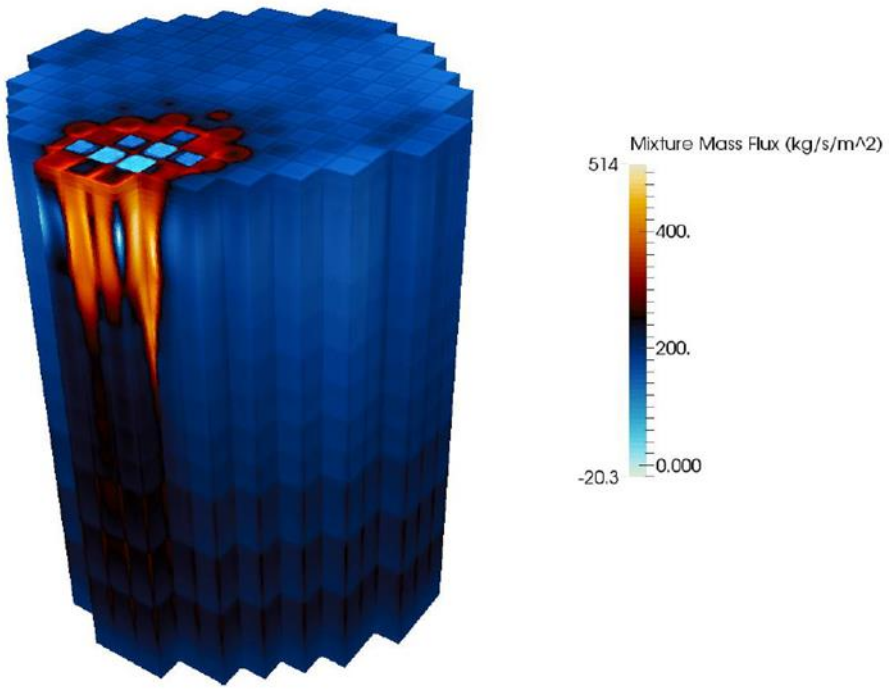

Figure 1.1 Mixture mass flux distribution computed by CTF (Sung et al., 2015)

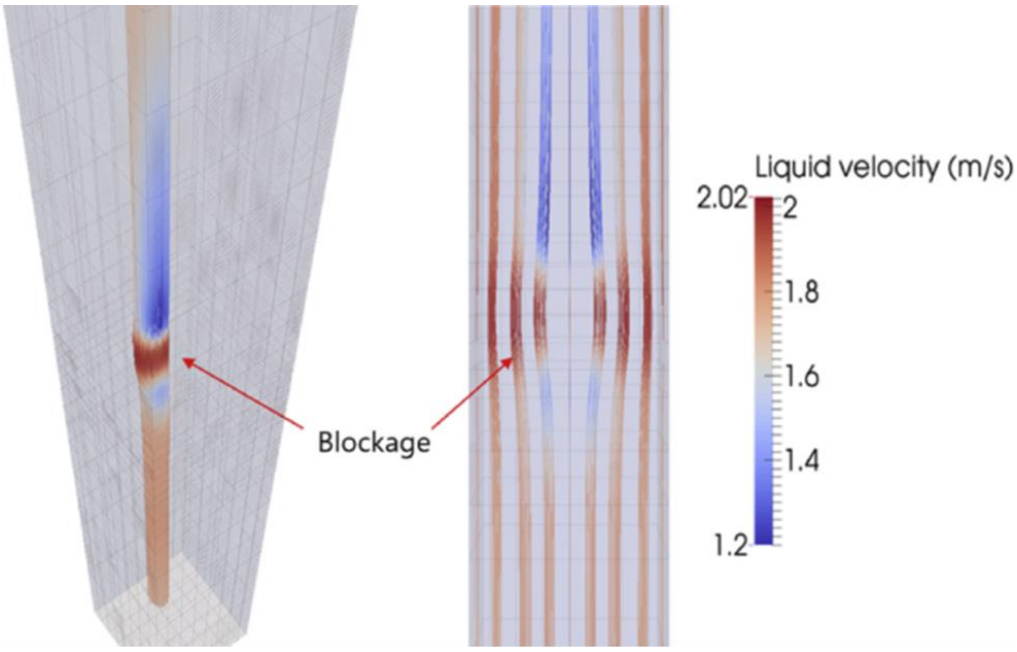

Figure 1.2 Cross flow and accelerated coolant at the blockage simulated by CUPID (Yoon et al., 2018)

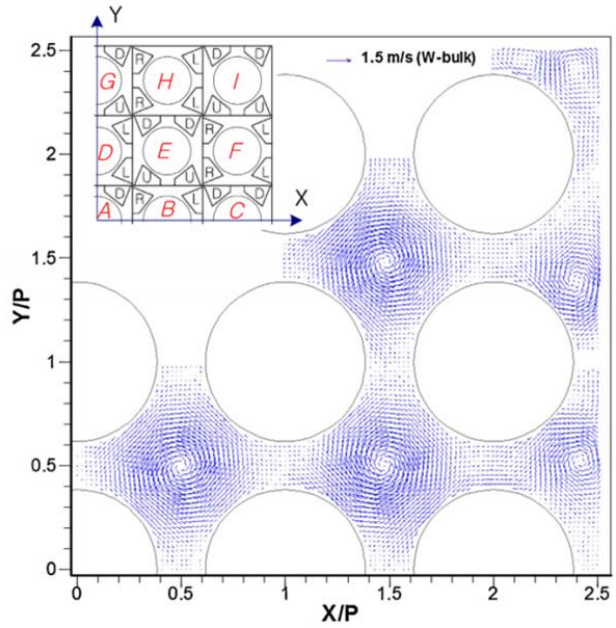

(a) The lateral velocity distribution using swirl type mixing vane

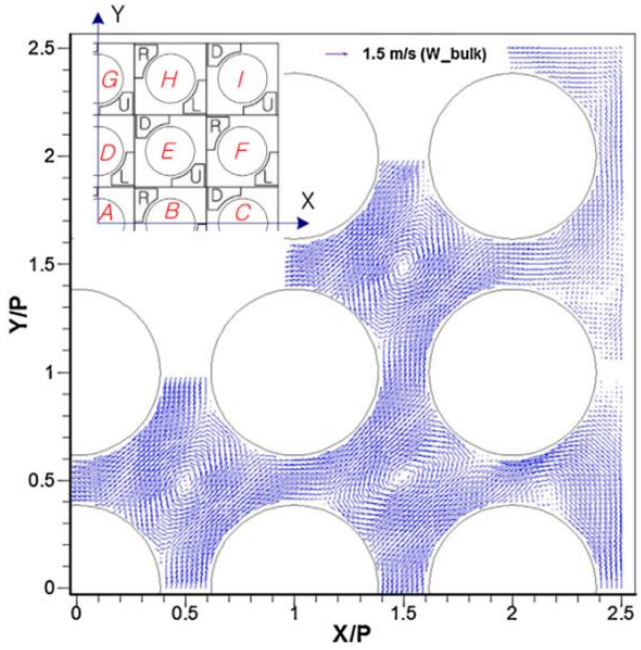

(b) The lateral velocity distribution using swirl type mixing vane

Figure 1.3 Vane-induced lateral velocity distribution analyzed by CFD scale (Chang et al., 2014)

1.2 Objective of Study and Scope

This study is a part of the multi-scale simulation using CUPID code. The entire system except the reactor vessel, such as cold leg, hot leg and steam generator, could be analyzed using a one-dimensional system scale code MARS. The CFD scale CUPID could simulate the reactor vessel which contains downcomer and nozzle and the subchannel scale CUPID could analyze the entire core. CUPID could use open medium approach same as a general CFD code, or the porous medium approach for simulating reactor core or steam generator. This is the multi-scale simulation using CUPID code that allows computation of various scales to be performed without external information exchanges. In this study, the subchannel scale analysis of APR1400 whole core was performed using more realistic model implemented CUPID.

As a previous study of this paper, the study which extended the capability of CUPID to subchannel scale analysis was progressed (Yoon, 2018). The fundamental subchannel models were implemented into CUPID; the crossflow model which contains friction factor model and form loss model, and the turbulent mixing model which consists of EM model and EVVD model. Afterward, the validations were performed against single-phase unheated/heated experiments and two-phase unheated tests. As follows, the preliminary whole core simulation of APR1400 was progressed using subchannel scale CUPID code. The condition of simulation was APR1400 core in hot full power, and the power was applied from the neutronics code, nTRACER (Jung, 2013). In the preliminary simulation, fuel rod heat conduction model was deactivated and the mixing vane attached spacer grid was not considered. The calculation result is described on Fig. 1.4. Therefore,

to improve the previous simulation and implement more realistic models on CUPID, this study has two objectives as follows.

First, the implementation of grid-directed cross flow model and verification of model were performed. For verification, the single assembly of APR1400 was simulated using subchannel scale CUPID code. Afterward the code-to-code comparison between CTF and CUPID was progressed. Second, the fuel rod heat conduction model was improved. Fuel rod is divided into four quarters, and the circumstantial heat conduction between quarter rods also could be considered. In addition, the CHF correlations were added for calculating DNBR. Fig. 1.5 shows the outline of this study.

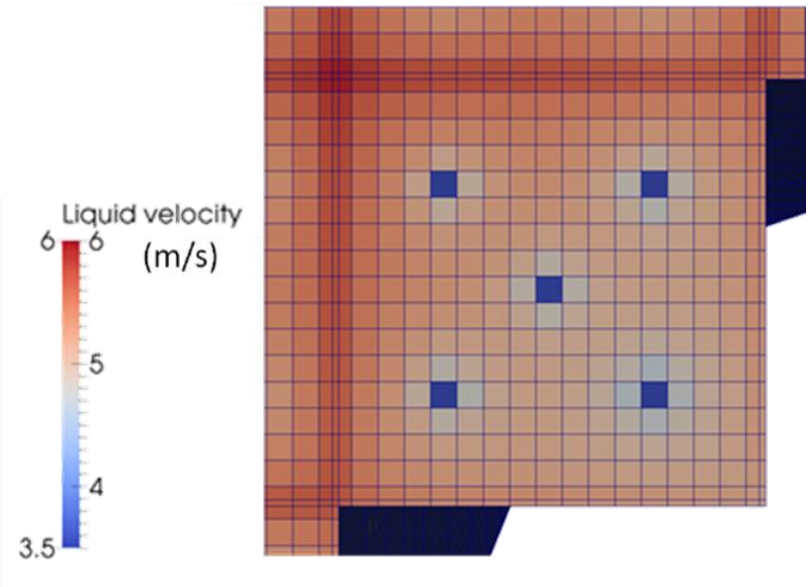

(a) Coolant velocity distribution of APR1400 whole core simulation

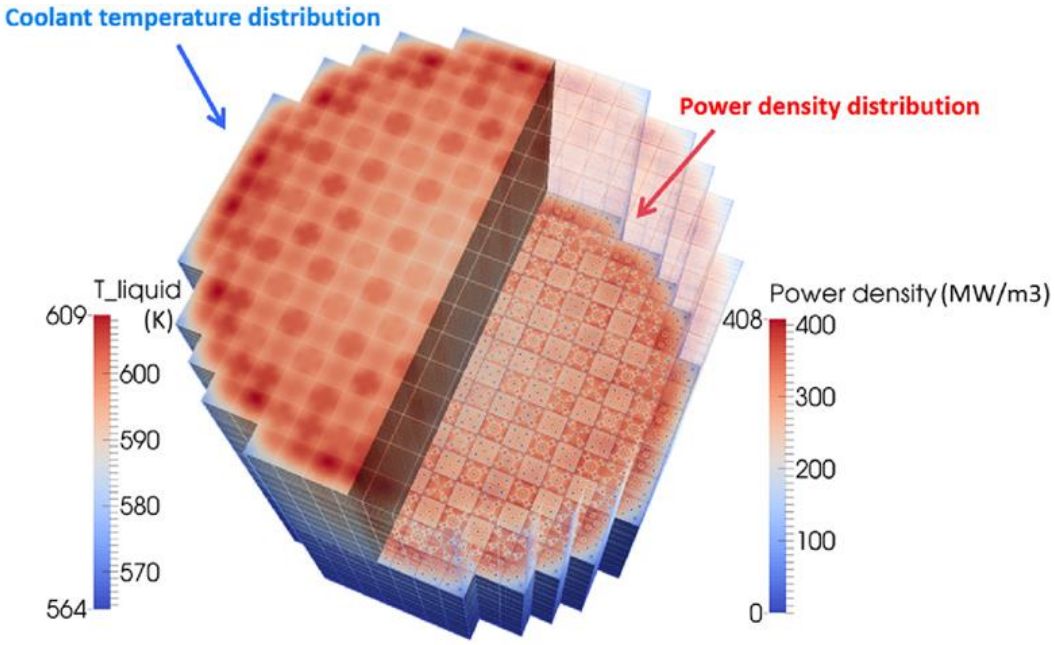

(b) Coolant temperature and power density distribution of APR1400 whole core simulation

Figure 1.4 Simulation result of APR1400 whole core using CUPID (Yoon, 2018)

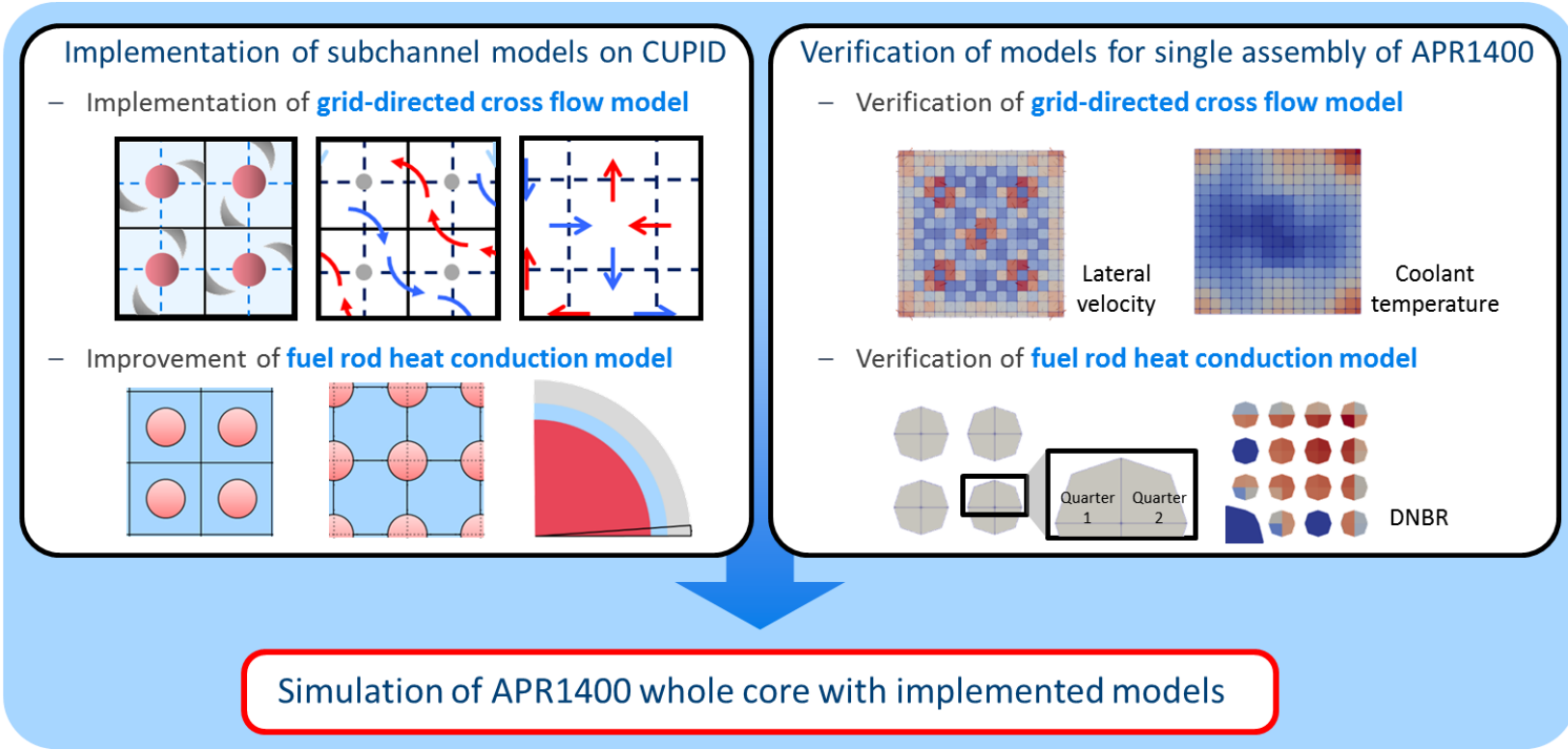

Figure 1.5 Outline of current study

Chapter 2

Implementation of Subchannel T/H Models to CUPID

2.1 Implementation of Grid-directed Cross Flow Model

The mixing vane attached spacer grid influences on the flow between adjacent channels. The considering of vane-induced coolant transfer is important to reliable subchannel scale thermal hydraulic analysis. CTF, the subchannel scale analysis code, used the grid-directed cross flow model for simulating the vane-induced coolant transfer. To use the model, it is necessary to set the direction of fluid from the shape of the mixing vane as shown in Fig. 2.1. Afterwards, the fluid direction described in Fig. 2.2 is simplified for subchannel scale analysis in a direction perpendicular to the cell face, as shown in Fig. 2.3.

CTF uses structured grid, especially staggered grid, which is optimized for subchannel scale analysis. The staggered grid has momentum information about each direction at cell faces and the scalar data in cell center as shown in Fig. 2.4 (a). It appears that CTF could simulate the coolant transfer through the gap using the grid-directed cross flow model, which was implemented into the momentum equation. The mass and energy were also transfer by coolant exchange.

In contrast, CUPID uses a collocated grid for computation whereas CTF uses

a staggered grid. This is because CUPID is the component analysis code, which enables not only subchannel scale but also CFD scale analysis. Therefore, CUPID uses an unstructured grid, particularly a cell-centered collocated grid. The collocated grid stores the momentum and scalar information into a cell center. So the momentum cancellation, which reduces the effect of grid-directed cross flow model, could be occurred in cell center as illustrated in Fig. 2.4 (b).

Thus, in order to apply the model for the code using collocated grid, grid-directed cross flow model was modified as follows: First, the model was additionally implemented into scalar equations; mass and energy equations. Second, additional turbulent mixing coefficient β' was introduced for vane-induced turbulent mixing. Also five guide tubes included in the CE type 16x16 fuel assembly were modeled. The changed distribution of the mixing vanes in the near the guide tube was considered. Finally, not only transverse coolant transfer caused by the spacer grid with mixing vanes, but also axial pressure drop was considered as a spacer grid model.

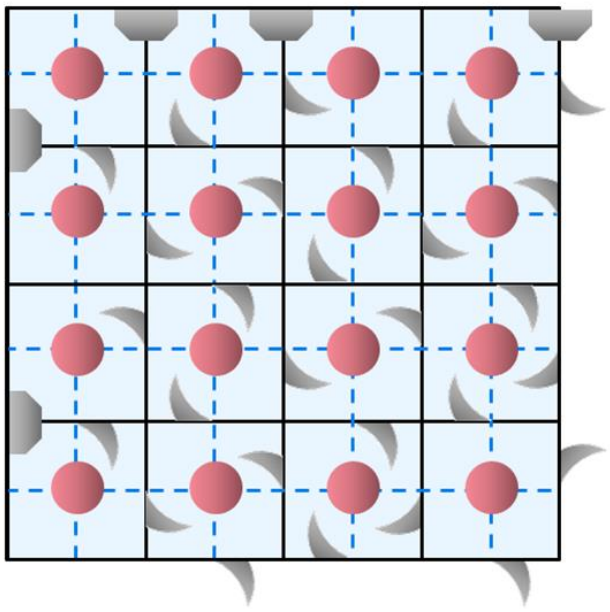

Figure 2.1 Example of mixing vane shape in assembly

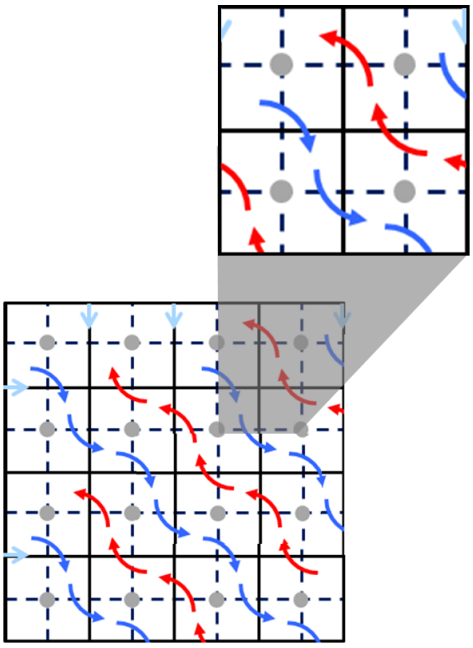

Figure 2.2 Direction of fluid from the shape of the mixing vane

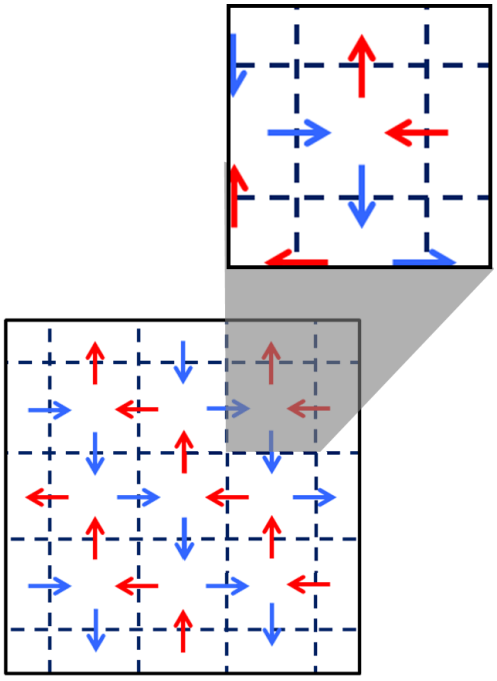

Figure 2.3 The simplified fluid direction for subchannel scale analysis

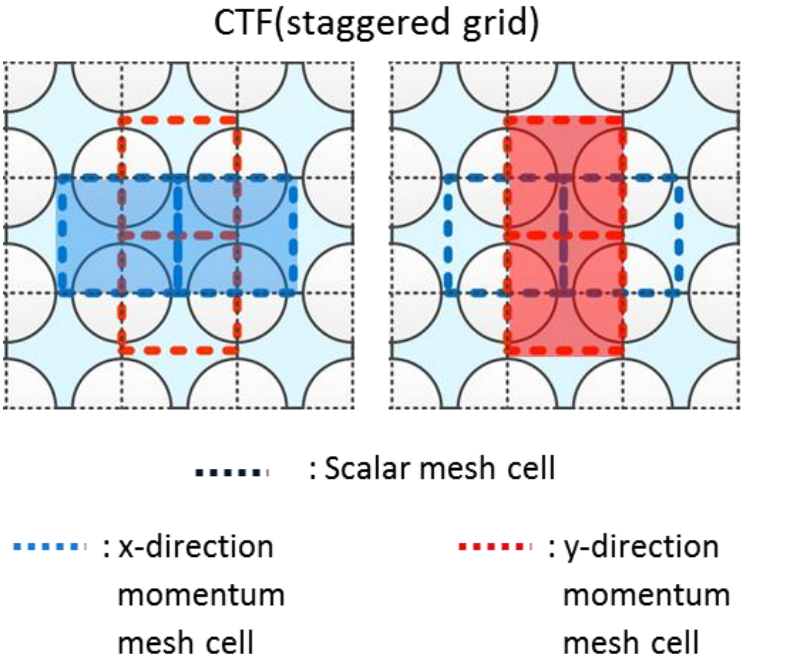

(a) Scalar and momentum mesh cell in staggered grid

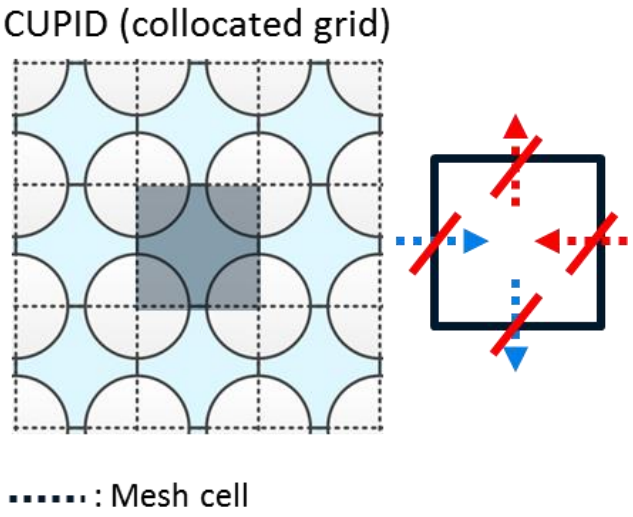

(b) Mesh cell and momentum cancelation in collocated grid

Figure 2.4 Difference between staggered grid and collocated grid

2.1.1 Additional Implementation of Model into Scalar Equation

The grid-directed cross flow model, which is a model for simulating the transverse coolant transfer caused by mixing vanes, was implemented into the CTF momentum equation such as equation 2-1 (Blyth, 2015).

$$\mathrm{M_k} = f^2 u_l \rho_l A \times u_l \quad (2\text{-}1)$$

Where $\mathrm{M_k}$: lateral momentum transfer due to grid-directed cross flow model

f : lateral convection factor (ratio of lateral to axial velocity)

A : gap area (gap size×cell height)

The lateral convection factor f, which is the ratio of the lateral to axial velocity, could be confirmed from the experiment or CFD calculation result. However, since the experimental data on APR1400 were inaccessible, the applied lateral convection factor on CUPID and CTF simulation was observed from the analysis of PSBT experiment. The PSBT 5x5 bundle test was conducted using spacer grids with mixing vanes (Rubin et al., 2010). It was confirmed that the lateral convection factor 0.27 could be used for subchannel scale analysis of the PSBT experiment (Blyth, 2017).

The grid-directed cross flow model was implemented into the CUPID momentum equation, and also into the mass and energy equation, as in equation 2-2. Scalar exchange between adjacent channels due to the model are not canceled, so it is possible to compensate for the momentum cancellation in the x and y directions caused by the data handling method of collocated grid.

$$\mathrm{M_e} = f u_l \rho_l A$$

$$\mathrm{M}_h = f u_l \rho_l A \times h_l \quad (2\text{-}2)$$

Where M_e, M_h : lateral mass and energy transfer due to grid-directed cross flow model.

2.1.2 Additional Turbulent Mixing Coefficient β'

To simulate the turbulent mixing in subchannel scale analysis, EVVD (Equal Volume exchange turbulent mixing and Void Drift) model that exchange same volume between adjacent channels could has been used for two-phase or single-phase heated condition simulation (Todreas and Kazimi, 1990). The effect of the EVVD model implemented into CUPID was confirmed in previous studies (Yoon, 2018).

Turbulence mixing coefficient β should be determined for applying turbulence mixing models. β is the ratio of lateral mass flow to axial mass flow, which can be confirmed from experimental or CFD analysis results. To take into account the additional turbulence mixture caused by mixing vanes, β' was introduced and turbulent mixing coefficient β was replaced to $\beta = \beta_{\mathrm{default}} + \beta'$.

Before introducing the β' into the turbulent mixing coefficient β, the following procedure was performed to confirm the β_{default}. Since experimental data about APR1400 core was not released, β_{default} needed to be determined from the previous study. β_{default} used for the subchannel scale analysis of experiments in the previous study were summarized as Table 2.1. The maximum value of β is 0.05 and the minimum is 0.005, so the β_{default} available for simulation could be between these.

Next, the β' added to the turbulent mixing model was derived from the options of CTF, grid-induced turbulent mixing model. This option multiplies factor (1 or more than one) by the $\beta_{default}$ to account for additional grid-induced mixing as described in Fig. 2.5 (Avramova, 2007). But in order to consider the cancellation of x and y direction momentum in collocated grid, it is more reasonable to add the factor in the corresponding direction as shown in Fig. 2.6 than multiply the factor by the total computing cells. Therefore, the mixing coefficient β', added to each direction of $\beta_{default}$ causing additional mixing, was determined by CUPID-CTF code to code comparison.

Table 2.1 Turbulent mixing coefficient β used in previous study

Experiments	Selected β for validation on previous study
CNEN 4x4 test (single-phase, unheated)	0.02
PNL 7x7 test (single-phase, unheated)	0.02
PNNL 2x6 test (single-phase, heated)	0.005 (min)
RPI air-water mixing test (two-phase, unheated)	0.05 (max)
GE 2x2 test (two-phase, heated)	0.05 (max)

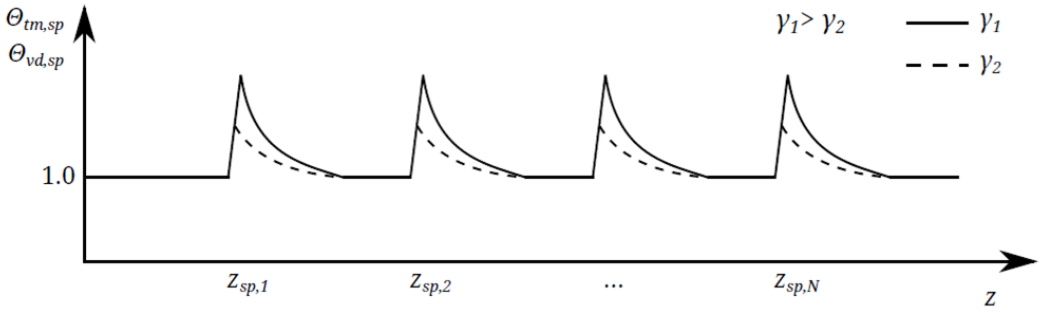

Figure 2.5 Schematic of spacer multiplier used in grid-induced turbulent mixing model (Avramova, 2007)

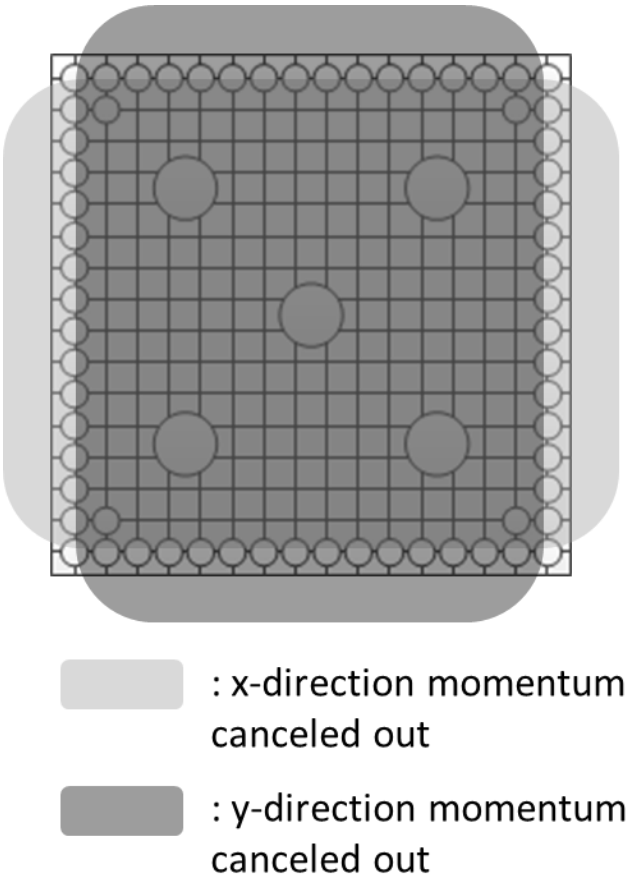

Figure 2.6 Momentum cancelation depended on the direction

2.1.3 The Mixing Vane Effect at the Near the Guide Tubes

The CE type 16x16 fuel assembly contains five guide tubes. Each guide tube replaced the four nuclear fuel rods and affects nine subchannels near the guide tube including the single center channel of the guide tube, four side channels of the guide tube and four corner channels of the guide tube. The changed subchannel porosity, which is the ratio of the fluid volume to the whole cell volume, due to the guide tube is described in Table 2.2.

As described in Table 2.2 and Fig. 2.7, porosities of subchannels are various in near the guide tube. In the case of CTF, the grid-directed cross flow model is applied to a cell face, porosity in the subchannel does not affect the cross low prediction. In the case of CUPID, the model is applied to the cell center, the difference in porosity in the vicinity of the guide tube causes the distorted prediction the cross flow. Thus, calibration for the porosity-induced error was progressed.

Because the porosity of the guide tube corner is 1.05 times larger than that the normal subchannel, the model is applied weakly. Therefore, the grid-directed cross flow model operated in the corner subchannel of the guide tube 1.05 times increased. On the other hand, in the side channel of the guide tube, the effect of model is stronger than normal subchannel caused by 0.57 times smaller porosity; the reduced value of the lateral correlation factor was applied on side channel of the guide tube. In addition, the model was applied taking into account the shape of the guide tube. Since a guide tube replaces the four fuel rods, the shape of the mixing vanes distribution is changed in near the guide tube. Fig. 2.8 shows the simplified coolant direction of single assembly considering all guide tubes, and Fig. 2.9 is an example of the input file including guide tube data. The direction of

fluid transfer could be deduced from the shape of the mixing vane geometry, which is described on Final Safety Analysis Report of APR1400 (FSAR). In addition, two different phenomena from the center subchannels appear near the guide tube. First, in the case of four guide tubes at the edge of the assembly described in Fig. 2.10 (a), the coolant passes through the guide tubes and does not change the direction. On the other case, for single guide tube in the center of the assembly, such as Fig. 2.10 (b), the coolant from the previous four guide tubes slightly blocked by the guide tube and changes its direction. The guide tube makes the grid-directed cross flow model more asymmetrically operate.

Table 2.2 Porosity of single assembly in the APR1400 reactor

Subchannel type	Porosity
Normal subchannel	0.571
Guide tube center	0.571 x 0.02 =0.011
Guide tube side	0.329
Guide tube corner	0.599

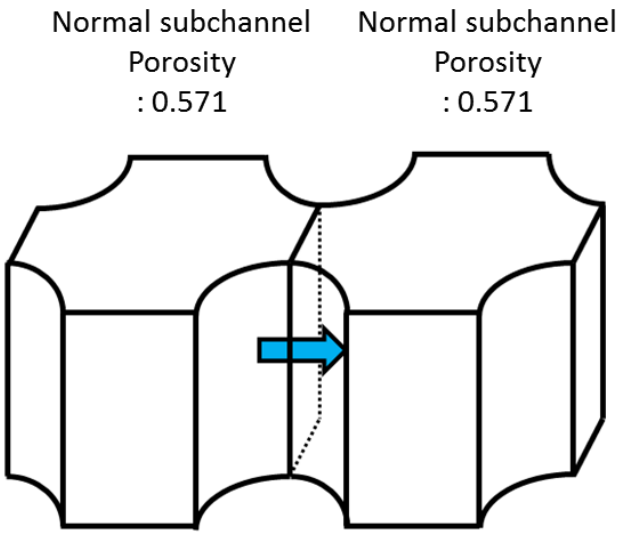

(a) Porosity of normal subchannels

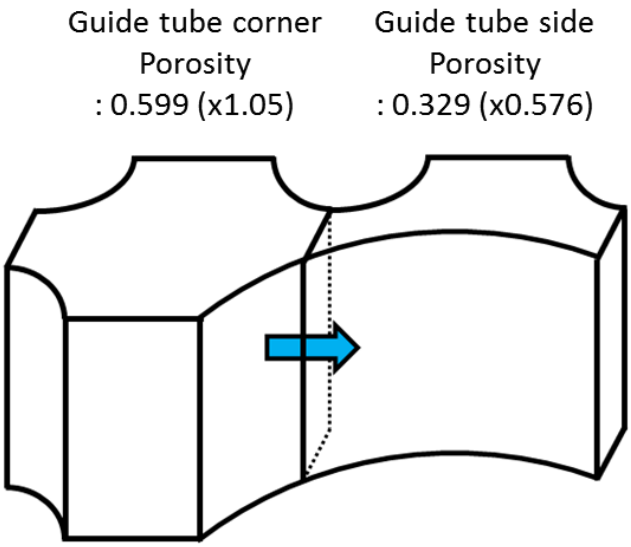

(b) Porosity of subchannels in vicinity of guide tube

Figure 2.7 Porosity of subchannels in single assembly of APR1400

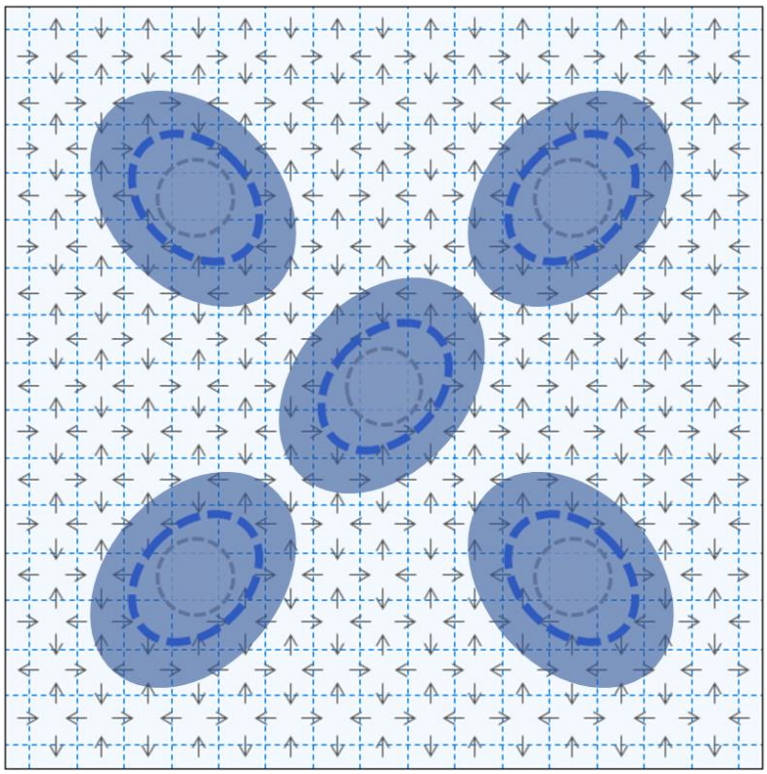

Figure 2.8 Simplified direction of vane-induced fluid transfer

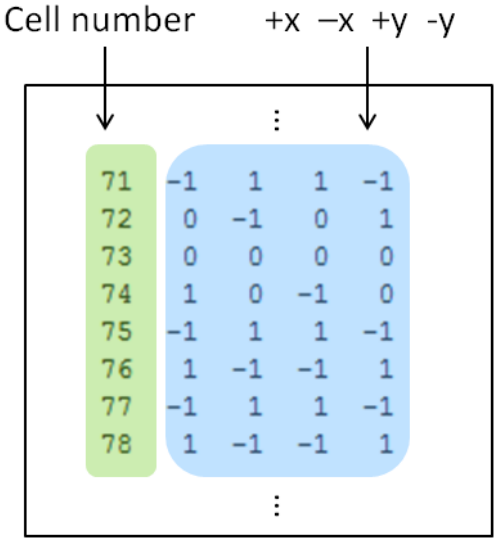

Figure 2.9 Example of input for applying fluid direction

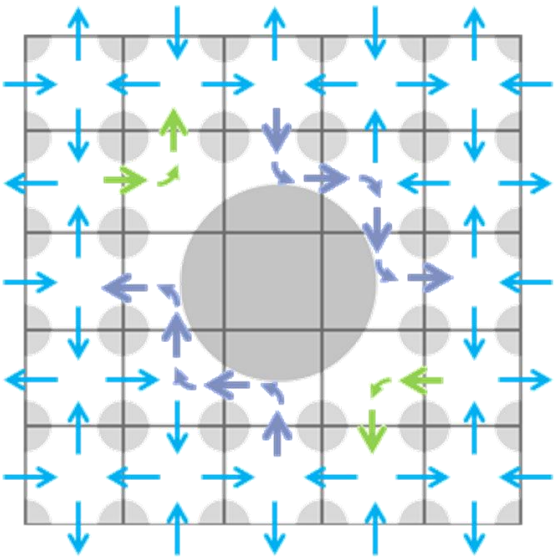

(a) Coolant transfer distribution of four guide tubes in the edge of the assembly

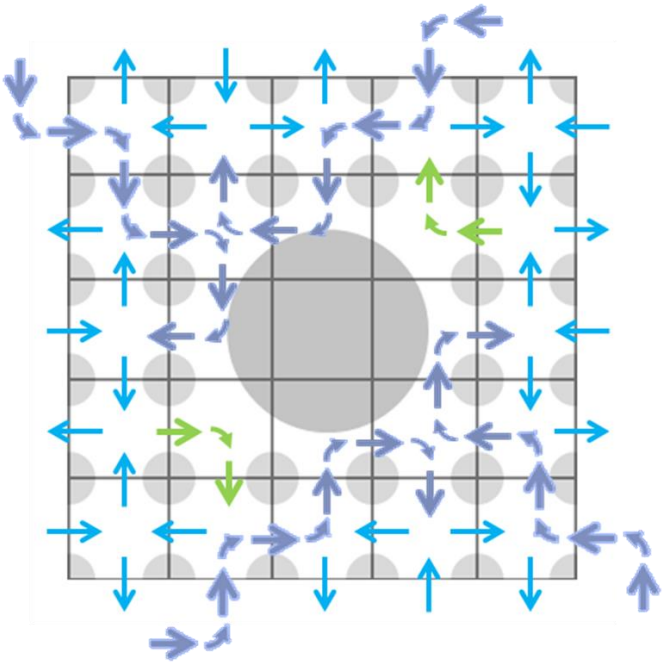

(b) Coolant transfer distribution of single guide tube in the center of the assembly

Figure 2.10 Coolant transfer distribution near the guide tube

2.1.4 Spacer Grid Induced Pressure Drop

The spacer grid fixes the shape of fuel rod bundle and prevents lateral vibration or axial fluctuations occurred by coolant flow. Thus, the coolant receives additional pressure drop during it passes through the spacer grid, even if the mixing vanes are not attached to the grid. There are total twelve spacer grids in the APR1400 reactor core; all of the grids contain mixing vane except the top and bottom spacer grids. Among them, ten of spacer grids were included in 3.81m heated length. They consisted of nine vane-attached ZIRLO spacer grids and single Inconel bottom grid without mixing vane. The following model was implemented to simulate the additional pressure drop caused by the spacer grid. This model was presented by MATRA report (Kwon, 2014).

$$\Delta \mathrm{M}_{\mathrm{SG}} = \frac{\mathrm{K}}{2}\frac{G^2}{\rho} \tag{2-3}$$

Where $\Delta \mathrm{M}_{\mathrm{SG}}$: additional axial momentum source due to spacer grid model

K : form loss coefficient

$\mathrm{G} = \sum \alpha_k \rho_k U_k$: mass flux

The form loss coefficient K depends on the length and shape of the spacer grid. However, the form loss coefficient of the spacer grid used in the APR1400 could not be accessible, so the coefficient was investigated with the previous study and the PSBT experiment. In the previous study, the form loss coefficient K was 1.0 for the CE 15x15 test (single-phase unheated), PNNL 2x6 test (single-phase hearted) and GE 3x3 test (two-phase unheated) simulation (Yoon, 2018). Likewise in the subchannel scale analysis of PSBT benchmark test, the form loss

coefficient was used as 1.0 for the simulation of mixing vane-attached grid (Blyth, 2017). It appears that the form loss coefficient could be fixed at 1.0 for simulation of this study. The axial pressure distribution and additional pressure drop caused by single spacer grid is described in Fig. 2.11.

Fig. 2.12 (a) describes the location of spacer grid in non-uniform mesh. Since the simulation of single assembly used uniform mesh, it is necessary to select the axial cell which is spacer grid model applied in the uniform mesh, as shown in Fig. 2.12 (b). The height of the spacer grid used to hold the APR1400 core and the axial length of the mesh for simulation are respectively 41.6 mm and 95.25mm. As the APR1400 heated length 3.81m was evenly divided into 40 parts, the height of mesh is longer than spacer grid. It suggests computing cell normally contains spacer grid such as Fig. 2.13 (a). Even if the spacer grid is located between the axial interfaces of the mesh, the model is applied to the cell where the center of the spacer grid is closer to the center of the mesh. In the case of Fig. 2.13 (b), model was operated on the lower cell whereas the pressure drop of upper cell increased in the case of Fig. 2.13 (c).7

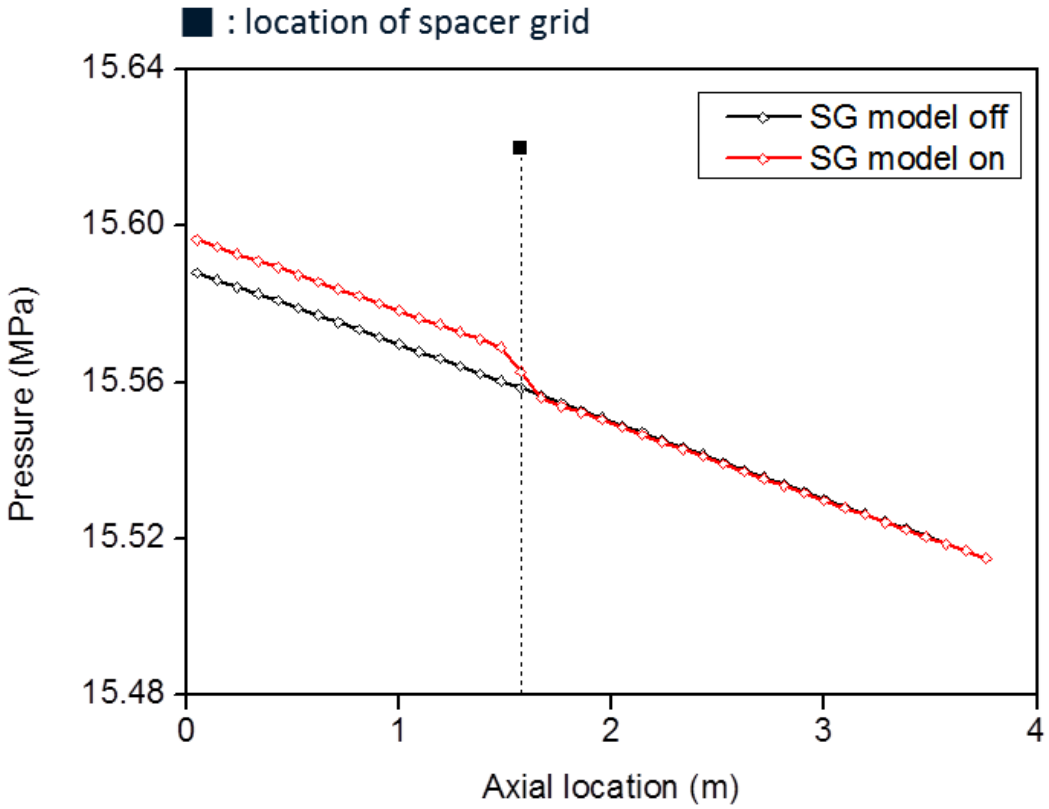

Figure 2.11 Additional pressure drop caused by spacer grid

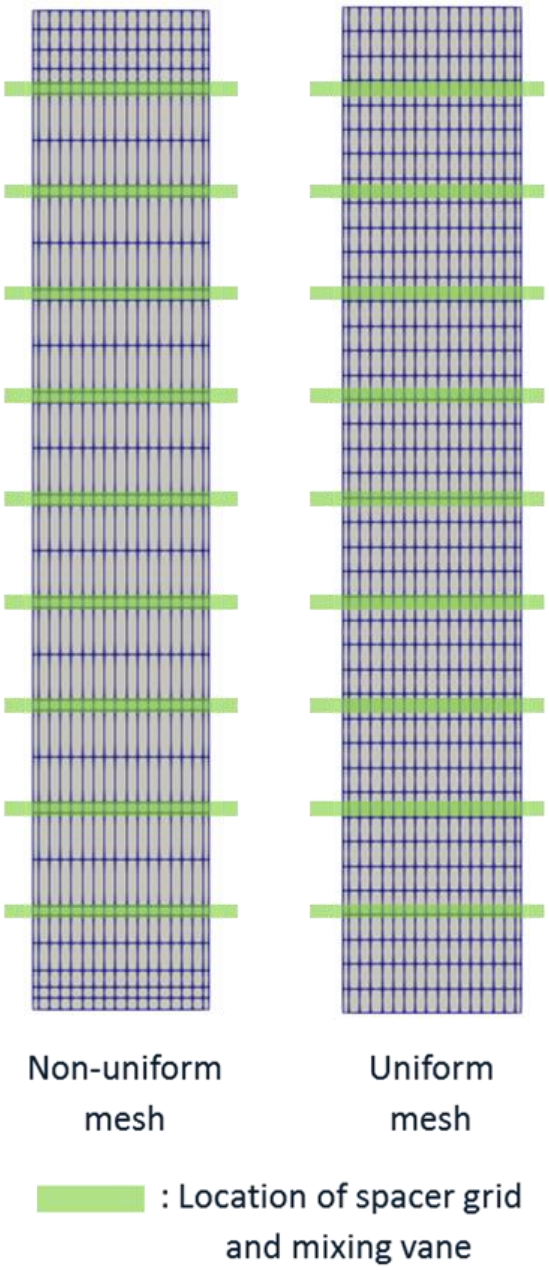

Figure 2.12 Location of spacer grid in the (a) axially non-uniform mesh and (b) uniform mesh

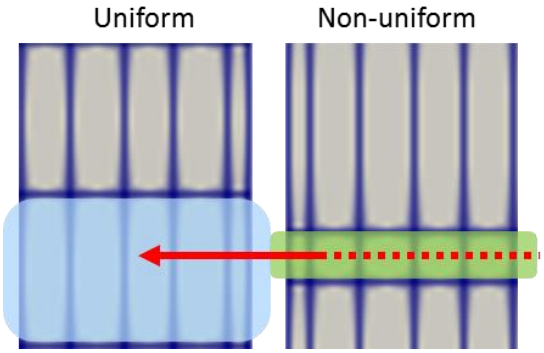

(a) Spacer grid included axial cell

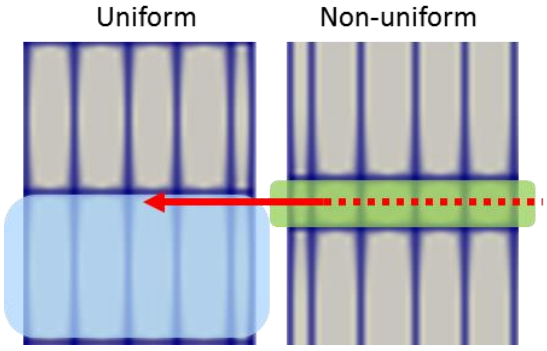

(b) Spacer grid located in the cell face : lower cell

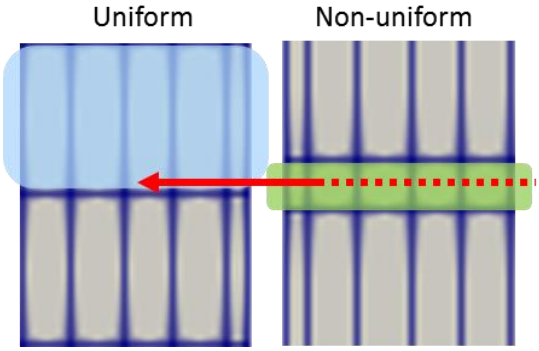

(c) Spacer grid located in the cell face : upper cell

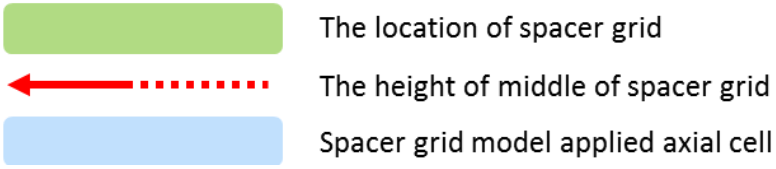

Figure 2.13 Spacer grid model applied axial cell

2.2 Improvement of Fuel Rod Heat Conduction Model

The subchannel is a space surrounded by the fuel rods and the walls, where the coolant temperature increased by the conducted heat from the fuel rod. Therefore, the accurate simulation of a rod bundle is necessary to perform reliable subchannel scale thermal hydraulic analysis. Fuel rod is composed of cladding, pellet and gap, which has different properties such as thermal conductivity and heat capacity. The material properties of the cladding and pellet were applied from material library for LWR accident condition analysis MATPRO as shown in equations 2-4 and 2-5 (Aybar and Ortego, 2005). Fig. 2.14 shows that the calculated thermal conductivity could capture the reference data.

$$k_{zircaloy} = 7.51 + 2.09 \times 10^{-2}T - 1.45 \times 10^{-5}T^2 + 7.67 \times 10^{-9}T^3 \quad (2\text{-}4)$$

$$k_{UO2} = \left[\frac{D}{1+(6.5-0.00469T')(1-D)}\right]\left[\frac{C_v}{(A+BT'')(1+3e_{th})}\right] + 5.2997 \times 10^{-3}Te^{-\frac{13358}{T}}\left\{1 + 0.169\left[\frac{13358}{T} + 2\right]^2\right\} \quad (2\text{-}5)$$

Where k_{UO2} : thermal conductivity of UO2 (W/m·K)

D : fraction of theoretical density

C_v : phonon contribution to the specific heat at constant volume (J/kg·K)

e_{th}: linear strain caused by thermal expansion (temperature>300 K)

T : fuel temperature (K)

T' : porosity correction for temperature

T'=6.50-T×4.69× 10^{-3} (temperature<1,364 K)

= -1 (temperature>1,877 K)

T′′=fuel temperature (temperature<1,800 K)

= 2,050 K (temperature>2,300 K)

A : a factor proportional to the point defect contribution

B : a factor proportional to the phonon-phonon scattering contribution

In addition, the gap between the pellet and the cladding is filled with gas to prevent contact between the pellet and the cladding. The heat transfer coefficient of the gap has an effect on the pellet center temperature. Therefore, the dynamic gap conductance model was implemented to calculate heat transfer coefficient of the gap (Chung et al., 2010). In the present study, it was assumed that as shown in equation 2-6 assumed that only helium exists in the gap.

$$H_{gap} = H_{rad} + H_{gas} + H_{solid} \tag{2-6}$$

$H_{rad} = \frac{q_r''}{T_1 - T_2}$: heat transfer coefficient due to thermal radiation

$H_{gas} = \frac{k_{gas}}{t_g + 1.845(g_1 + g_2)}$: heat transfer coefficient due to conduction in the fill gas

$H_{solid} = \frac{5k_m}{(R_1^2 + R_2^2)^{\frac{1}{2}}} \left(\frac{\mathrm{P_{int}}}{H_M}\right)^n \left(\frac{R_1}{\lambda_1}\right)$: heat transfer coefficient due to physical contact between the fuel pellet and the cladding

Where q_r'' : radiant heat flux leaving the fuel surface

$q_r'' = \sigma_{SB}\left[\frac{1}{\epsilon_1} + \frac{A_1}{A_2}\left(\frac{1}{\epsilon_2} - 1\right)\right]^{-1}[T_1^4 - T_2^4]$

$T_1 - T_2$: temperature difference between fuel and cladding

ϵ : emissivity

k_{gas} : fill gas mixture thermal conductivity

t_g : gas gap width(from deformation model)

g : temperature jump distances

$k_m = \frac{2k_1k_2}{k_1+k_2}$

R : mean surface roughness

$\frac{\mathrm{P_{int}}}{H_M}$: ratio of the interface pressure to the Meyer hardness

λ_1 : wave length

n=1.0 when $\frac{\mathrm{P_{int}}}{H_M} > 0.01$, n=0.5 when $\frac{\mathrm{P_{int}}}{H_M} < 0.0001$

$\left(\frac{\mathrm{P_{int}}}{H_M}\right)^n$=1 when $0.0001 < \frac{\mathrm{P_{int}}}{H_M} < 0.01$

$\left(\frac{R_1}{\lambda_1}\right) = \exp[0.5285 \times ln(R_1 - 5.738)]$

Each fuel rod is divided into four quarters. Not only one dimensional heat transfer from the fuel rod to the subchannel, but also circumstantial heat conduction among the quarter rods was considered. The inner temperature of the guide tube is set to be equal to the coolant temperature for neglecting heat transfer between the coolant and the guide tube. This is to prevent the guide tube from working as a heat sink. After that, the fuel rod I/O system was established for post-processing of the simulation result using fuel rod heat conduction model. The produced data includes fuel rod temperature, power and DNBR distribution.

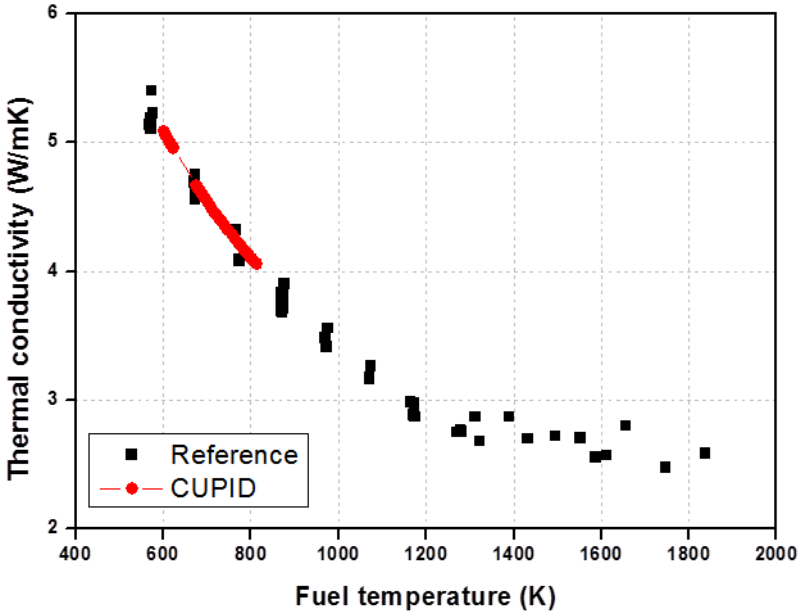

(a) Thermal conductivity of pellet

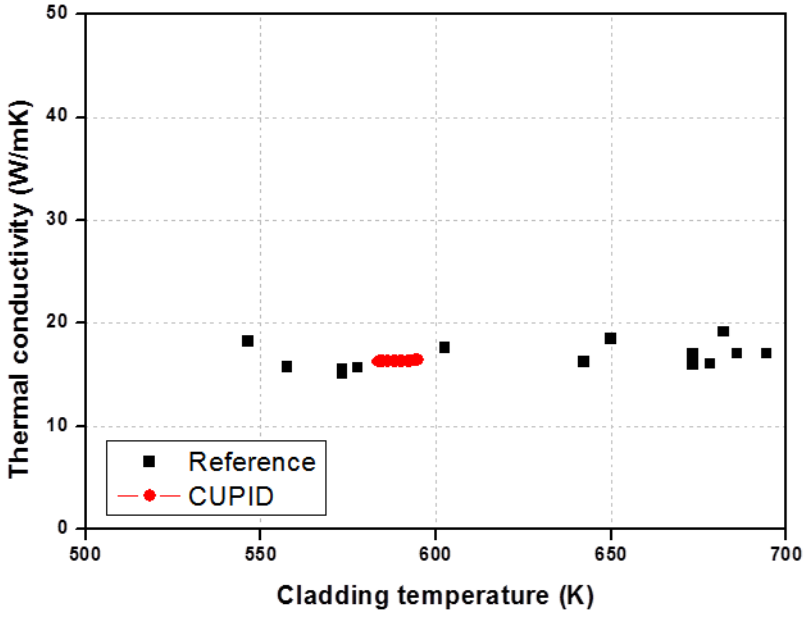

(b) Thermal conductivity of cladding

Figure 2.14 Thermal conductivity comparison reference and CUPID simulation

2.2.1 Improvement of Default Fuel Rod Heat Conduction Model Applied to CUPID

Depending on the location, corner, side and center subchannels face one, two and four fuel rods, respectively, as illustrated in Fig. 2.15. However, default model of fuel rod heat conduction in CUPID was a rod-centered approach, modeled as a single subchannel contact with one fuel rod. In this default model, the averaged value of power of fuel rods was entered into the subchannel. However, near the guide tube, such as side and center of guide tube subchannels, the power of the common fuel rods and guide tube are averaged. Since power is not applied to the guide tube, the internal temperature distribution of these channels could be distorted. Therefore, the model was improved as the subchannel could face the proper number of fuel rods as a channel-centered cell. The difference between rod-centered and channel-centered cells is illustrated in Fig. 2.16.

Likewise, the fuel rod faces four subchannels which have different temperatures and pressures. So, the fuel rod was divided into four quarters to be contact with each subchannel and also contain individual temperature information as shown in Fig. 2.17. It implies that one-dimensional heat conduction between each quarter of fuel rod and subchannel is required. Heat is conducted from the pellet center of the fuel rod through the gap and the cladding in turn, and the fuel rod temperature increased. Then the heat is transferred to the subchannel through the convection of the coolant, which depends on the subchannel temperature. In other words, a single fuel rod has four cladding surface temperatures as described in Fig. 2.18, allowing for more precise calculation of the DNBR distribution of the fuel rod. The equation, differentiating the one-dimensional heat conduction equation of fuel rod, is shown below. It is applied to the solid fuel cell.

$$k_{j+1}2\pi r_{j+1}\frac{T'_{j+1}-T'_j}{r_{cen,j+1}-r_{cen,j}} + k_j 2\pi r_j \frac{T'_{j-1}-T'_j}{r_{cen,j}-r_{cen,j-1}} + \dot{q}\pi\left(r_{j+1}^2 - r_j^2\right) \quad (2\text{-}7)$$

$$= \rho C_{p_j}\pi\left(r_{j+1}^2 - r_j^2\right)\frac{T'_j - T_j}{dt}$$

Where T : Temperature of previous step

T′ : Temperature of current time step

The subchannel scale thermal hydraulic analysis using CUPID was performed using the fuel rod heat conduction model, and the I/O system was established. In the activated fuel rod heat conduction model, related variables were cladding surface temperature, fuel rod center temperature and power. These variables could not be investigated and averaged value of the four fuel rods could be confirmed before the formation of the I/O system.

In addition, it is possible to simulate actual experimental condition and various type of fuel rods by adjusting rod pitch and radius of fuel rod. Therefore, the Westinghouse type 17x17 fuel assembly and the CE type 16x16 fuel assembly including five guide tubes could be produced as shown in Fig. 2.19. The guide tube of the CE type assembly replaces the four fuel rods, which deduces that the guide tube is divided into 16 sections.

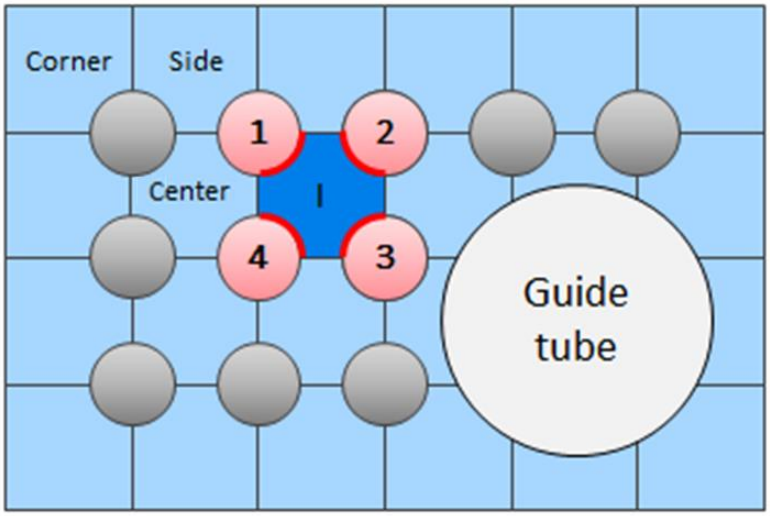

Figure 2.15 Subchannel-rod connectivity

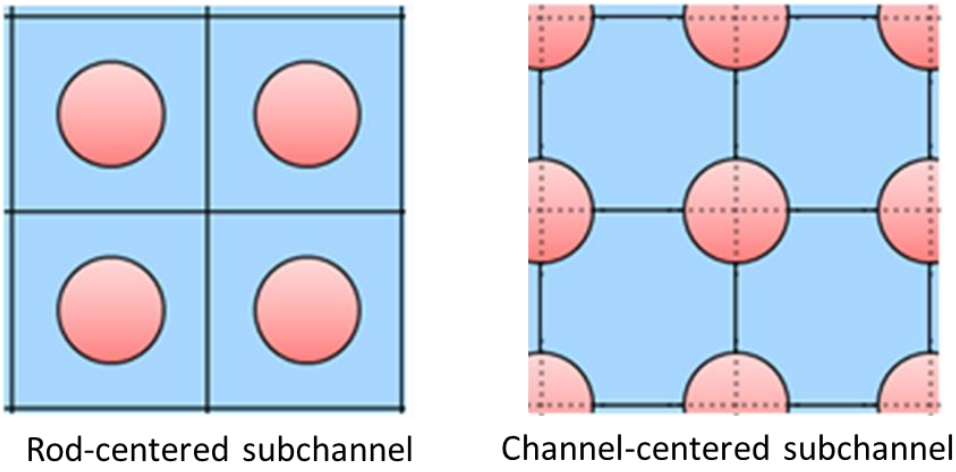

Figure 2.16 Difference between rod-centered and channel-centered channel

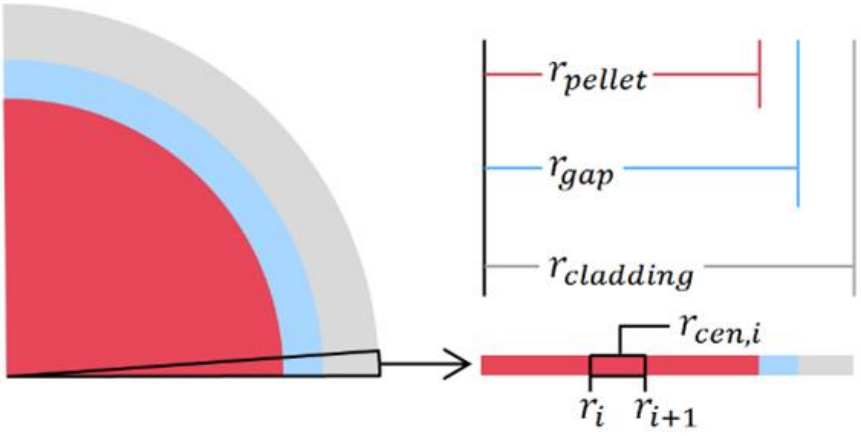

Figure 2.17 Schematic view of quarter fuel rod

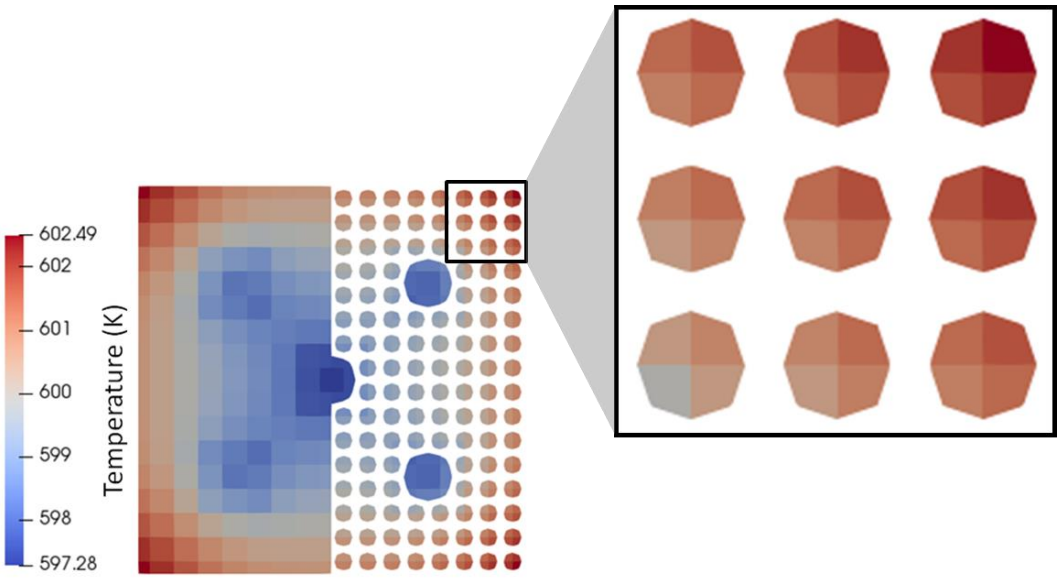

Figure 2.18 Single fuel rod divided into four sections

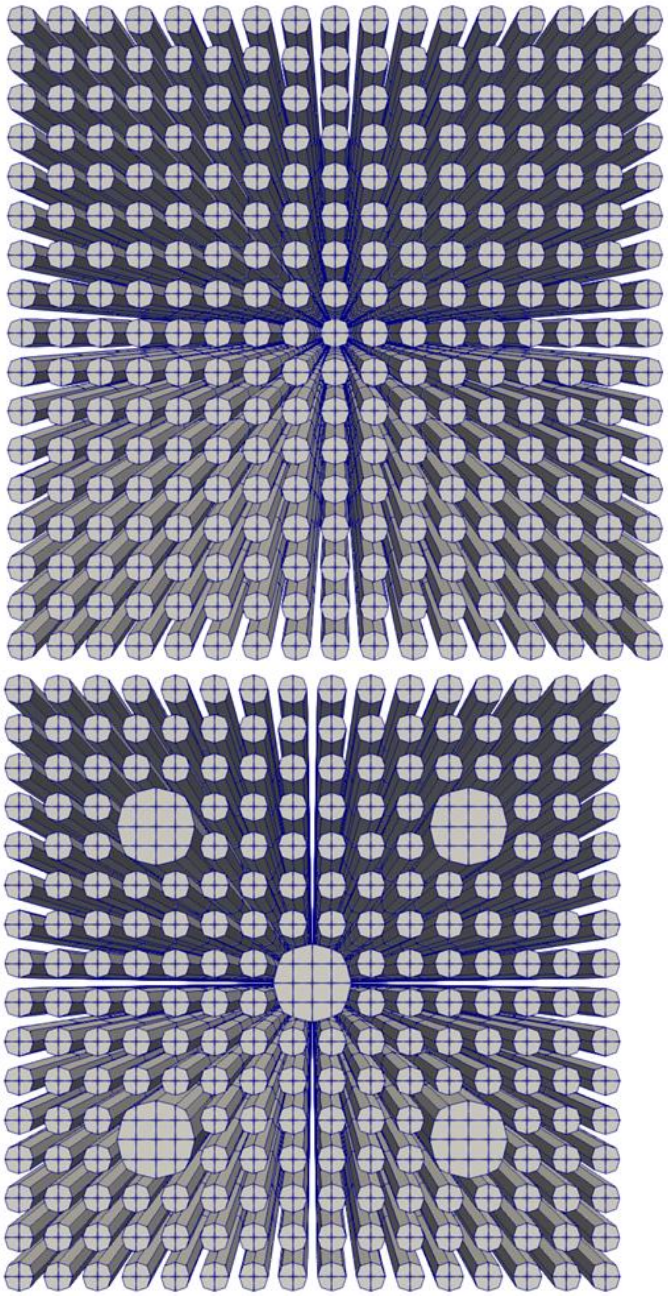

Figure 2.19 Visualized WH type and CE type assemblies

2.2.2 Circumstantial Heat Conduction between Quarter Fuel Rods

In order to apply more precise heat conduction model, the single rod was split up into four quarter fuel rods. Each quarter fuel rod faces the subchannel, which has its own liquid temperature; the difference in coolant temperature makes the difference of cladding surface temperature among the quarter rods. However, circumstantial heat conduction occurs between adjacent quarter fuel rods, so it is reasonable that the pellet center temperature becomes similar. The circumstantial heat conduction model, $\mathrm{Sc_{circum}}$, was added into the source term of differentiated fuel rod model as follows:

$$k_{j+1}2\pi r_{j+1}\frac{T'_{j+1}-T'_j}{r_{cen,j+1}-r_{cen,j}}+k_j 2\pi r_j\frac{T'_{j-1}-T'_j}{r_{cen,j}-r_{cen,j-1}}+\dot{q}\pi\left(r_{j+1}^2-r_j^2\right)$$
$$+\boldsymbol{Sc_{circum}}=\rho C_{p_j}\pi\left(r_{j+1}^2-r_j^2\right)\frac{T'_j-T_j}{dt} \qquad (2\text{-}8)$$

$$Sc_{circum}=-k_j\frac{\Delta T_{quarter1}}{0.5\pi r_{cen,j}}\left(r_{j+1}-r_j\right)-k_j\frac{\Delta T_{quarter2}}{0.5\pi r_{cen,j}}\left(r_{j+1}-r_j\right) \qquad (2\text{-}9)$$

$\mathrm{\Delta T_{quarter}}$, the temperature difference between adjacent quarter fuel rods, has two limitation $\mathrm{\Delta T_1}$ and $\mathrm{\Delta T_2}$. These limiters are required to guarantee numerical stability during the transient calculation as the circumstantial conduction was treated in an explicit way. First, $\mathrm{\Delta T_1}$ is smaller value between temperature difference of quarter fuel rods and $\mathrm{\Delta T_{limit}}$. In addition, $\mathrm{\Delta T_2}$ is temperature difference between quarter rods which causes the $\mathrm{\Delta T_{limit}}$ change of the fuel

temperature. Circumstantial heat conduction was simulated using a smaller value of ΔT_1 and ΔT_2 as $\Delta T_{quarter}$.

$$\Delta T_1 = T_j - T_{neigh,j}, \qquad \left|T_j - T_{neigh,j}\right| \le \Delta T_{limit}$$

$$\Delta T_1 = \pm \Delta T_{limit}, \qquad \left|T_j - T_{neigh,j}\right| > \Delta T_{limit}$$

$$k_j \frac{\Delta T_2}{0.5\pi r_{cen,j}}\left(r_{j+1} - r_j\right) = \rho C_p A \frac{\Delta T_{limit}}{dt}, \qquad \Delta T_2 = \frac{0.5\pi r_{cen,j}}{k_j\left(r_{j+1} - r_j\right)} \rho C_p A \frac{\Delta T_{limit}}{dt}$$

$$\Delta T_{quarter} = min(\Delta T_1, \Delta T_2) \tag{2-10}$$

If ΔT_{limit} is too small (=0.1 K), the temperature difference at the pellet center is maintained by the reduced effect of the circumstantial heat conduction model as shown in Fig. 2.20 (a). Otherwise, if ΔT_{limit} is too large (=5.0 K), the instability of calculation occurs and pellet center temperature diverged as illustrated in Fig. 2.20 (b). On the other hand, Fig. 2.20 (c) describes the calculation result using a proper ΔT_{limit} (=1.0 K) that the conversed temperature at the pellet center of the quarter fuel rods.

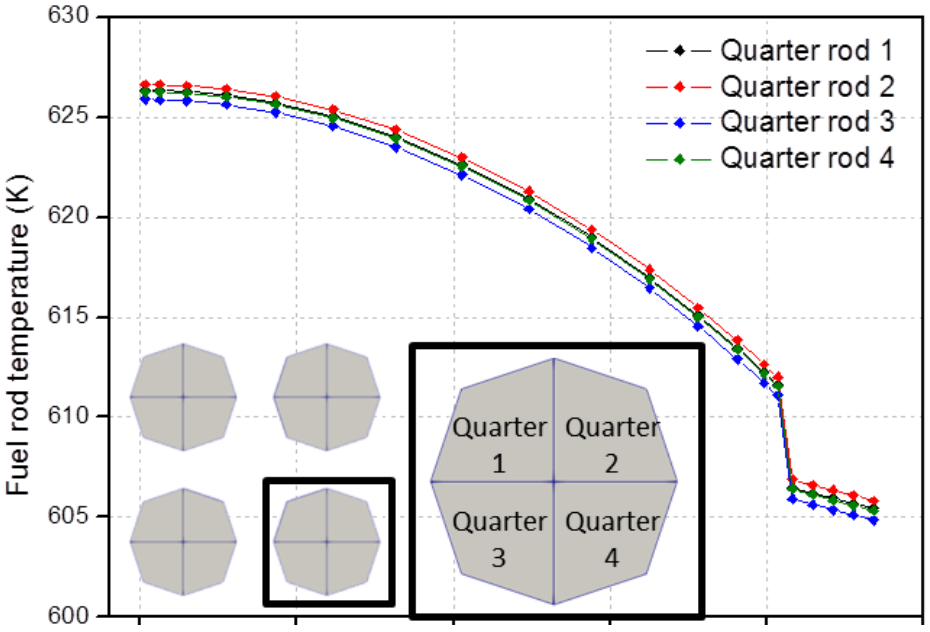

(a) Fuel rod internal temperature distribution when ΔT_{limit}=0.1 K

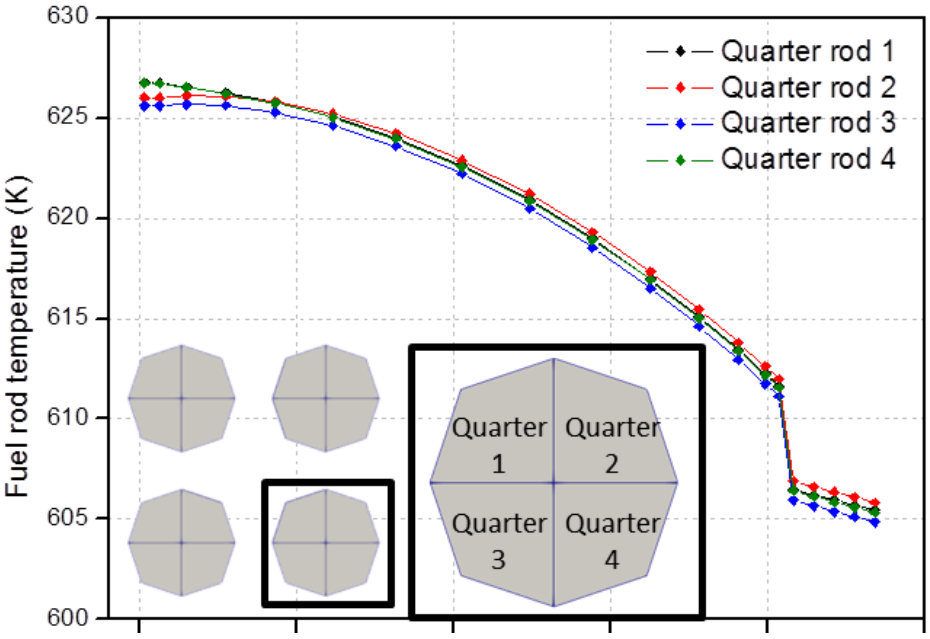

(b) Fuel rod internal temperature distribution when ΔT_{limit}=5.0 K

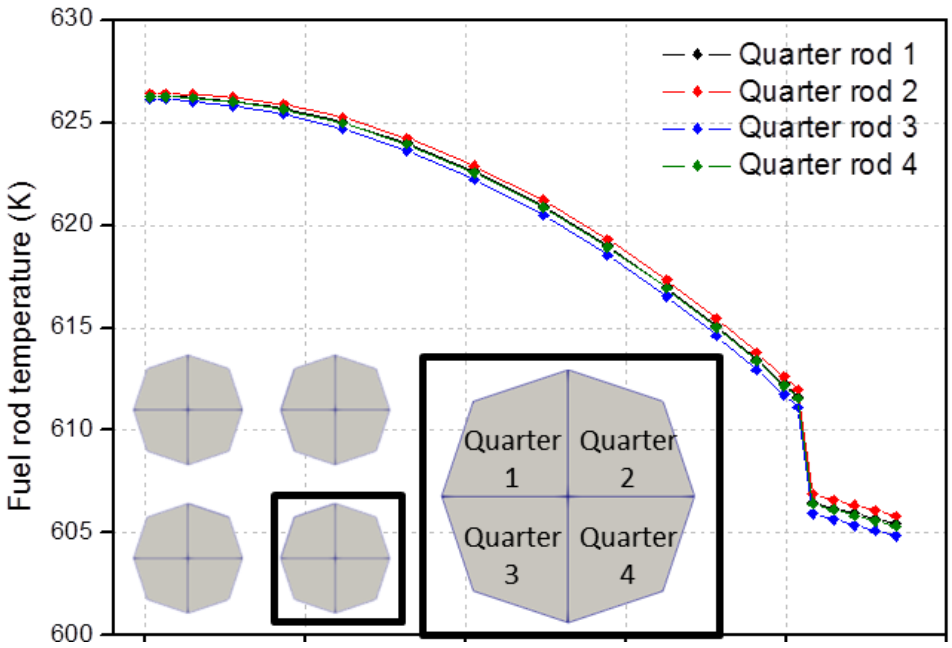

(c) Fuel rod internal temperature distribution when ΔT_{limit}=1.0 K

Figure 2.20 Fuel rod internal temperature distribution caused by circumstantial heat conduction

2.2.3 Implementation of CHF Model

DNBR, which is the ratio of CHF generated power to fuel rod power, is one of the most important parameter of the reactor core thermal hydraulic analysis. Since the fuel rod power in hot full power has a cosine shape, it is expected that the minimum DNBR could occur at the center of the fuel rod. But it is necessary to implement the CHF model and calculate the DNBR in order to determine the accurate location and its value of the minimum DNBR.

The use of an appropriate CHF model is required for DNBR prediction. However, the KCE-1 model, the CHF model currently used for simulation of APR1400, is not released as a commercial model. Thus, relatively more simple model, Biasi correlation (Biasi et al., 1967) and the more accurate CE-1 model (Tong, 2018) were implemented into CUPID to confirm the DNBR distribution change caused by the difference of CHF model. The Biasi and CE-1 correlation are as follows.

Biasi correlation:

$$q''_{biasi} = (5.9691 \times 10^6) G^{-\frac{1}{6}} \left(F(P) G^{-\frac{1}{6}} - X \right) D_H^{-n} \qquad (2\text{-}11)$$

$$D_H < 1cm : n = 0.6, \qquad D_H > 1cm : n = 0.4$$

CE-1 correlation:

$$q''_{CE-1} = \frac{A'(A-BX)}{C} \times 3.1546 \times 10^6 W/m^2 \qquad (2\text{-}12)$$

Where $A' = b_1 \left(\frac{d}{d_m} \right)^{b_2}$, $A = (b_3 + b_4 p) G^{(b_5 + b_6 p)}$

$B = G H_{fg}$, $C = G^{(b_7 p + b_8 G)}$

G : mass flux, P : pressure, X : quality

H_{fg} : latent heat of evaporation

d : subchannel equivalent diameter

d_m : matrix channel equivalent diameter

$b1 = 2.8922 \times 10^{-3}, \quad b2 = -0.50749$

$b3 = 405.32, \quad b4 = -9.9290 \times 10^{-2}$

$b5 = -0.67757, \quad b6 = 6.8235 \times 10^{-4}$

$b7 = 3.1240 \times 10^{-4}, \quad b8 = -8.3245 \times 10^{-2}$

Several variables such as flow rate, cladding and coolant temperature are used for DNBR calculations, in addition to the power of the fuel rod. The fuel rods divided into four sections have the same power, but DNBR is different because the cladding and fluid temperature are different from each other. As a preliminary calculation to determine the effect of the model difference, the distribution of DNBR and the size of the minimum DNBR were verified in a single assembly simulation with uniform power.

Since all fuel rods had the same power and the coolant temperature gradually increased as the flow goes up, the minimum DNBR appeared at the outlet. Under this condition, the minimum DNBR was 4.04 and 3.91 calculated using the Biasi correlation and CE-1 correlation respectively, and CE-1 correlation showed more conservative value. In addition, the location of the minimum DNBR and the distribution of DNBR were changed as shown in Fig. 2.21 and Fig. 2.22. In particular, the calculation result using the CE-1 correlation showed the minimum DNBR at the corner subchannel of the guide tube. This could be confirmed by calculating the each four fuel rods rather than using averaging power.

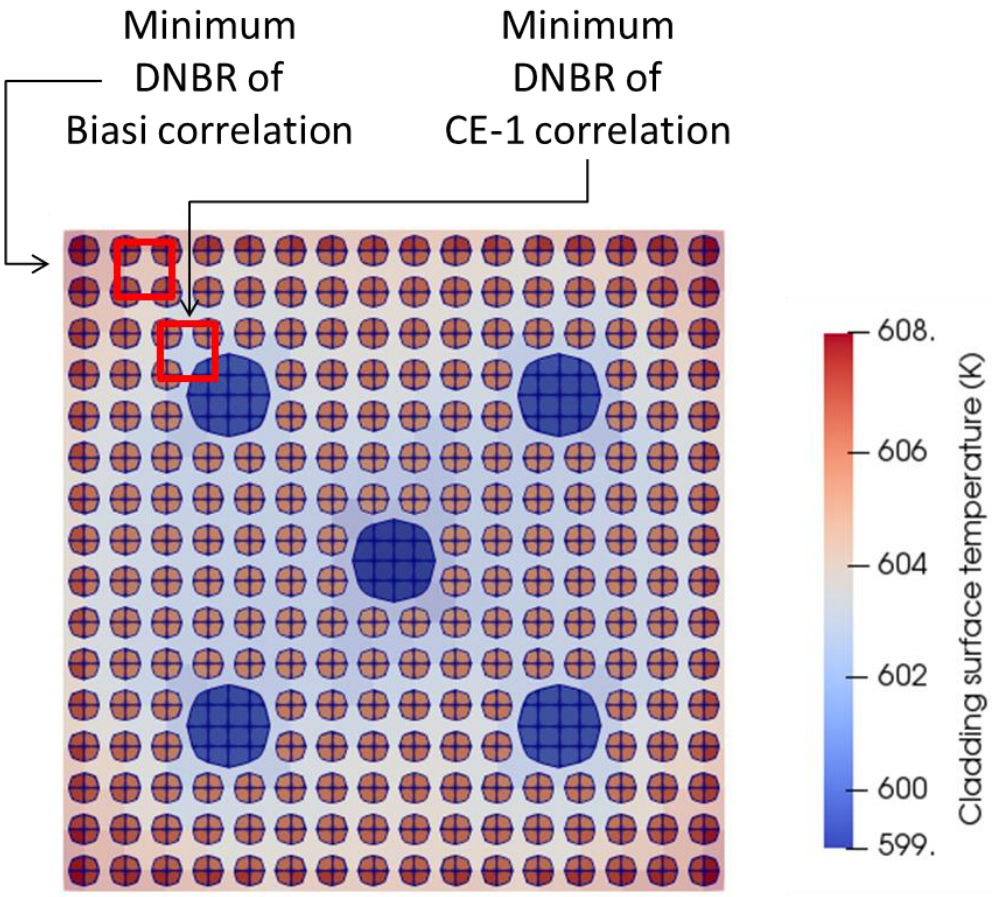

Figure 2.21 Cladding surface temperature distribution and location of minimum DNBR

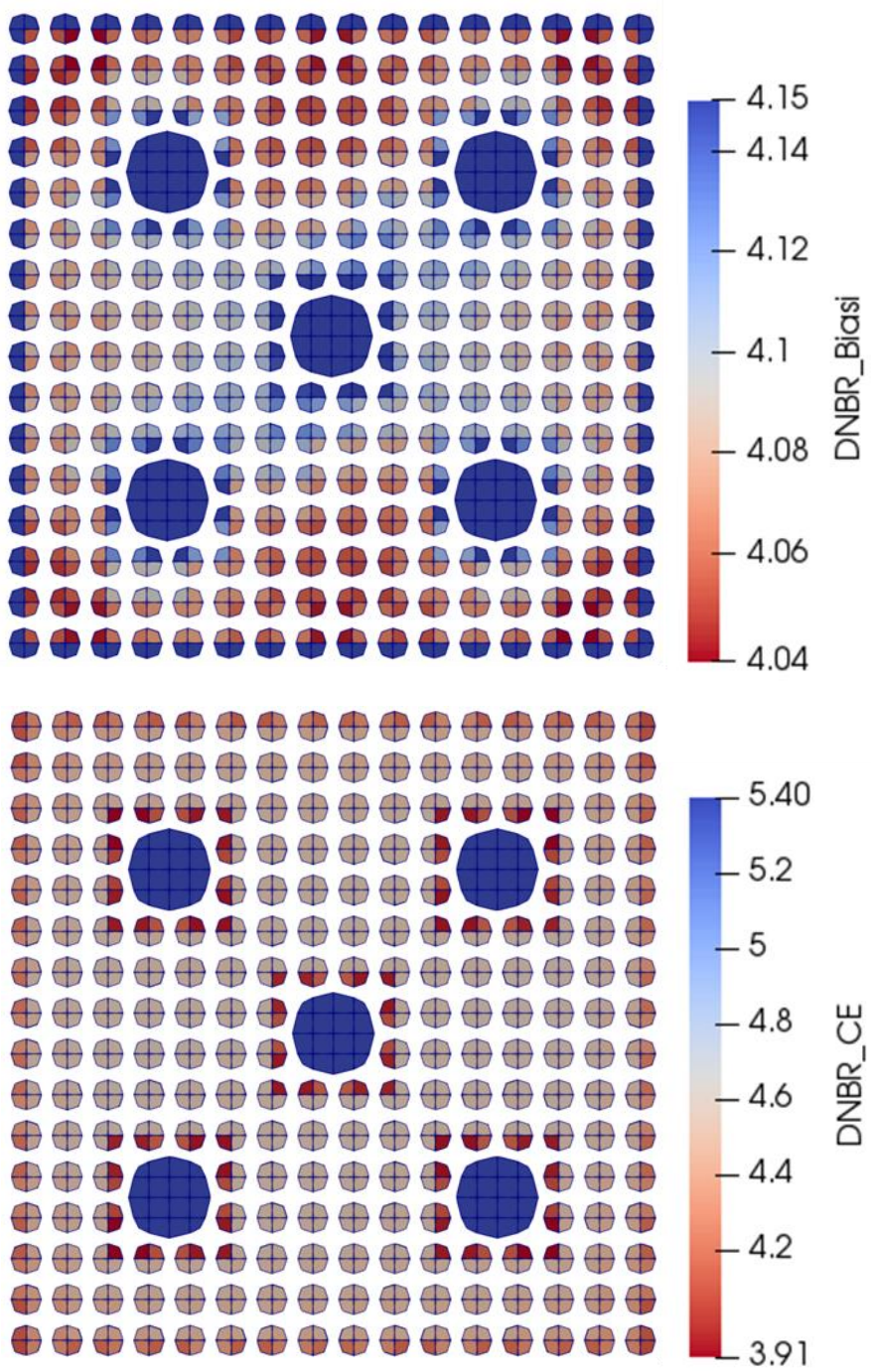

Figure 2.22 DNBR distribution using Biasi correlation and CE-1 correlation

Chapter 3

Verification of Models for Single Assembly of APR1400

3.1 Simulation of APR1400 Single Assembly

Prior to the whole core simulation of APR1400, preliminary calculations were progressed for a single assembly for verification of the models. As shown in Fig. 3.1, the heated length 3.81m was equally divided into 40 parts in the axial direction, and the ghost cells were added to the outlet as the same height. Water gaps among the assemblies and in the space between shroud and channel were not modeled for single assembly simulation, instead the adiabatic wall faced the corner and side subchannels. The mesh was generated using SALOME (Ribes and Caremoli, 2017) and the number of fluid cells and solid cells were 11,849 (17x17x41) and 839,680 (16x16x4x20x41), respectively.

The CE type Plus7 fuel assembly which was used for APR1400 has 16x16 rod bundle and five guide tubes. The guide tube affects nine subchannels, four of them are corner of the guide tube, four are sides of the guide tube and the last one is the center of the guide tube. CTF and CUPID used different methods to simulate a guide tube center subchannel. For the mesh used for the CTF simulation, it was assumed that the center subchannel of guide tube is an empty space. Therefore,

coolant flow of inside and the fluid exchange with surrounding channels were prevented in the center of the guide tube. On the other hand, the mesh used for CUPID calculation considered the center of guide tube as a fluid cell; the porosity was 2% of the normal subchannel. It allowed a small amount of bypassed flow through the guide tube. Fig. 3.2 describes the difference between guide tube center subchannel of CTF and CUPID.

For single assembly calculation, APR1400 core power was applied from the simulation result using nTRACER, a neutronics code. The power distribution was entered from the assembly 23, which is the inner assembly, faces with water gap instead of the shroud. The averaged power of single assembly was 16.527 MW and the total power of the assembly 23 was 18.050 MW. Fig. 3.3 shows the position of the assembly 23 in the whole core.

The grid used for the nTRACER simulation was non-uniform in the axial direction. Therefore the volumetric power density was applied on uniform mesh proportional to the overlaid length of non-uniform mesh as shown in Fig. 3.4. For example, the linear power applied on channel i is $q_i' = (q_p' \times l_{ip} + q_q' \times l_{iq} + q_r' \times l_{ir})/l_i$ and the linear power applied on channel j is $q_j^{'} = (q_r^{'} \times l_{jr})/l_j = q_r^{'}$.

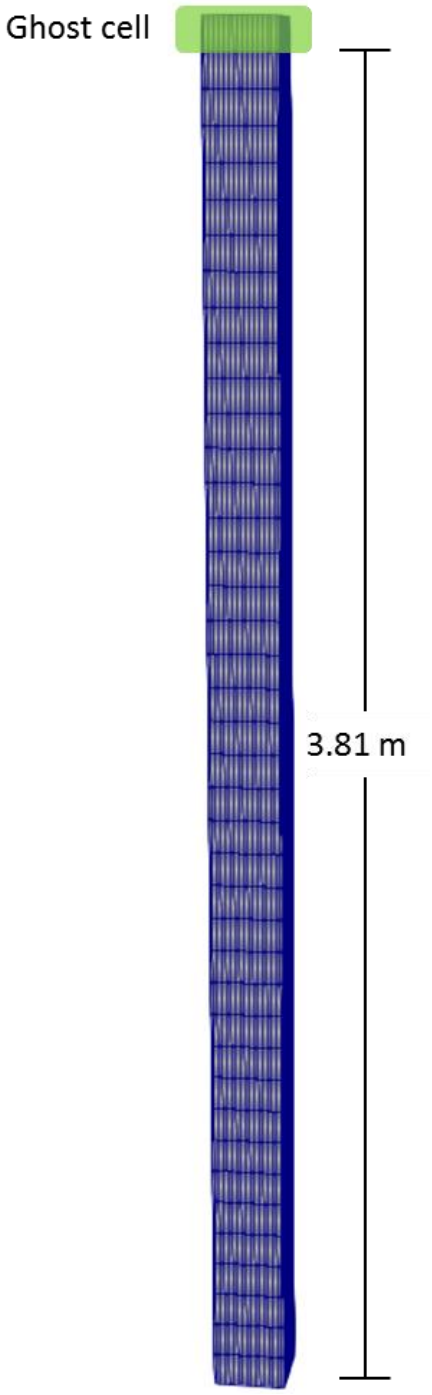

Figure 3.1 Axially uniform mesh of single assembly

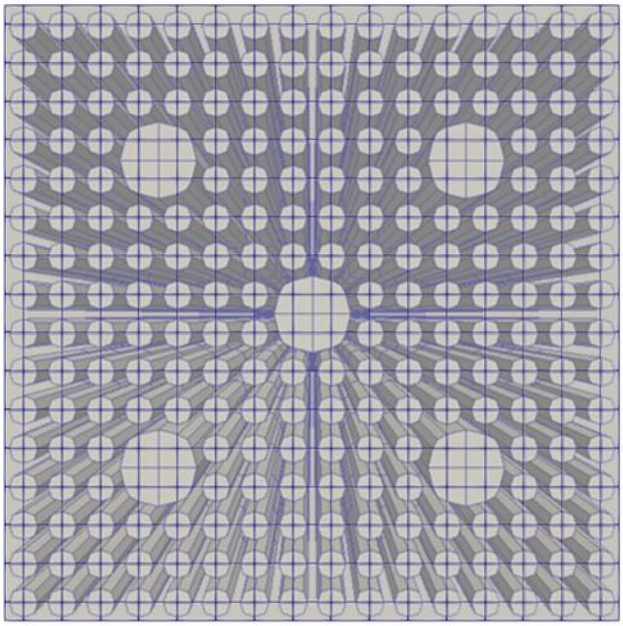

(a) Fluid mesh of CUPID

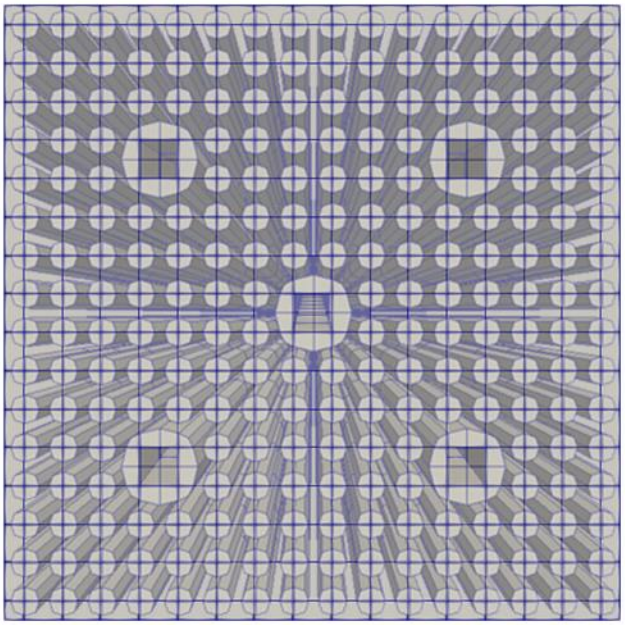

(b) Fluid mesh of CTF

Figure 3.2 Difference of CUPID and CTF on considering center of guide tube

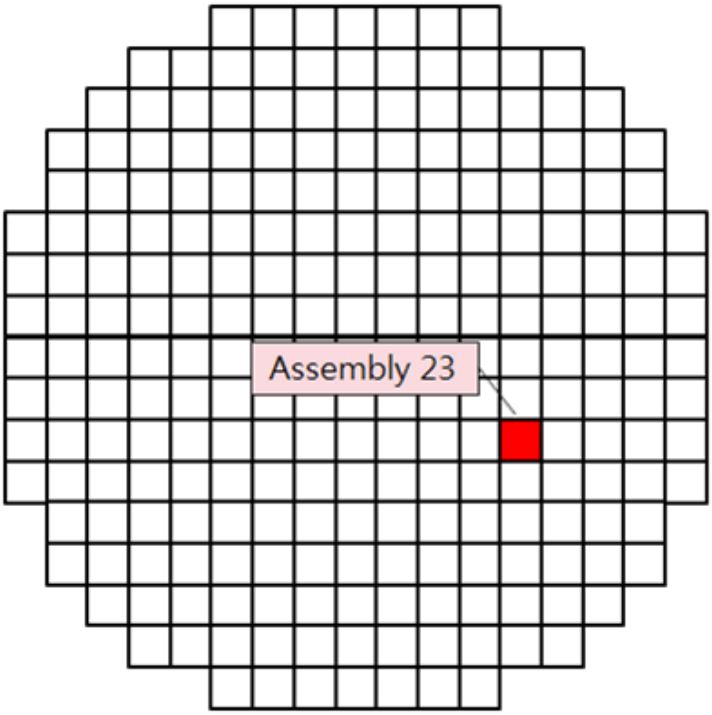

Figure 3.3 Location of the assembly 23 in the whole core of APR1400

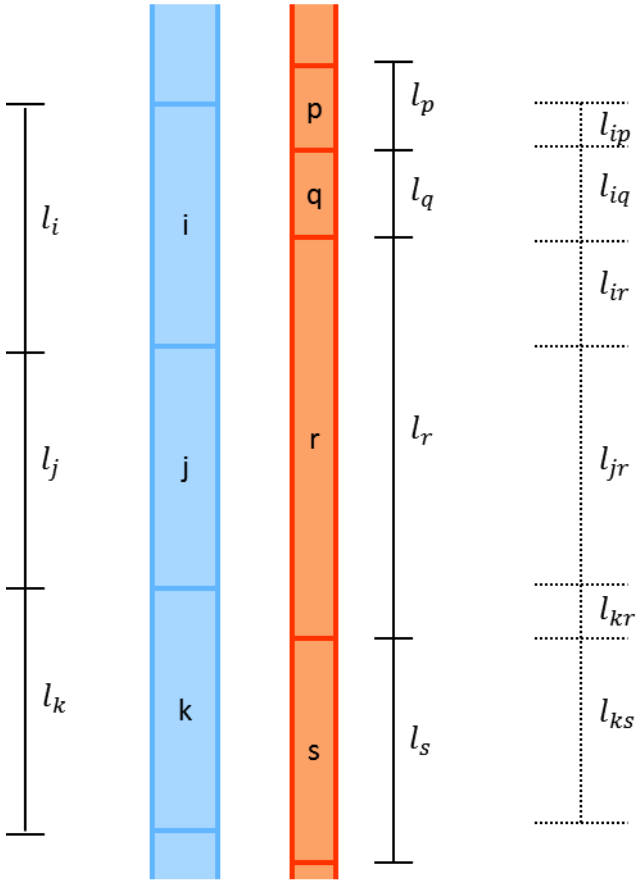

Figure 3.4 Example of uniform mesh and non-uniform mesh

3.2 Verification of Grid-directed Cross Flow Model

The grid-directed cross flow model was implemented to simulate the thermal hydraulic phenomena induced by mixing vane. Some modification of the model was progressed to make the model applicable for the collocated grid and model was verified against the APR1400 single assembly. Since the experimental data of APR1400 was not accessible, the code-to-code comparison between CUPID and CTF was performed.

3.2.1 Verification of Modified Grid-directed Cross Flow Model

In order to compensate the momentum cancellation in the center subchannel, the model was implemented into not only momentum equation but also scalar equation such as mass and energy. Then, β' was added on $\beta_{default}$, which is the originally used turbulent mixing coefficient, to induce the additional turbulent mixing caused by mixing vane. β' made the simulation result using CUPID could reproduce the result from CTF calculation. According to the previous study, the maximum and minimum values of turbulent mixing coefficient $\beta_{default}$ were 0.05 and 0.005. The value of $\beta_{default}$ was 0.005 for the same phenomenon in the single assembly simulation, which was single-phase heated condition. Therefore, $\beta_{default}$ of 0.005 was used for APR1400 single assembly analysis.

Since the momentum cancellation occurred in each direction, β' was added to the x and y direction respectively in the EVVD model. In addition, β' was not implemented in the vicinity of guide tube because the model was not canceled near the guide tube. To select the β' the code-to-code comparison between

CUPID and CTF was conducted, as shown below. As illustrated in Fig. 3.5 (a) and (b), the simulation results of CUPID and CTF are similar due to the implementation of β' on the EVVD model. In addition, the temperature distribution of the coolant and cladding surface at the outlet is getting flatten as the β' increases as shown in Fig. 3.6 and Fig. 3.7.

The simulation result of applying modified grid-directed cross flow model is following. Fig. 3.8 and Fig. 3.9 shows that the coolant stream line is uniform in the axial direction before applying the model, whereas the stream line rotates and moves transversely after the model implementation. In particular, non-uniform lateral fluid transfer occurring near the guide tube was observed. Fig. 3.10 provides the more detailed description of the lateral velocity at the mixing vane location. The transverse velocity was large in the subchannel where momentum was not cancelled, such as corner subchannel or near the guide tubes. On the other hand, in the center subchannel, it could be confirmed from the simulation result that the lateral velocity was small due to the momentum cancellation.

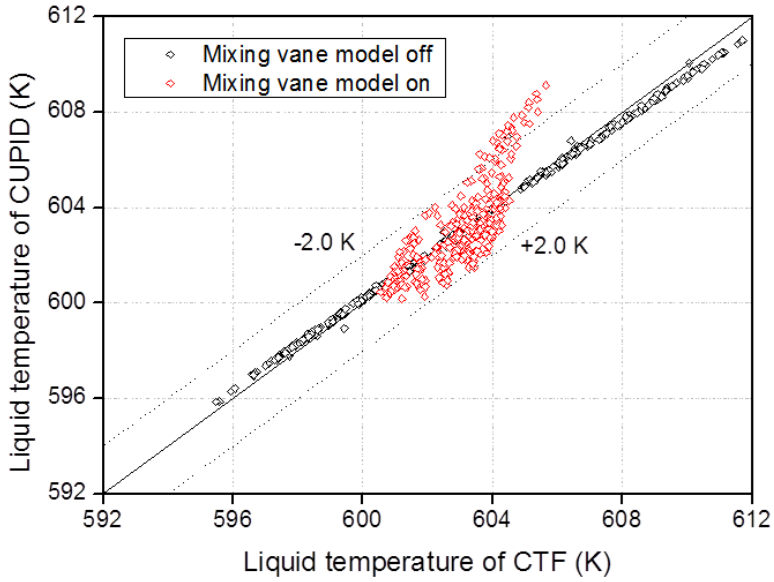

(a) Comparison of liquid temperature between CUPID and CTF without β′

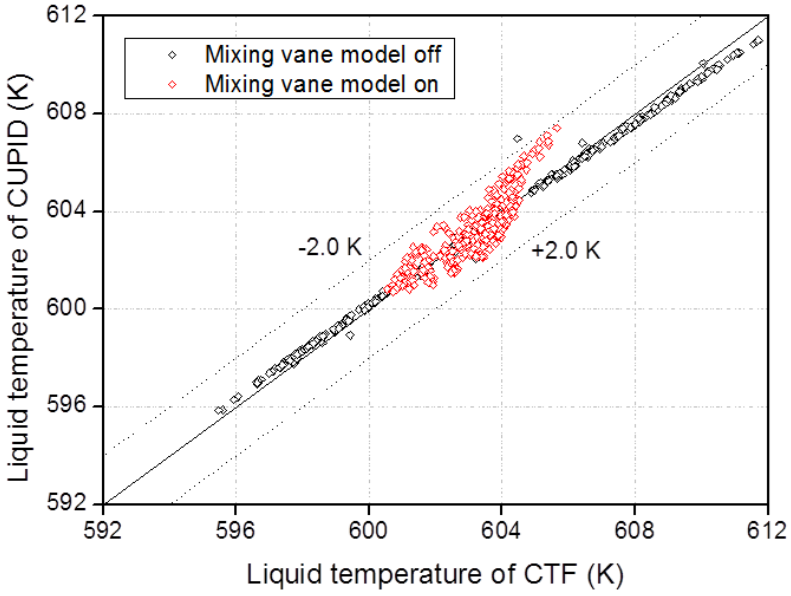

(b) Comparison of liquid temperature between CUPID and CTF with β′

Figure 3.5 Code-to-code comparisons of outlet temperature between CUPID and CTF

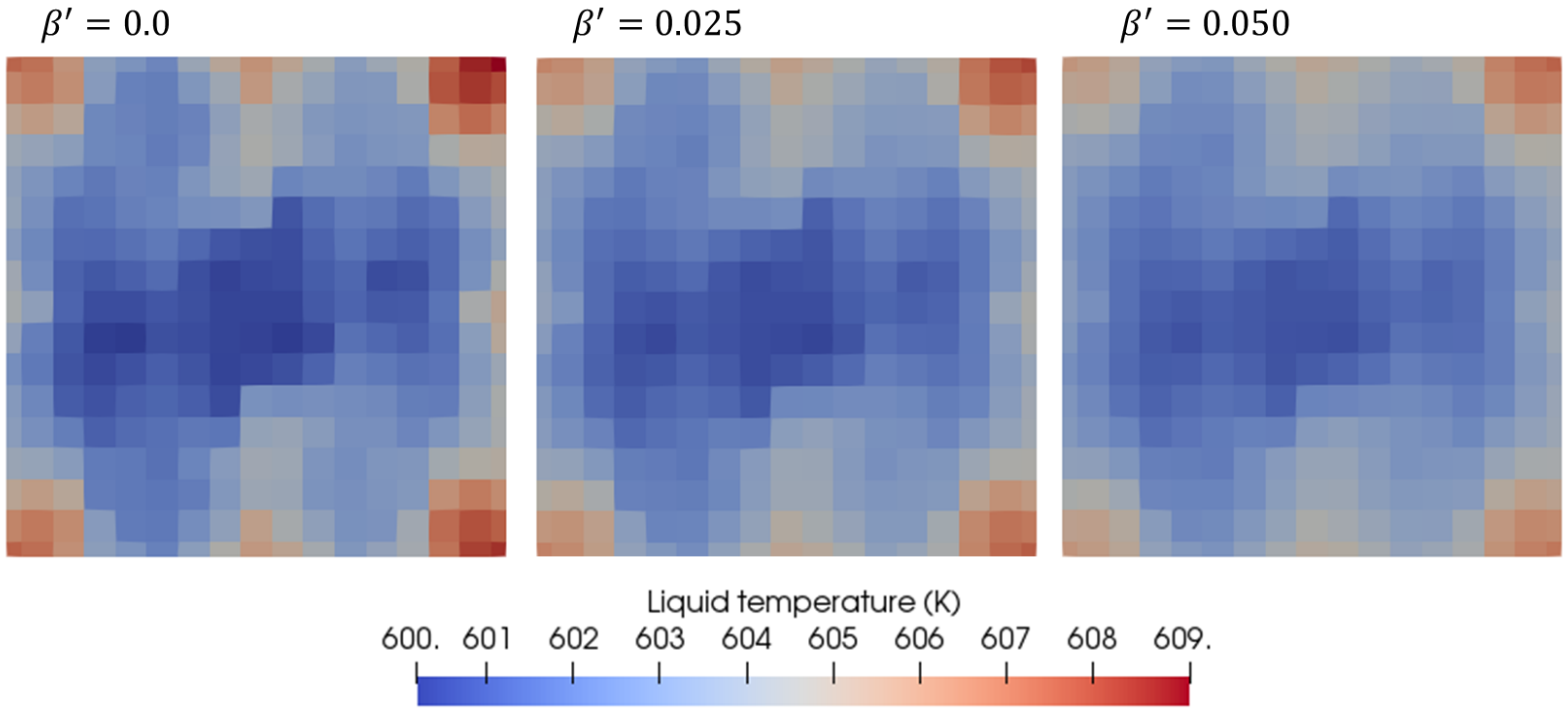

Figure 3.6 Liquid temperature distribution at the outlet when β' is 0, 0.025 and 0.05

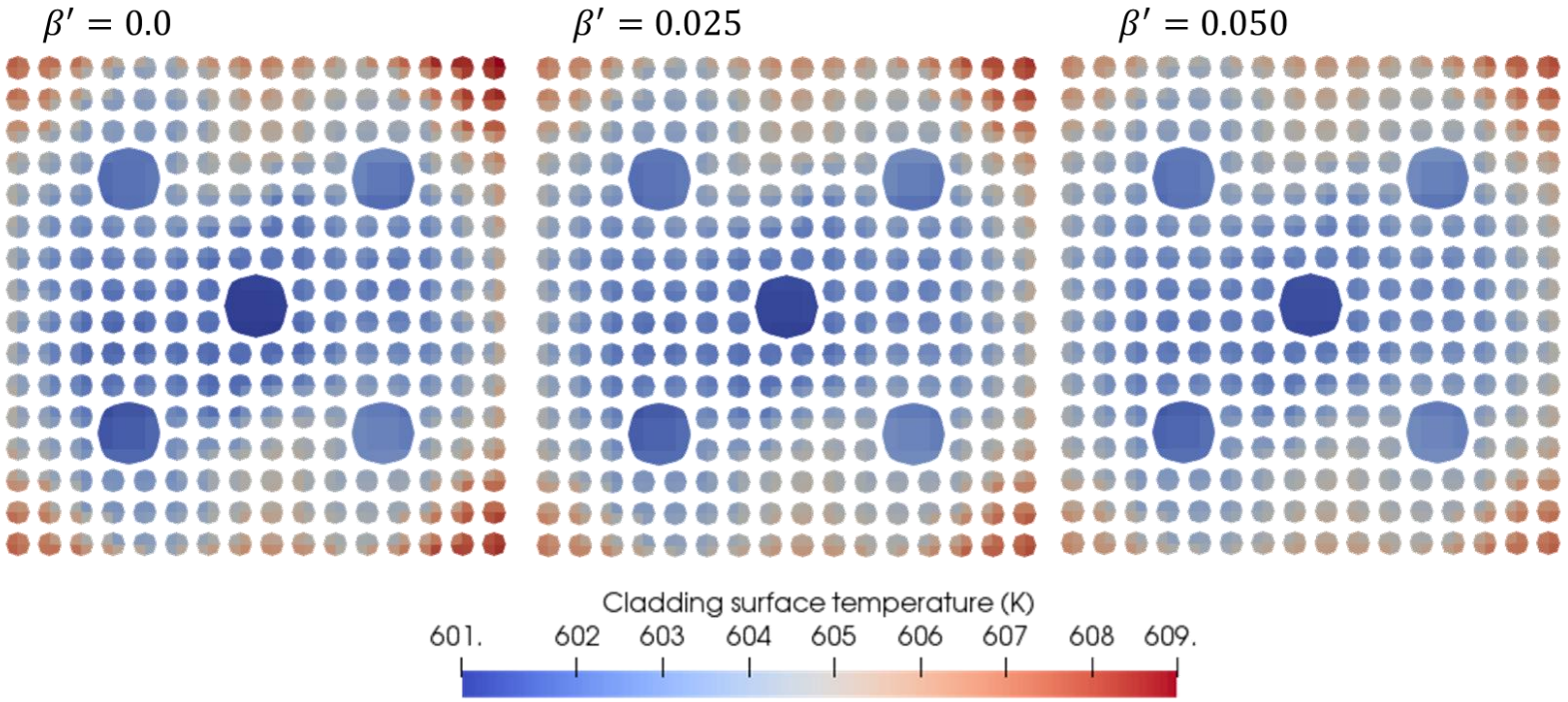

Figure 3.7 Cladding surface temperature distribution at the outlet when β' is 0, 0.025 and 0.05

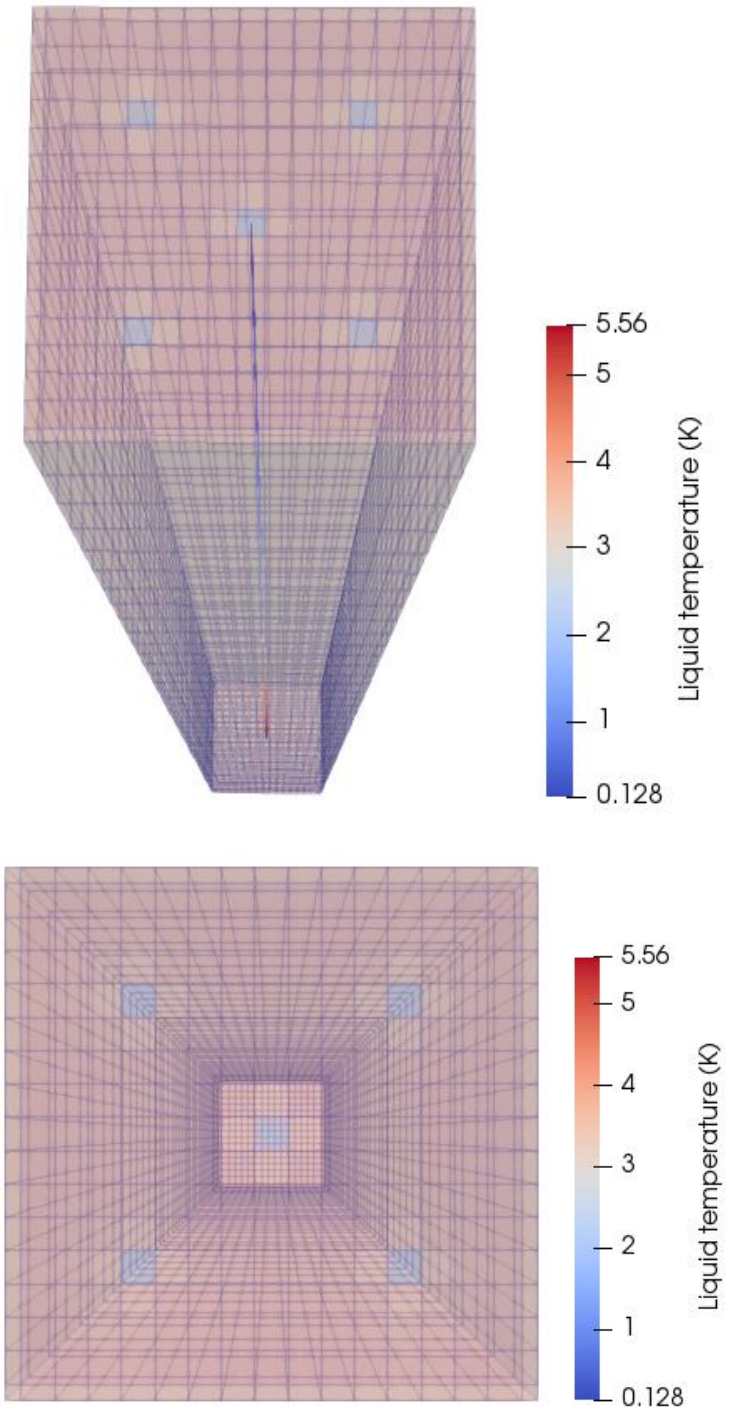

Figure 3.8 Stream line of coolant: deactivated mixing vane model

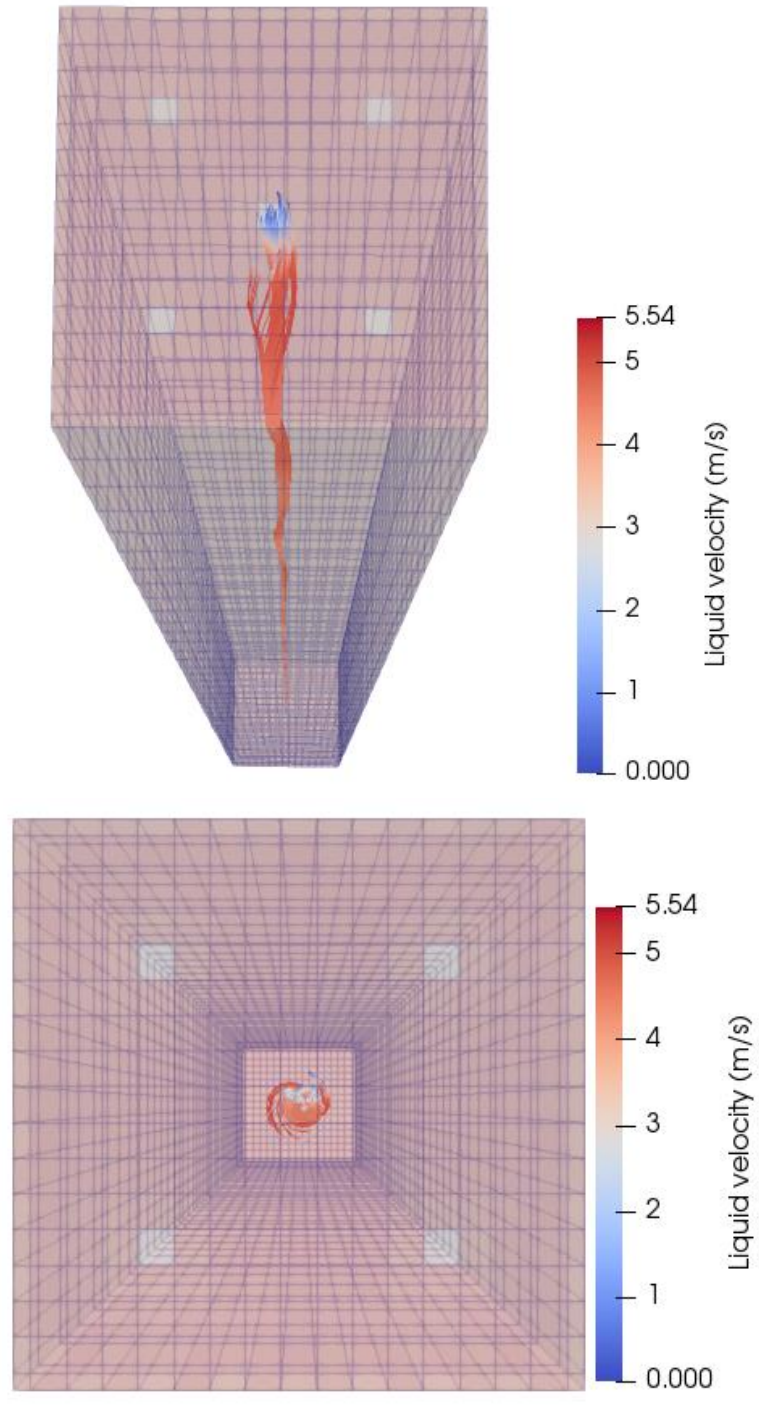

Figure 3.9 Stream line of coolant: activated mixing vane model

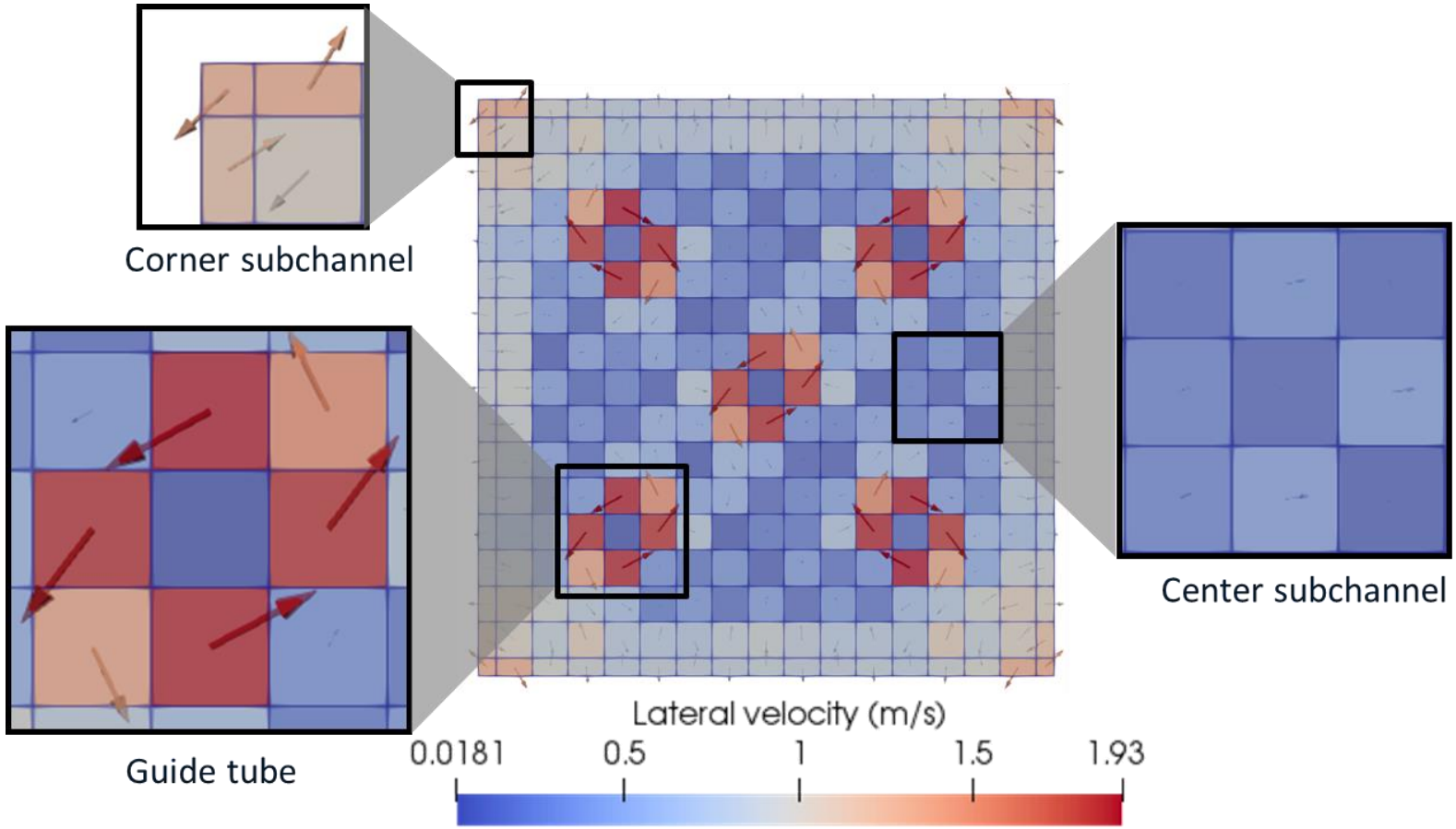

Figure 3.10 Liquid lateral velocity distribution at the mixing vane layer

3.2.2 Code-to-code Comparison between CUPID and CTF

From the simulation of APR1400 single assembly, the grid-directed cross flow model was verified for reproducing the coolant transfer and temperature distribution change due to mixing vanes. Afterwards, the code-to-code comparison of CUPID and CTF was progressed for quantitative comparison of the mixing vane model. First, the CUPID and CTF outlet temperature and the axial velocity were comparable within the error of 1 K and 0.2 m/s as illustrated in Fig. 3.11 (a) and (b). The temperature distribution, which was as large as 595 K~612 K before adding the mixing vane model, decreased as 600 K~606 K after the model implementation.

Next, the comparison of outlet centerline extraction was performed as shown in Fig. 3.12. For temperature, the CUPID calculation result was flatter than results from CTF, but CUPID and CTF had a similar distribution. The axial velocity distribution also could be comparable. The largest difference occurred at the near the guide tube.

In addition, the pressure drop generated by the spacer grid was considered. The heated section of APR1400 contains ten spacer grids, which consist of nine mixing vane-attached spacer grids and single non-mixing vane grid at the inlet. Since CTF could not simulate the spacer grid at the entrance section, nine spacer grids except the inlet supporting grid were simulated for code-to-code comparison. The calculation result is represented on Fig. 3.13. The additional pressure drop due to spacer grid was 161.72 kPa, and the code-to-code comparison showed similar pressure drop simulation of CUPID and CTF.

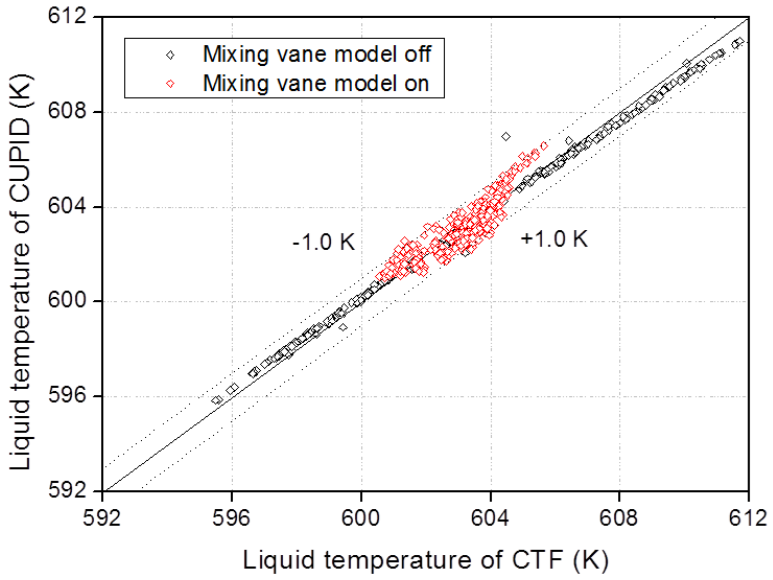

(a) Liquid temperature comparison between CUPID and CTF

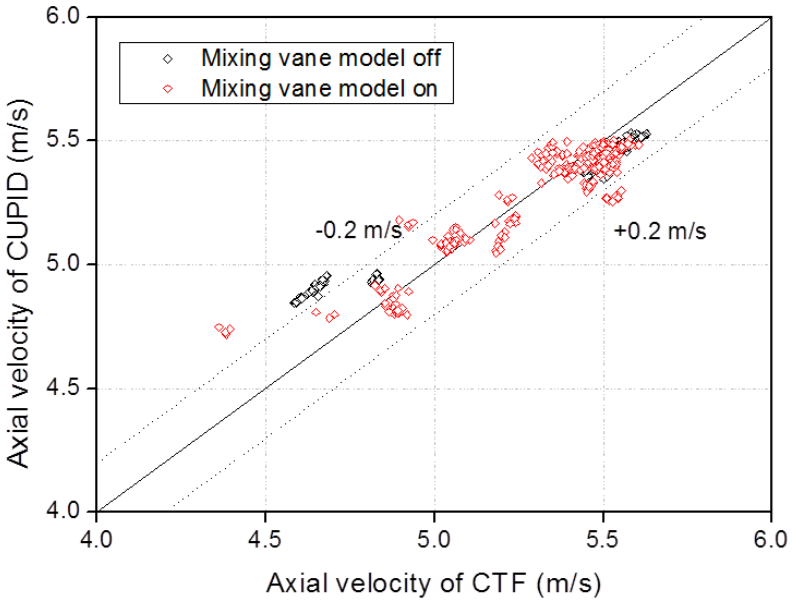

(b) Axial velocity comparison between CUPID and CTF

Figure 3.11 Code-to-code comparisons between CUPID and CTF at the outlet

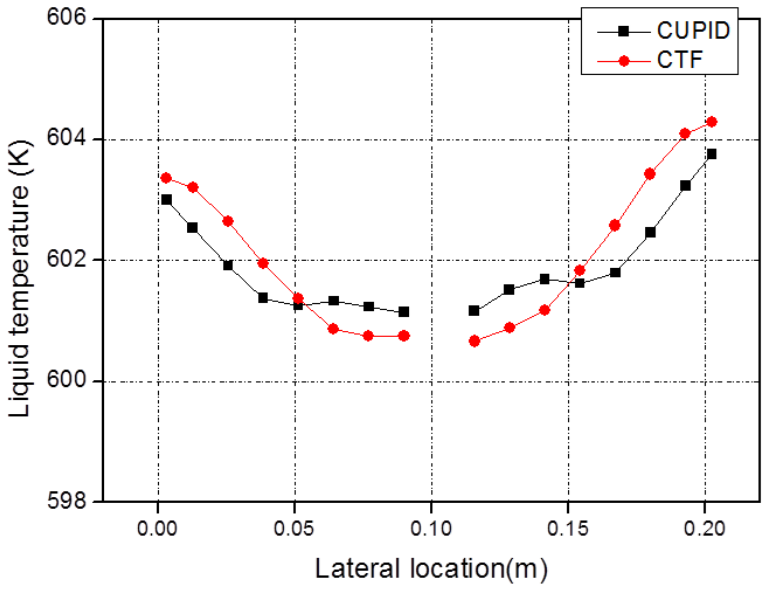

(a) Centerline liquid temperature comparison between CUPID and CTF

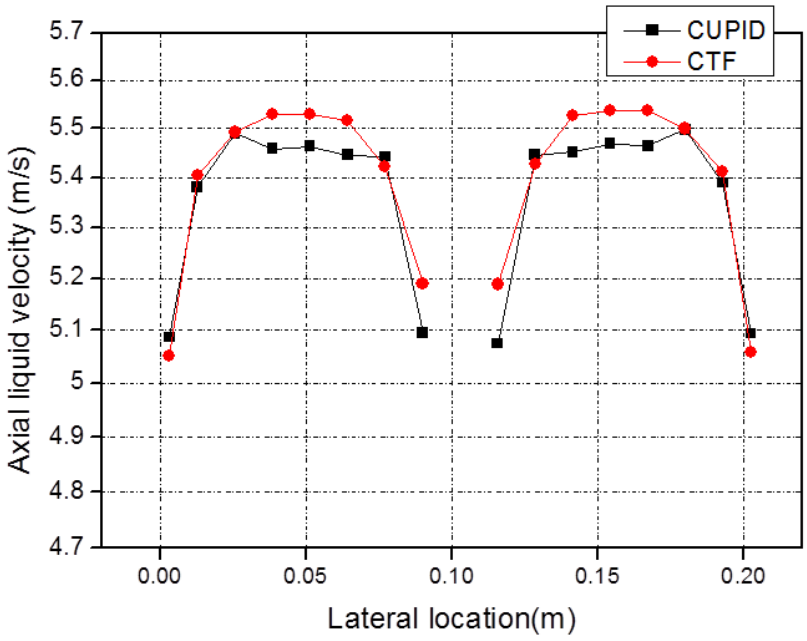

(b) Centerline axial velocity comparison between CUPID and CTF

Figure 3.12 Code-to-code comparisons between CUPID and CTF at the centerline of outlet

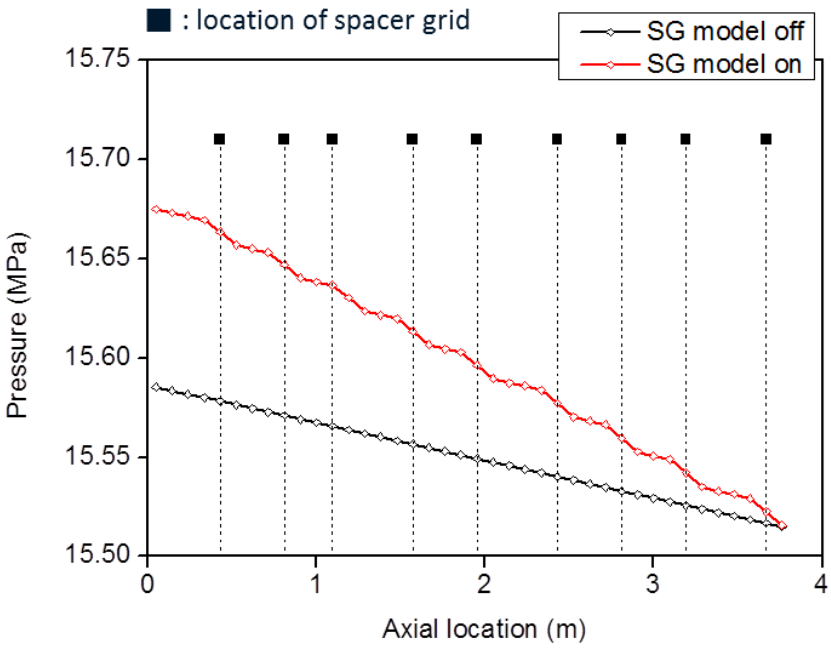

(a) CUPID axial pressure distribution using deactivated and activated spacer grid pressure drop model

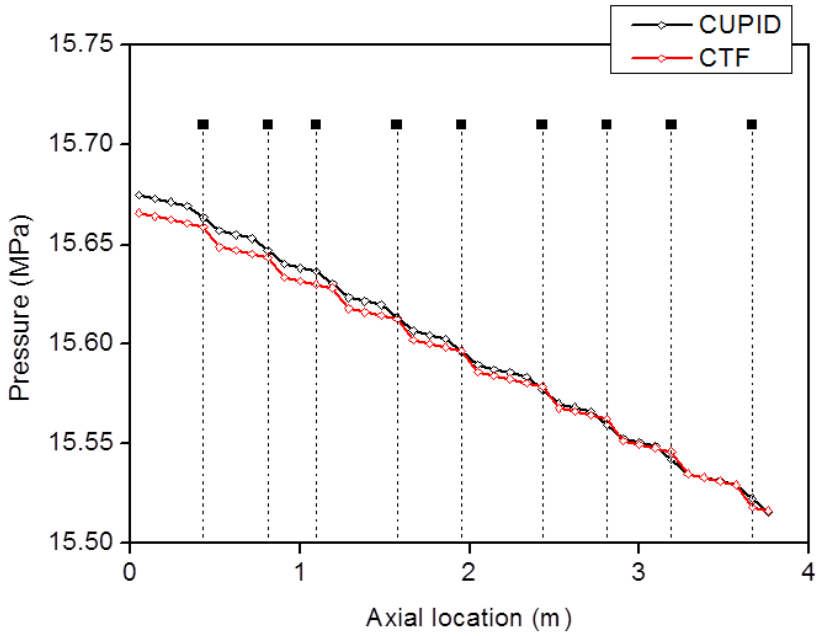

(b) Axial pressure comparison between CUPID and CTF

Figure 3.13 Axial pressure distribution

3.3 Verification of Fuel Rod Heat Conduction Model

By using the fuel rod heat conduction model, the variables related to fuel rod could be used including cladding surface temperature, pellet center temperature and entered power. The cladding surface and the coolant temperature increased as the flow approached to the outlet, but the maximum temperature was observed below the outlet due to the mixing vane and power distribution. The outlet cladding surface and the fluid temperatures are described in Fig. 3.14 (a) and (b). On the other hand, the pellet center temperature had a cosine shape similar with the power distribution, and Fig. 3.14 (c) and (d) compare the volumetric power and pellet center temperature at the center of the highest power.

Moreover, the circumstantial heat conduction among quarter fuel rods was progressed. For example, the difference of cladding surface temperature of the corner fuel rod in Fig. 3.15 is 0.66 K while the difference of pellet center temperature is 0.29 K. The temperature difference caused by the coolant temperature generally decreased at the inside of the pellet.

In addition the DNBR distribution using Biasi correlation and CE-1 correlation could be evaluated. After the implementation of the grid-directed cross flow model, the minimum DNBR increased in both cases. The minimum DNBR rose 3.43% using Biasi correlation, whereas 13.56% elevated using CE-1 correlation. The CE-1 correlation reproduced more conservative DNBR distribution than Biasi correlation.

For calculation of CHF, the hydraulic diameter or heated diameter was required as well as temperature and velocity information. The definition of hydraulic diameter was $4A/P_{wetted}$ and heated diameter was $4A/P_{heated}$. The

normal subchannel had same P_{wetted} which was the length of the wall and P_{heated} the length of the heated surface, but the lengths were different in the side, corner and near the guide tube. Particularly, the hydraulic diameter of corner subchannel was smaller than the normal subchannel whereas heated diameter was the same.

Because Biasi correlation is an equation for CHF calculation inside the heated round tube, the heated diameter and the hydraulic diameter are not distinguished. Therefore, although the coolant and cladding surface temperature of the corner subchannel were lower than that of the neighbor subchannels, DNBR increased due to small hydraulic diameter. On the other hand, when DNBR was calculated using the CE-1 correlation considering the heated diameter, DNBR decreased on account of higher temperature and low velocity since heated diameter was same. Fig. 3.16 illustrates the location of the minimum DNBR simulated by each correlation. Because the power distribution was the axially cosine shape, the minimum DNBR occurred at the middle of the test section; the cladding surface temperature continuously increased after the location of the minimum DNBR.

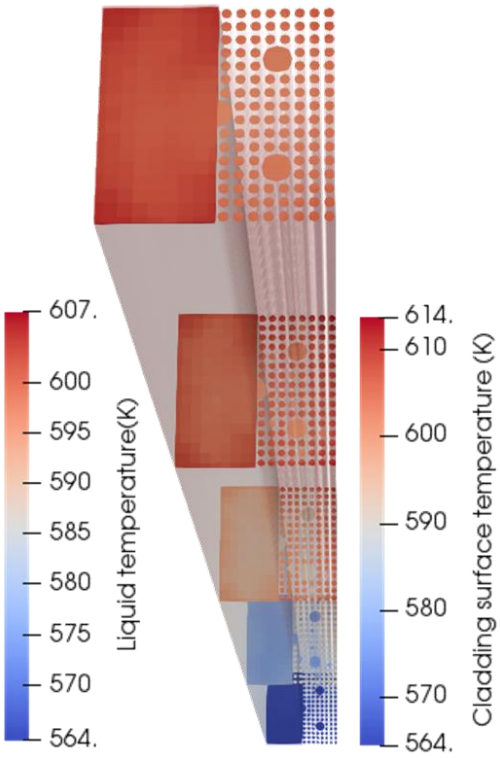

(a) Distribution of liquid and cladding surface temperature

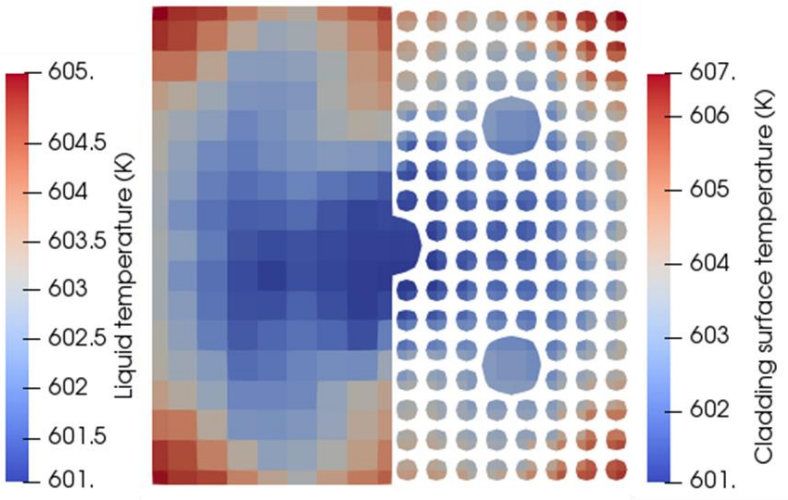

(b) Distribution of outlet liquid and cladding surface distribution

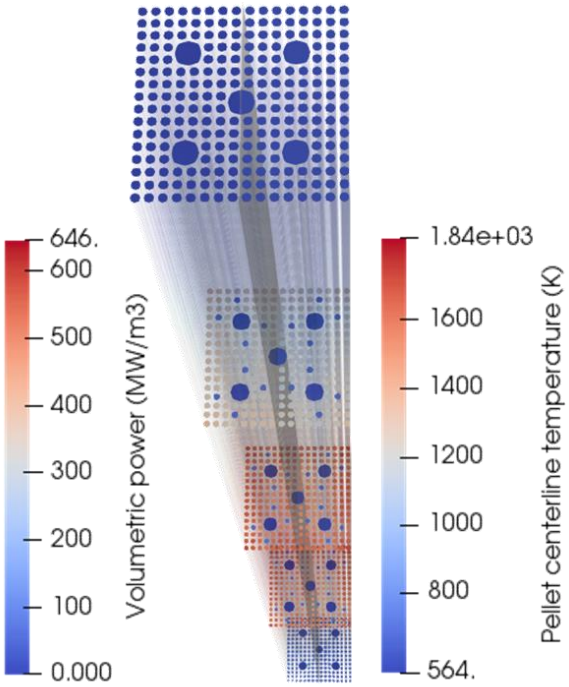

(c) Distribution of volumetric power and pellet centerline temperature

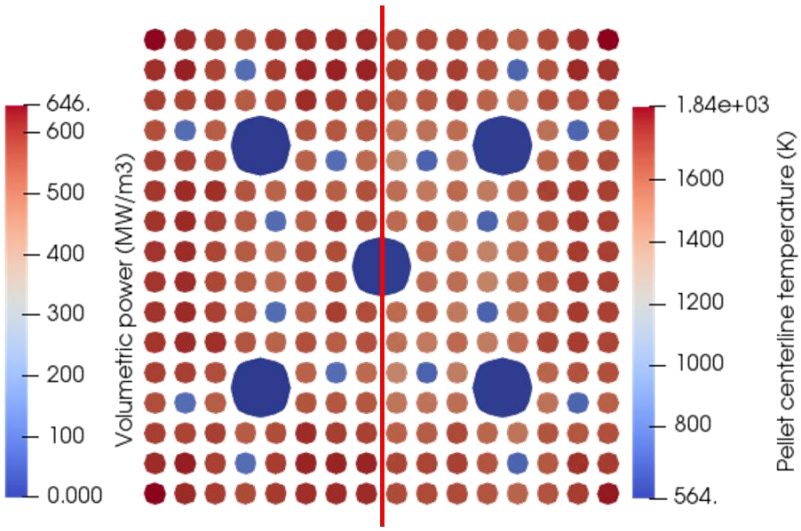

(d) Distribution of volumetric power and pellet centerline temperature at the largest volumetric heat source

Figure 3.14 Simulation result of single assembly

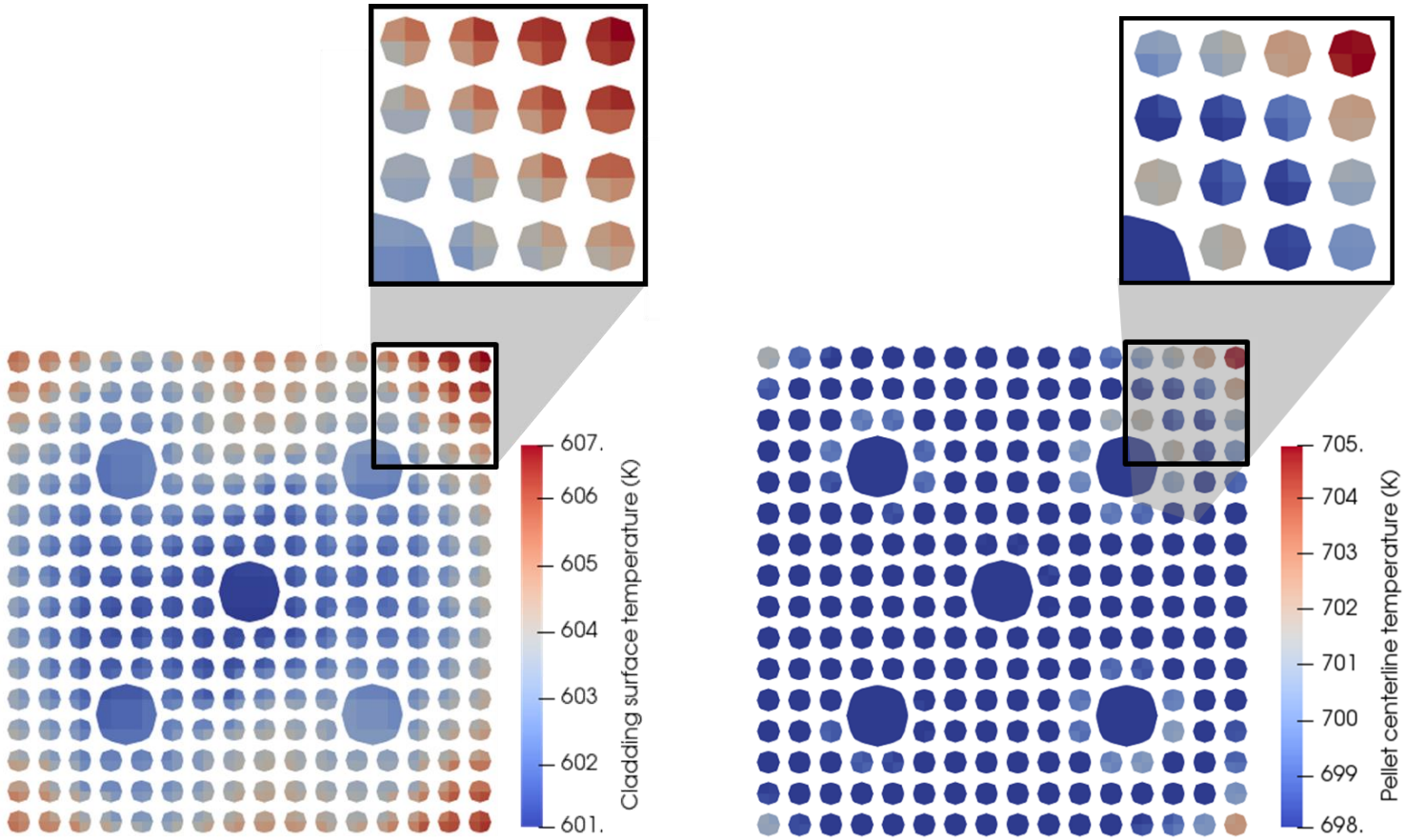

Figure 3.15 Distribution of outlet cladding surface and pellet centerline temperature

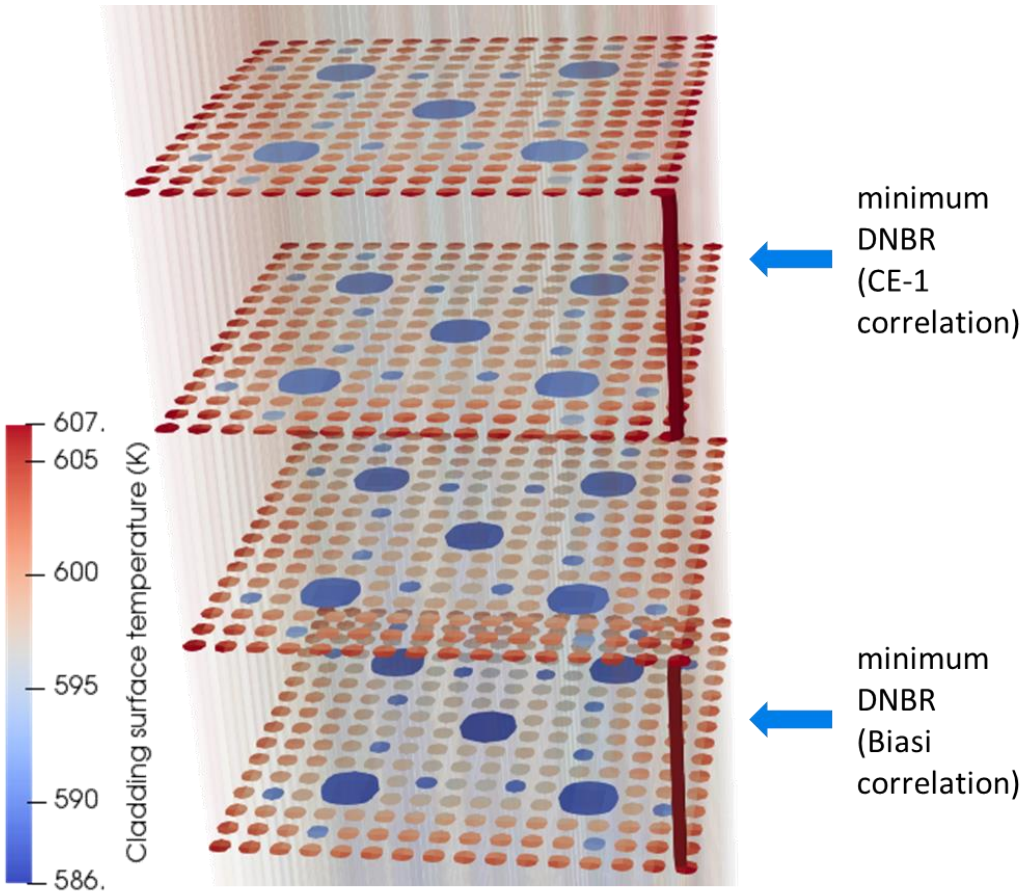

Figure 3.16 Location of minimum DNBR and cladding surface temperature

Chapter 4

Simulation of APR1400 Whole Core with Implemented Models

4.1 Simulation of APR1400 Whole Core

After the preliminary calculation for the single assembly, the APR1400 whole core was simulated. For the simulation, the generation of mesh was performed using open form mesh generation tool SALOME (Ribes and Caremoli, 2017). The whole core consists of 241 fuel assemblies, which are the CE type 16x16 assembly contained five guide tubes. Same as the single assembly simulation, the heated section of whole core was uniformly divided into 40 sessions, and the ghost cells were added on above of the outlet. The number of the fluid cells was 3,226,577 (17x17x41x241 + water gap) and the number of the solid cells was 202,362,880 (16x16x4x20x41x241).

4.1.1 Whole Core Modeling for Subchannel Scale Analysis using CUPID

The major difference between the APR1400 simulation of the single assembly and the whole core was existence of the water gap. For the single assembly simulation, water gaps were not considered, and the corner or side subchannel

faced the adiabatic wall. For the whole core simulation, on the other hand, the water gap between assemblies was modeled. It induced the smaller friction at the corner or side subchannel of the whole core simulation than the single assembly result. Furthermore, in the outer assembly, the shroud was added to simulate the friction with the wall.

For simulation, the 13 subchannel types were established which contain normal subchannel such as corner, side and center subchannel, guide tube, water gap and near the shroud. The subchannel type was same as the previous study (Yoon, 2018). The physical information such as porosity, permeability and hydraulic diameter was different depending on the type, and especially the porosity of the guide tube center subchannel was extremely reduced.

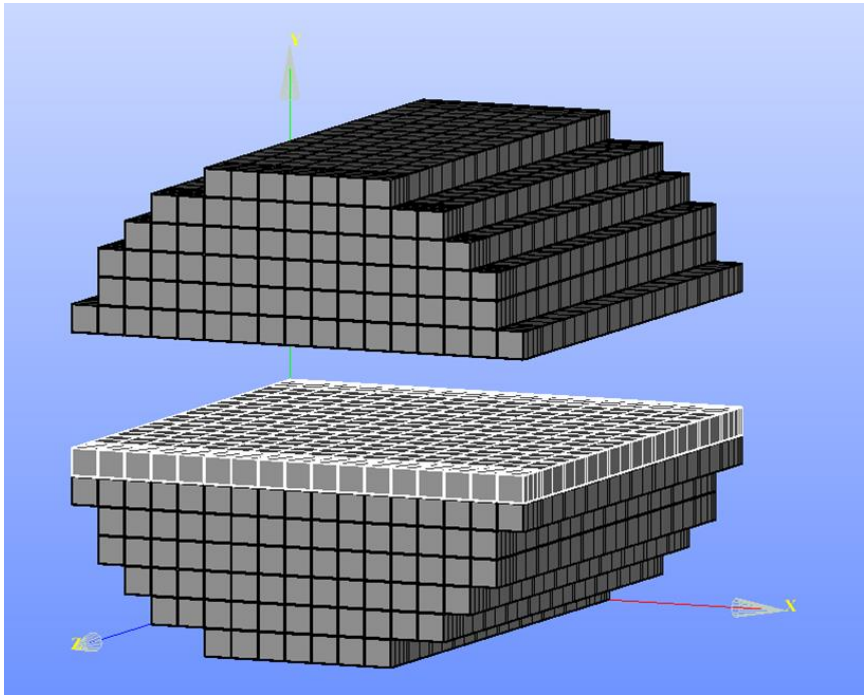

Figure 4.1 Generated mesh using SALOME

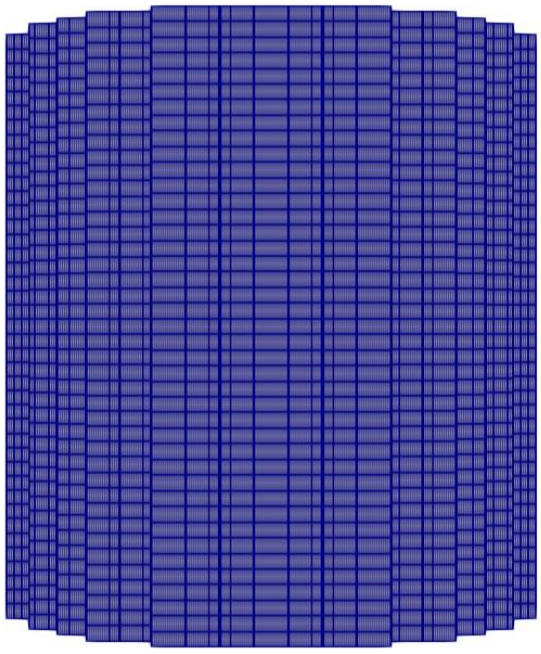

Figure 4.2 Axial distribution of whole core mesh

4.1.2 Implementation of Power Distribution from nTRACER

The axially non-uniform power distribution from nTRACER was implemented for the APR1400 whole core simulation same as single assembly calculation. nTRACER calculation result had information about quarter core instead of the entire core, so it was symmetrically applied on the opposite sides of the reflective boundary. The implemented power distribution could be visualized as shown in Fig. 4.3.

In spite of the quarter fuel rods had the same power, the difference of coolant temperature and velocity induced the different cladding surface and DNBR. Power was not applied to the guide tube, water gaps and near the shrouds channels. The coolant transfer was prevented from surrounding to the center subchannel of guide tube unlike the water gap or near the shroud. The total applied power for whole core analysis in hot full power condition of APR1400 was 3,983 MW, which was the same as the power given in the final safety analysis report of APR1400 of Shin Kori Units 3 and 4.

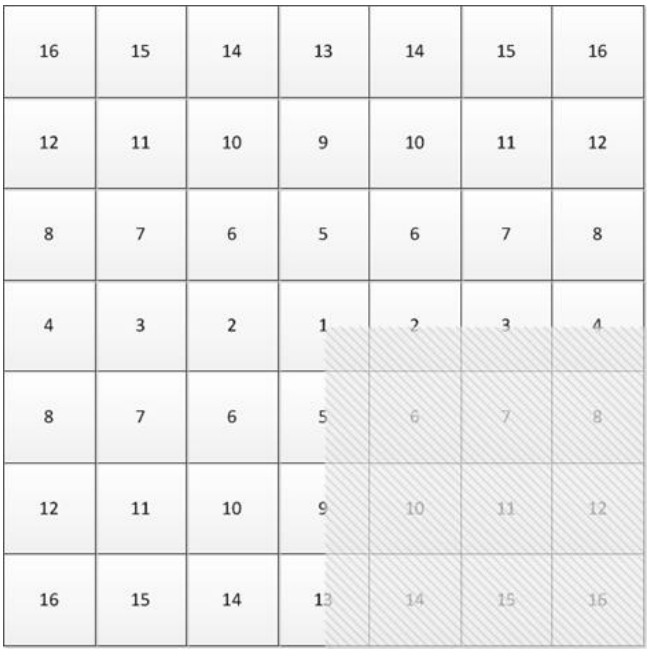

(a) Original power distribution of nTRACER

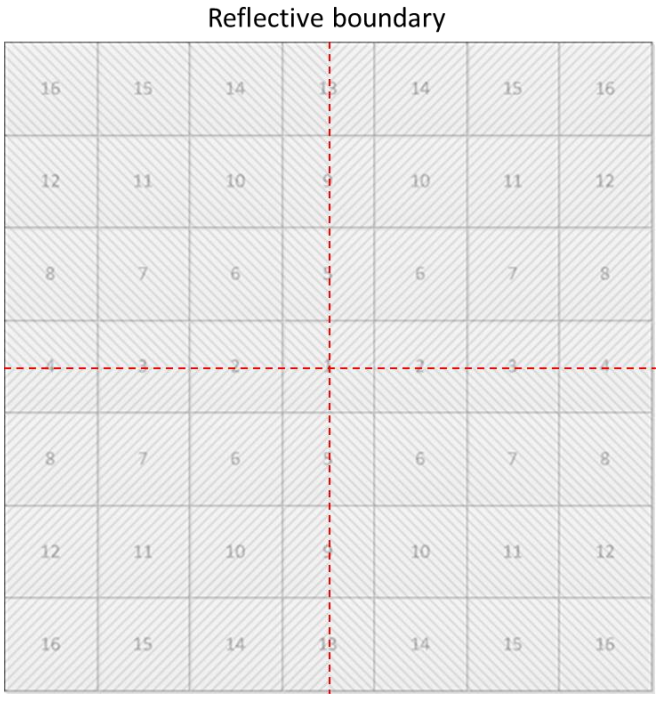

(b) Implemented power distribution into CUPID

Figure 4.3 Example of power implementation

4.1.3 Improvement of CUPID Parallel Processing Method

Despite the single assembly could be calculated using a few cores in a Windows environment, the simulation of APR1400 required higher computing power in cluster. This is because the APR1400 mesh includes 241 assemblies as well as additional computing cells such as water gap and the near the shroud. The fuel rod heat conduction model requires significantly large memory due to the additional analysis of 202 million solid cells. So, the CUPID parallel processing method was developed into a more efficient calculation.

For the simulation using multi-core processor, the calculation domain was divided into each processor. Afterward, the information of the entire geometry was saved on the temporary array and distributed among the processor. Before the modification of memory handling method, the all processor received the necessary information from the each temporary array as illustrated in Fig. 4.4 (a). By contrast, only master rank allocated the temporary array including data of geometry after the improvement. The slave ranks received data from the master rank instead of their own temporary array; it makes the slave ranks could save the memory as shown in Fig. 4.4 (b). In this way, effective memory management becomes possible by using the modified memory handling method. CUPID already had an option to use the method, but the option could not be activated to the porous media method used for subchannel scale analysis. So, the source code was modified to apply this method for subchannel scale thermal hydraulic analysis, and decreased the memory usage.

After using the modified memory handling method, the limitation in core usage, in the cluster of the present study, was overcome. The Intel (R) Xeon (R) CPU E5-2660 v2 and Intel (R) Xeon (R) CPU E5-2680 v4 were used for the

calculation and the problem time was 1.5 seconds to reach steady state condition. The calculation wall clock time depending on core usage is described in Fig. 4.5, and the simulation time was reduced to 59 minutes with 136 cores. The MPI domain decomposition was used to automatically distribute computing cells to each processor for the whole core simulation. Using 136 processors, each processor calculated average 23,724 fluid cells and the maximum difference of the number of allocated fluid cells was 33. The evenly distributed computational domain by MPI domain decomposition is illustrated in Fig. 4.6.

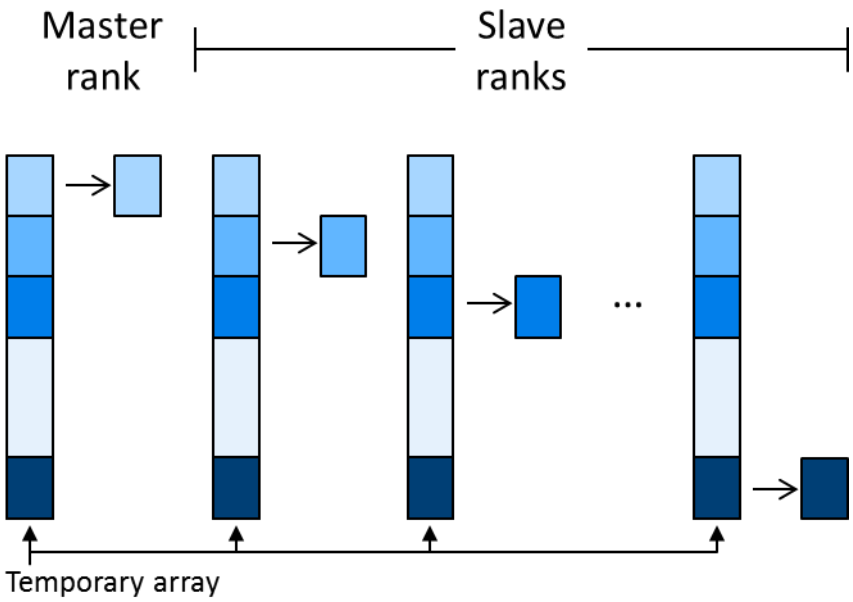

(a) Memory handling method before modification

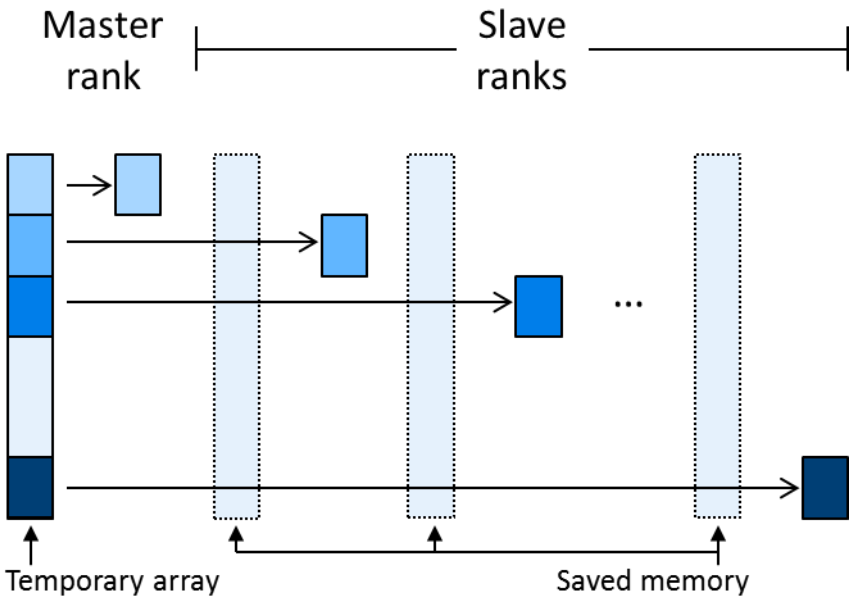

(b) Memory handling method after modification

Figure 4.4 Schematic draw of memory handling method

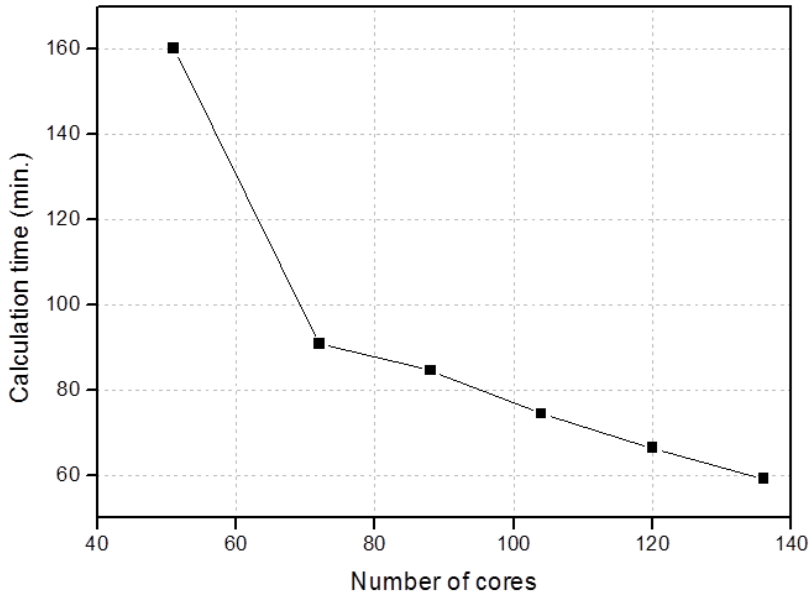

Figure 4.5 Wall-clock calculation time against number of cores

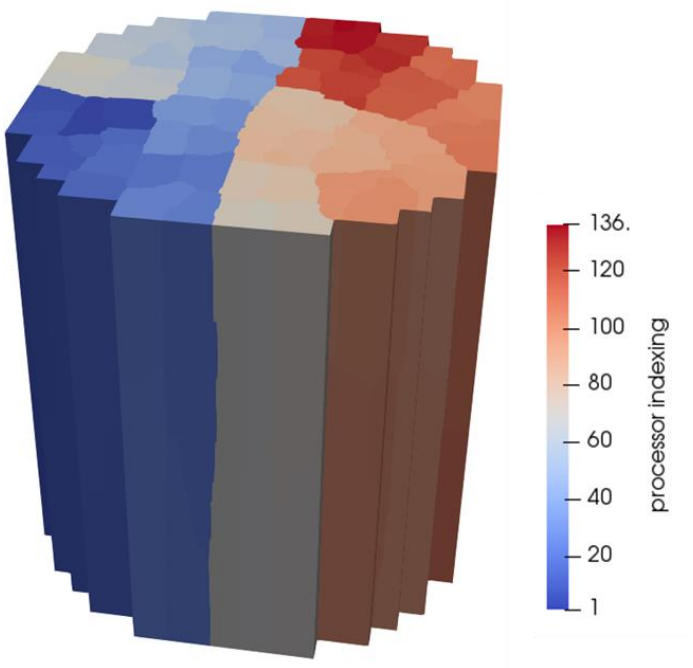

Figure 4.6 Processor indexing

4.2 Verification of Grid-directed Cross Flow Model

The whole core simulation of APR1400 was progressed using a grid-directed cross flow model, a model to simulate fluid transfer induced by mixing vanes. The code-to-code comparison between CUPID and CTF was progressed using the mixing vane model by the single assembly simulation. The grid-directed cross flow model was implemented to scalar equations as well as the momentum equation, and the turbulent mixing coefficient β was replaced by $\beta_{\mathrm{default}} + \beta'$. The single assembly simulation, which was performed by using β_{default} as 0.005, was extended to whole core. According to the previous study, the range of β_{default} was 0.005 to 0.05 (Yoon et al., 2018). Since the actual experimental data were not usable, the minimum and maximum values of β_{default} was suggested for the APR1400 core simulation.

First, the effect of grid-directed cross flow model to coolant temperature distribution was observed. When the mixing vane model was deactivated, the temperature distributions were dominantly influenced by the turbulent mixing coefficient β_{default}. Fig. 4.7 describes the significantly flattened coolant temperature distribution when β_{default} was 0.05 than 0.005. On the other hand, when the model was activated, the liquid temperature distribution was flatten even the 0.005 β_{default} was used. The vane-induced coolant mixing decreases the difference of fluid temperature as illustrated in Fig. 4.8.

Next, the lateral velocity distribution of the coolant at the mixing vane layer was investigated. Contrary to the temperature distribution, the lateral velocity was not significantly affected by the β_{default}. When the grid-directed cross flow model was deactivated, the lateral velocity was small as 0.03 m/s regardless of

the $\beta_{default}$ as illustrated in Fig. 4.9. Whereas when the model was activated, the lateral velocity was high as 2.24 m/s. Fig. 4.10 depict the asymmetrical fluid transfer due to the guide tube effect of mixing vane.

The axial fluid velocity was more affected by the physical information such as porosity and hydraulic diameter than mixing vane model. Fig. 4.11 shows the axial velocity of single assembly simulation and Fig. 4.12 describes the axial velocity of the assembly 23, the location of entered power into single assembly simulation. In the single assembly calculation result, flow velocity was slow at the corner subchannel where the hydraulic diameter was relatively small; whereas the velocity was fast at the corner and water gap because of the high porosity and hydraulic diameter in the whole core simulation. In addition, in both of the single assembly and whole core simulation, it could be found that the axial coolant velocities were low at the guide tube where the porosity was exceptionally small.

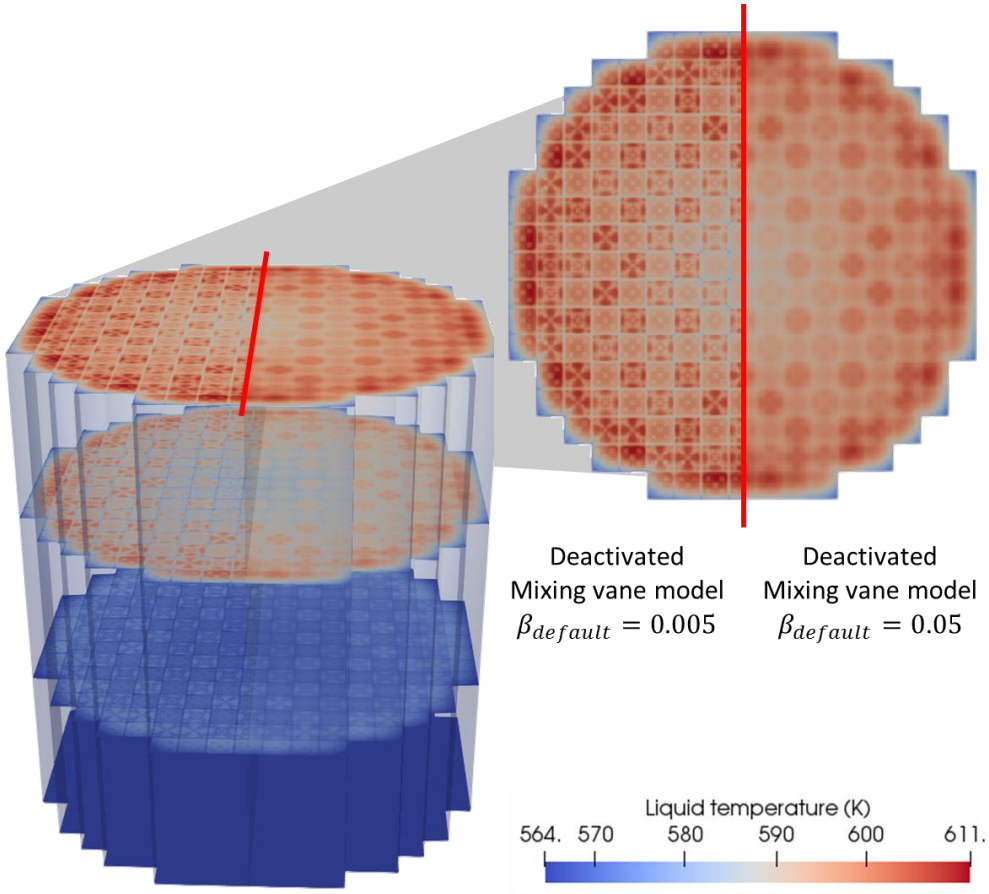

Figure 4.7 Liquid temperature distribution without mixing vane model

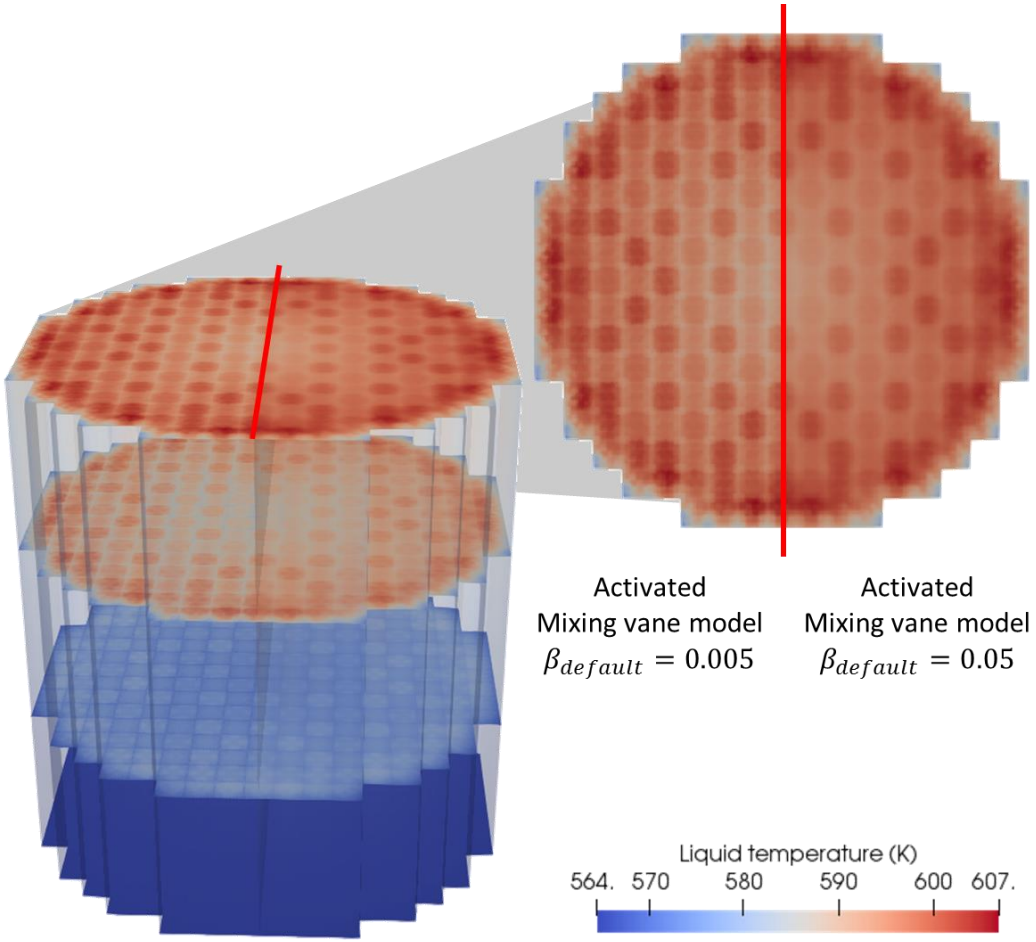

Figure 4.8 Liquid temperature distribution with mixing vane model

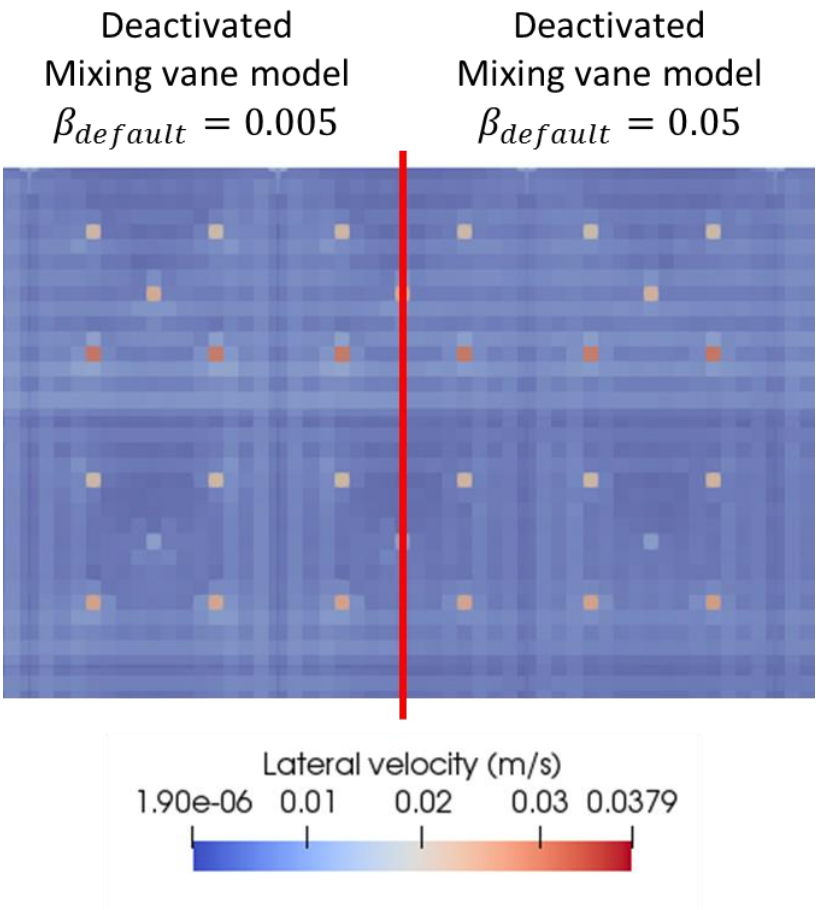

Figure 4.9 Lateral velocity distribution without mixing vane model

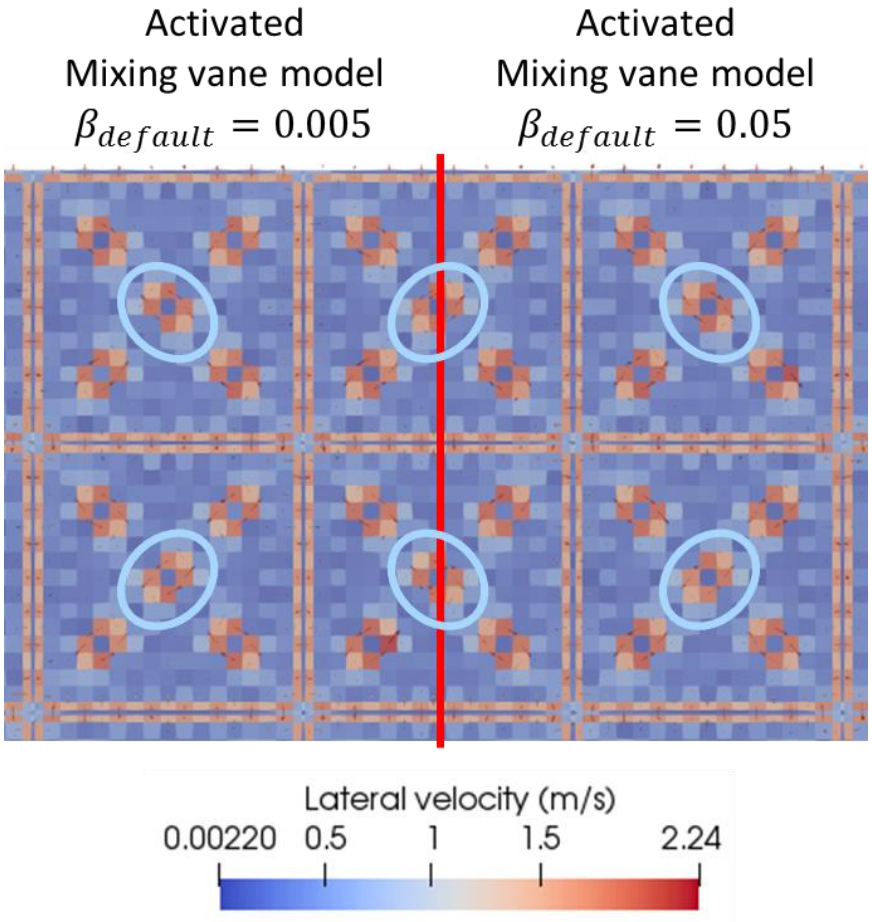

Figure 4.10 Lateral velocity distribution with mixing vane model

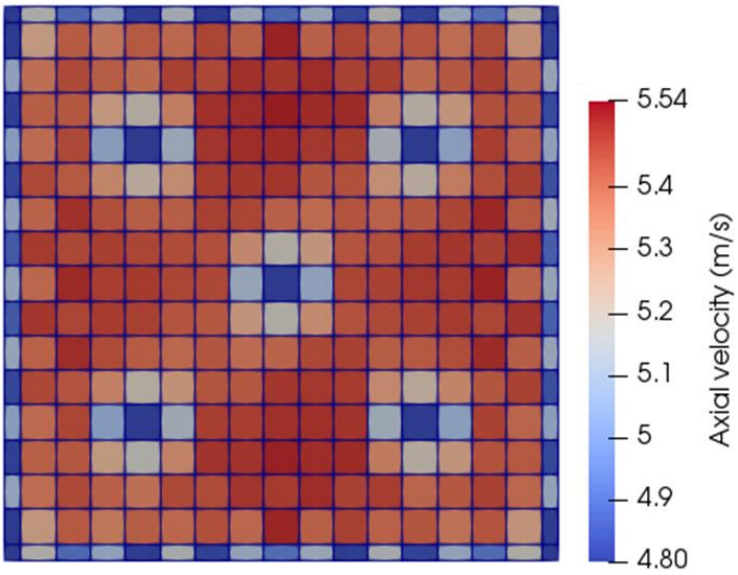

Figure 4.11 Axial velocity distribution of single assembly

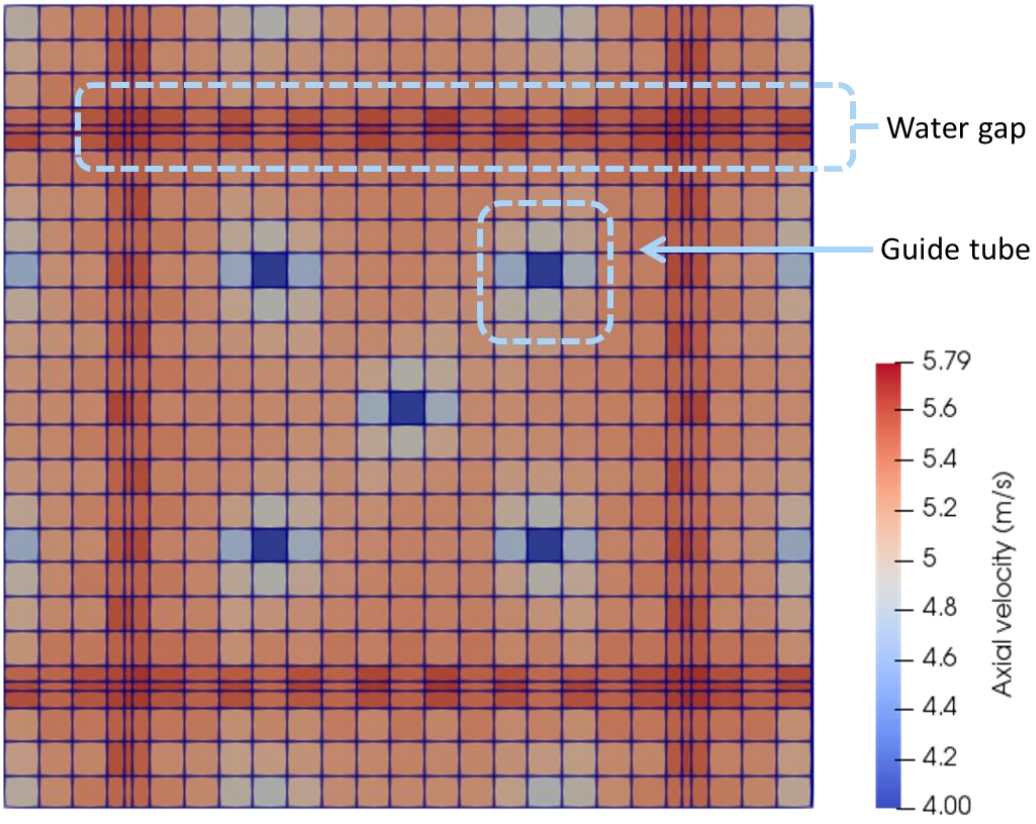

Figure 4.12 Axial velocity distribution of APR1400 simulation (assembly 23)

4.3 Verification of Fuel Rod Heat Conduction Model

The fuel rod heat conduction model was applied for APR1400 whole core simulation. The power distribution, cladding surface temperature and coolant temperature distribution are shown in Fig. 4.13. Reactor power had cosine shape, which is the highest at the middle point, and liquid and cladding temperature gradually increased as it got closer to the outlet Fig. 4.14 shows the cladding surface temperature distribution of single assembly simulation and whole core simulation at assembly 23. In the whole core simulation, the temperature was reduced by the fluid exchange with surrounding assemblies through the water gap.

Next, the comparison DNBR distribution and minimum DNBR was conducted between single assembly simulation result and the assembly 23 of whole core simulation under the same power condition. As shown in Fig. 4.15, the location of minimum DNBR of single assembly and APR1400 whole core are respectively center and corner subchannel when CHF calculated by Biasi correlation. This result was physically unacceptable because the temperature was lower and velocity was higher in the corner subchannel of the whole core simulation. This is because Biasi correlation used hydraulic diameter instead of heated diameter for CHF calculation. In the corner subchannel, the hydraulic diameter of single assembly was small because this channel faced the adiabatic wall, whereas hydraulic diameter was large in the whole core simulation which had water gaps. Since Biasi correlation computed low CHF when the hydraulic diameter was large, the minimum DNBR of whole core simulation was occurred at the corner subchannel; physically inaccurate result.

To calculation, on the other hand, the CE-1 correlation used heated diameter

which was same at the corner subchannel of single assembly simulation and whole core simulation. Therefore, the minimum DNBR was located on the corner subchannel due to low coolant speed and high temperature. In contrast, the whole core DNBR was higher at the corner subchannel than near subchannel where had higher velocity and lower temperature. The minimum DNBR calculated by CE-1 model increased by 16.81%. Fig. 4.16 shows distribution of DNBR using each correlation. The hydraulic and heated diameters of each simulation and minimum DNBR were summarized in Table 4.1. These results explained the importance of choosing the CHF correlation which is optimized on simulation geometry.

In addition, cladding surface temperature and fuel rod center line temperature could be influenced by the mixing vane. The cladding surface and the pellet center temperature are described in Fig. 4.17. The outlet cladding surface temperature in the assembly 23 was reduced from 607.96 K to 601.74 K, and the outlet pellet center temperature decreased from 723.52 K to 719.38 K due to mixing vane.

Table 4.1 Minimum DNBR depending on CHF correlation by hydraulic and heated diameter

	Simulation of single assembly	Simulation of APR1400 whole core (Assembly 23)
Hydraulic diameter of corner subchannel (mm)	4.641	12.637
Heated diameter of corner subchannel (mm)	12.637	12.637
Minimum DNBR (by Biasi correlation)	2.41	2.20 (corner subchannel)
Minimum DNBR (by CE-1 correlation)	2.26 (corner subchannel)	2.58

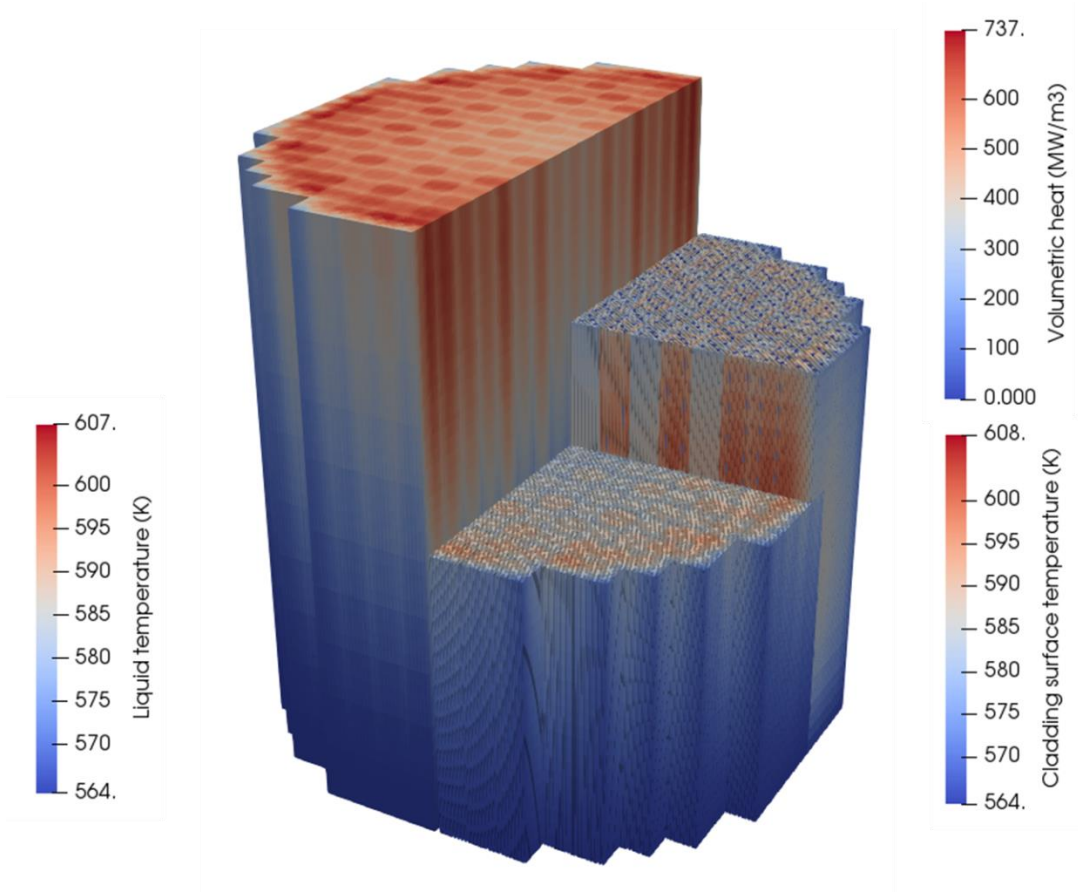

Figure 4.13 Simulation results of APR1400 whole core

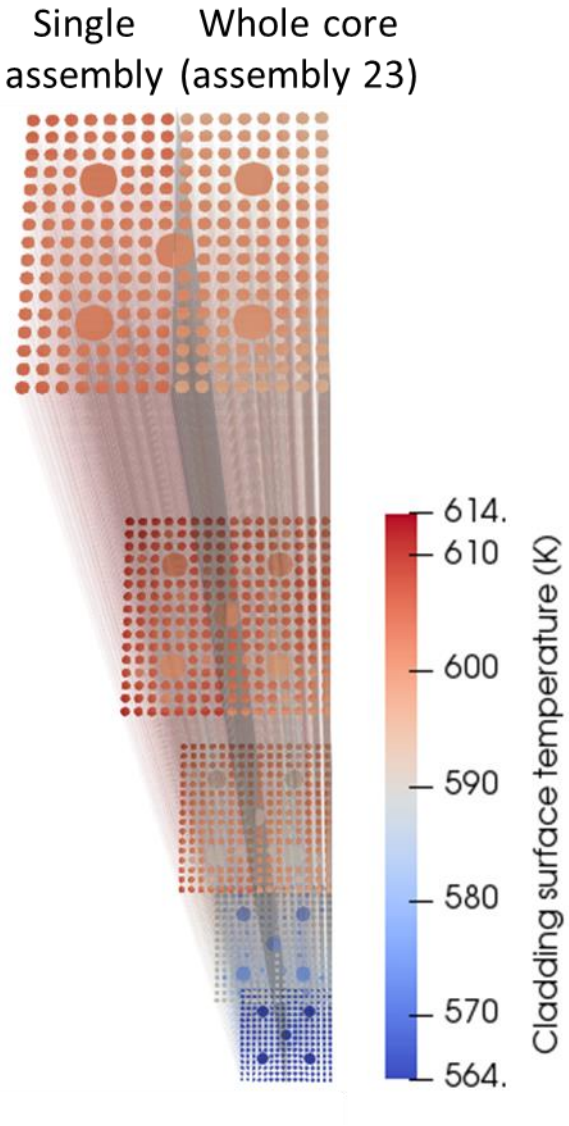

Figure 4.14 Cladding surface temperature distribution of whole core simulation and single assembly

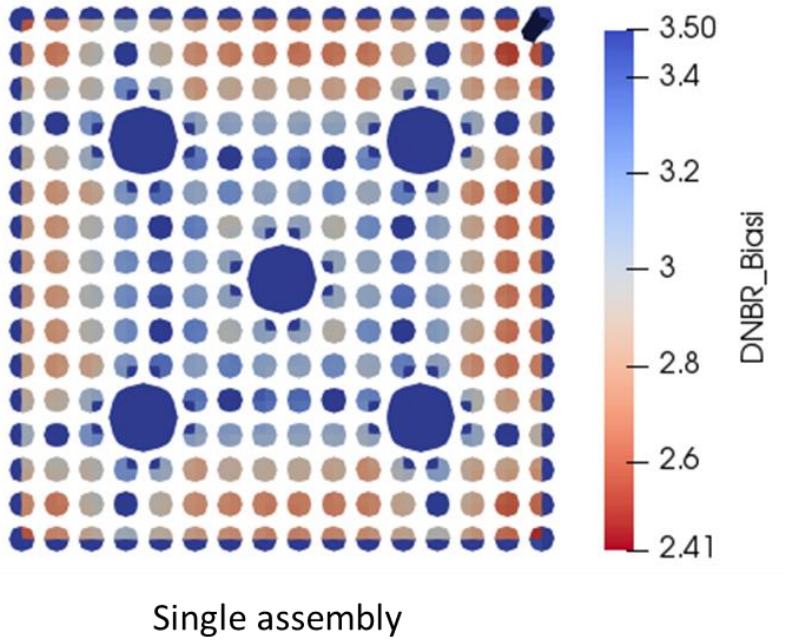

(a) DNBR distribution of single assembly using Biasi correlation

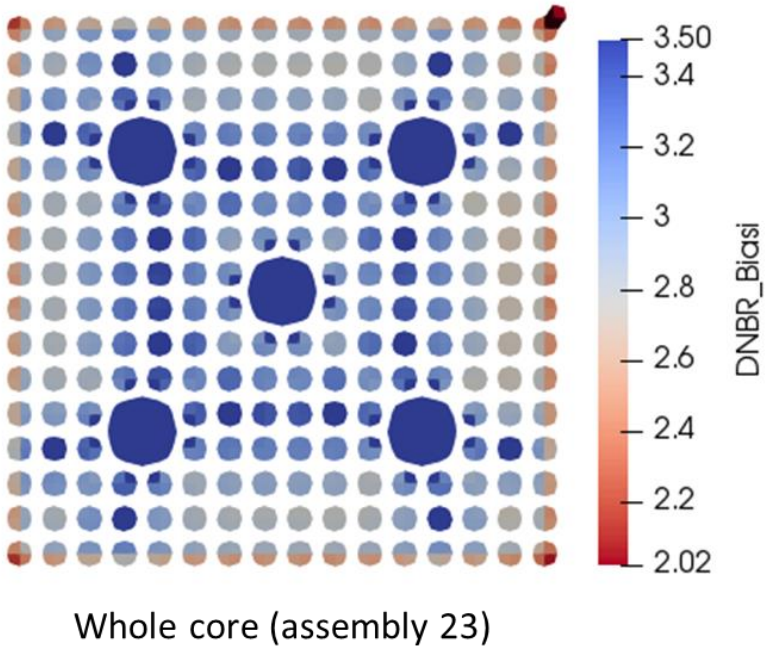

(b) DNBR distribution of whole core using Biasi correlation

Figure 4.15 DNBR distribution and minimum DNBR using Biasi correlation

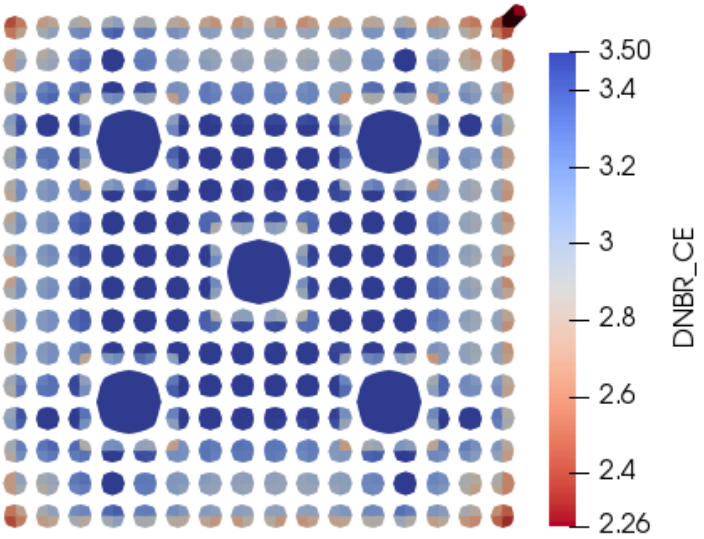

(a) DNBR distribution of single assembly using CE-1 correlation

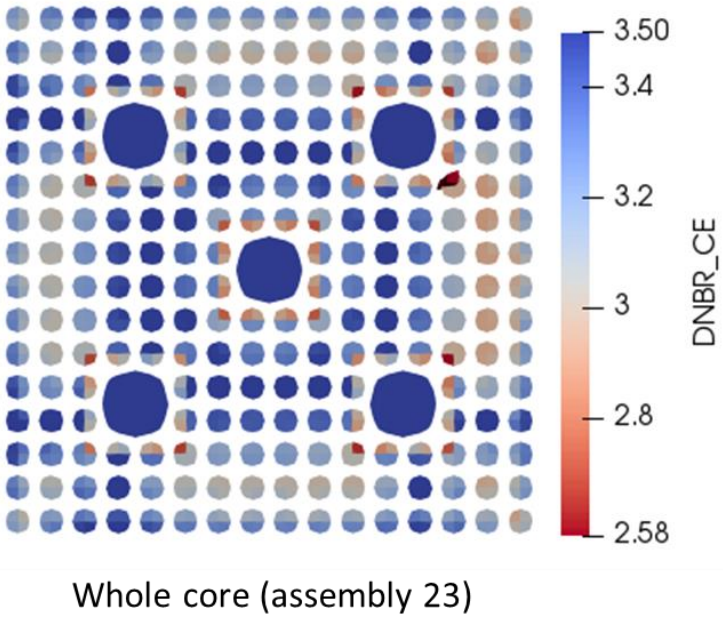

(b) DNBR distribution of whole core using CE-1 correlation

Figure 4.16 DNBR distribution and minimum DNBR using CE-1 correlation

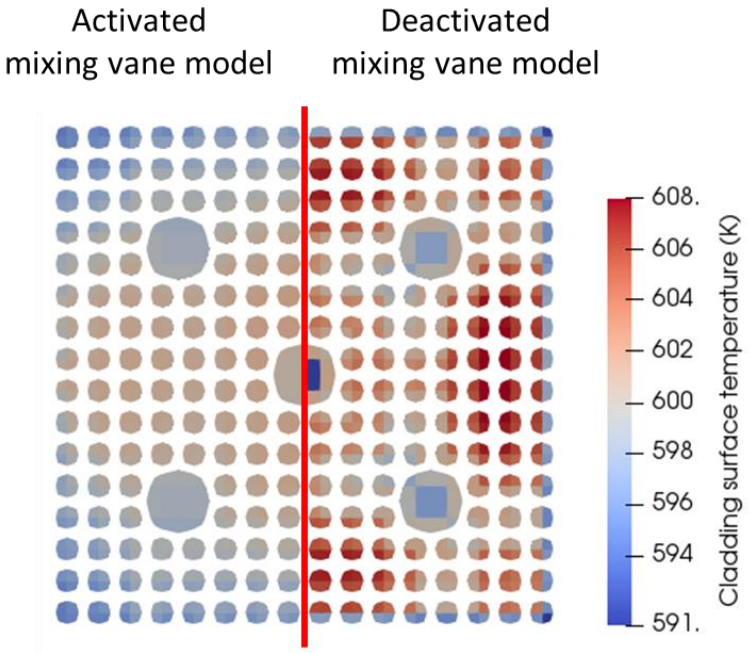

(a) Distribution of cladding surface temperature depending on mixing vane model

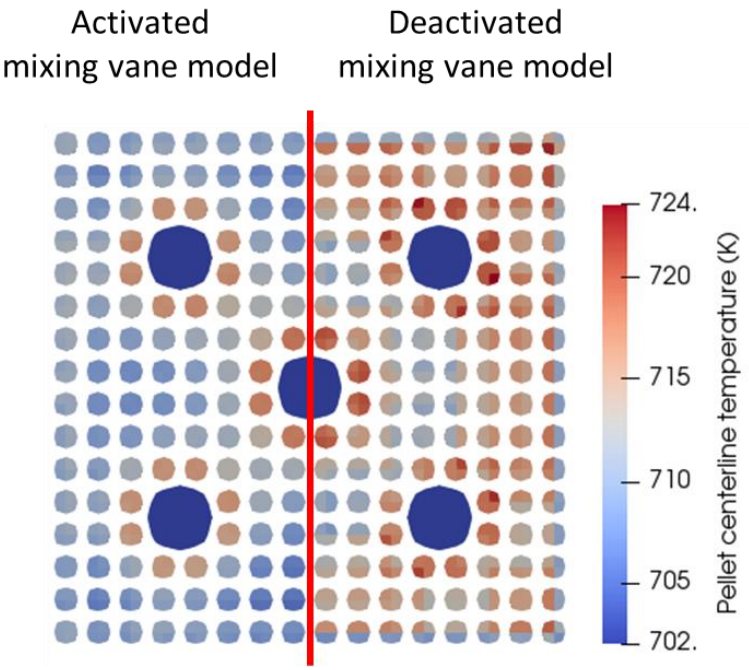

(b) Distribution of pellet centerline temperature depending on mixing vane model

Figure 4.17 Mixing vane effect on outlet cladding and pellet centerline temperature

Chapter 5

Conclusions

5.1 Summary

In the present study, the improvement of subchannel scale analysis capability of CUPID with grid-directed cross flow and fuel rod model was progressed. For the more realistic calculation, vane-induced coolant transfer should be simulated. The subchannel scale thermal hydraulic analysis code CTF used grid-directed cross flow model to simulate the cross flow caused by mixing vane. Since CUPID uses collocated grid while CTF uses staggered grid, the grid-directed cross flow model needed to be modified for applying on CUPID. The modifications of model are as follow: the additional implementation of model into scalar equation and the additional turbulent mixing coefficient β'. Afterward, the effect of the guide tubes was considered and the pressure drop caused by spacer grid was modeled.

Meanwhile, the improvement of fuel rod heat conduction model was conducted. The default one-dimensional heat conduction model was modified. Since the single fuel rod faces four subchannels which have relatively different temperature and velocity, the fuel rod divided into four sections. In addition, the circumstantial heat conduction among the quarter rods was considered. The CHF model was implemented and the DNBR distribution was investigated.

After the implementation of model, the verification of models against the

single assembly of APR1400 was progressed. Because the experimental data of reactor core were inaccessible, the code-to-code comparison between CUPID and CTF was conducted. The simulation results from CUPID and CTF were comparable.

Moreover, the whole core of APR1400 with implemented models was simulated. Power distribution was applied from the neutronics code, nTRACER. For multi-core simulation, the CUPID parallel processing method was improved. The simulation result of APR1400 whole core shows the effect of grid-directed cross flow model and the fuel rod heat conduction model. From this, the capability of the subchannel scale analysis using CUPID by considering the effect of the mixing vane and the fuel rod heat conduction was improved, and the basis for the subchannel scale analysis of accident condition was established.

5.2 Future Recommendations

In this study, the subchannel scale analysis capability of CUPID with grid-directed cross flow model and fuel rod model was improved. For this improvement, the simulations were performed for single assembly of APR1400 and whole core. Since the simulation and experiment result about reactor core is inaccessible, the code-to-code comparison was performed between CUPID and CTF, which is the subchannel scale thermal analysis code.

Thus, for the additional validation of grid-directed cross flow model, quantitative validation against experimental data and plant data are required. In

addition to calculate more accurate pellet center temperature using fuel rod heat conduction model, the gap model needed to be improved considering deformation of fuel rod and the changes in material properties.

References

Avramova, M. N., Development of an innovative spacer grid model utilizing computational fluid dynamics within a subchannel analysis tool, PhD thesis, Pennsylvania State University, 2007.

Avramova, M. N., & Salko, R. K., *CTF Theory Manual* (No. ORNL/TM--2016/430), Oak Ridge National Laboratory (ORNL), 2016.

Aybar, H. S., & Ortego, P., A review of nuclear fuel performance codes, *Progress in Nuclear Energy*, 46(2), 127-141, 2005.

Biasi, L., Clerici, G. C., Garribba, S., Sala, R., & Tozzi, A., *Studies on Burnout. Part 3, A New Correlation for Round Ducts and Uniform Heating and Its Comparison with World Data*, ARS SpA, Milan. Univ., Milan, 1967.

Blyth, T. S., *Improvement of COBRA-TF Subchannel Thermal-Hydraulics Code (CTF) Using Computational Fluid Dynamics*, CASL Technical Report, CASL-U-2015-0020-000, 2015.

Blyth, T. S., *Development and Implementation of CFD-Informed Models for the Advanced Subchannel Code CTF*, The Pennsylvania State University, 2017.

Chang, S. K., Kim, S., & Song, C. H., Turbulent mixing in a rod bundle with vaned spacer grids: OECD/NEA–KAERI CFD benchmark exercise test, *Nuclear*

Engineering and Design, 279, 19-36, 2014.

Chung, B. D., Kim, K. D., Bae, S. W., Jeong, J. J., Lee, S. W., Hwang, M. K., & Yoon, C., *MARS code manual volume I: code structure, system models, and solution methods* (No. KAERI/TR--2812/2004), Korea Atomic Energy Research Institute, 2010.

Daeubler, M., Trost, N., Jimenez, J., Sanchez, V., Stieglitz, R., & Macian-Juan, R., Static and transient pin-by-pin simulations of a full PWR core with the extended coupled code system DYNSUB, *Annals of Nuclear Energy*, 84, 31-44, 2015.

Gensler, A., Schmidt, A., Kuehnel, K., & Wehle, F., LWR core safety analysis with Areva's 3-dimensional methods, *Atw. Internationale Zeitschrift fuer Kernenergie*, 59(2), 82-88, 2013.

Jung, Y. S., Shim, C. B., Lim, C. H., & Joo, H. G., Practical numerical reactor employing direct whole core neutron transport and subchannel thermal/hydraulic solvers, *Annals of Nuclear Energy*, 62, 357-374, 2013

Kawahara, A., Sadatomi, M., Hirakata, Y., & Endo, M., Hydrodynamic effects of mixing vane attached to grid spacer on two-phase annular flows, *Nuclear Engineering and Design*, 310, 648-655, 2016.

Kim, H. C., Lee, Y. J., & Han, S. H., Assessment of the Effects on PCT Evaluation

of Enhanced Fuel Model Facilitated by Coupling the MARS Code with the FRAPTRAN Code, Proceedings of the KNS 2016 Autumn Meeting, 2016.

Kwon, H., *Validation of a Subchannel Analysis Code MATRA Version 1.1.*, KAERI/TR-5581/2014, KAERI, 2014.

Li, X., & Gao, Y., Methods of simulating large-scale rod bundle and application to a 17 × 17 fuel assembly with mixing vane spacer grid, *Nuclear Engineering and Design*, 267, 10-22, 2014.

NRC, U.S., "50.46 Acceptance criteria for emergency core cooling systems for light-water nuclear power reactors", https://www.nrc.gov/reading-rm/doc-collections/cfr/part050/part050-0046.html, accessed July 30, 2018

NRC, U.S., Technical and Regulatory Basis for the Reactivity-initiated Accident Interim Acceptance Criteria and Guidance, 2015

Ribes, A., & Caremoli, C., Salome platform component model for numerical simulation, *In Computer Software and Applications Conference, COMPSAC 2007, 31st Annual International* (Vol. 2, pp. 553-564), IEEE, 2007.

Rubin, A., Schoedel, A., Avramova, M., Utsuno, H., Bajorek, S., & Velazquez-Lozada, A., OECD/NRC Benchmark based on NUPEC PWR subchannel and bundle tests (PSBT), Volume I: Experimental Database and Final Problem Specifications, *US NRC OECD Nuclear Energy Agency*, 2010.

Salko, R., Lange, T., Kucukboyaci, V., Sung, Y., Palmtag, S., Gehin, J., & Avramova, M., Development of COBRA-TF for Modeling Full-Core, Reactor Operating Cycles, *Advances in Nuclear Fuel Management V (ANFM 2015)*, 2015.

Sung, Y., Kucukboyaci, V., Cao, L., & Salko, R. K., COBRA-TF Evaluation and Application for PWR Steamline Break DNB Analysis, *NURETH-16, Paper, 13431,* 2015.

Todreas, N. E., & Kazimi, M. S., *Nuclear systems II: Elements of thermal hydraulic design (Vol. 2)*, Taylor & Francis, 1990.

Tong, L. S., *Boiling heat transfer and two-phase flow*, Routledge, 2018.

Yoon, S. J., Kim, S. B., Park, G. C., Yoon, H. Y., & Cho, H. K., Application of CUPID for subchannel-scale thermal–hydraulic analysis of pressurized water reactor core under single-phase conditions, *Nuclear Engineering and Technology*, 50(1), 54-67, 2018.

국문초록

최근 컴퓨팅 파워가 증가함에 따라, 부수로 해석 코드와 중성자 수송 코드를 연계한 전노심 봉단위 해석이 활발하게 수행되고 있다. 안전기준이 사고 상황 핵연료 상태를 고려하게 개정됨에 따라, 전노심 봉단위 해석은 안전 마진을 보다 정확하게 계산할 수 있다.

보다 현실적인 부수로스케일 원자로 노심 열수력 해석을 위해 혼합날개로 인한 유체 횡방향 이동을 재현할 필요가 있다. 그러나 CUPID를 이용한 부수로스케일 열수력해석을 진행한 선행 연구에서는 혼합날개를 고려하지 않았다. 따라서 지지격자 유도 횡류 모델을 대입하여 혼합날개의 영향을 모사하는 것이 본 연구의 목적 중 하나이다. 또한 선행 연구에서 핵연료봉 열전도 모델이 사용되지 않았으므로, CUPID 내장 핵연료봉 열전도 모델을 개선하여 부수로스케일 해석에 사용하는 것이 본 연구의 또 다른 목적이다.

혼합날개로 인해 발생하는 유체 이동을 모사하기 위하여, 부수로스케일 열수력 해석 코드인 CTF는 지지격자-유도 횡류 모델을 운동량 방정식에 추가하여 사용한다. CTF가 사용하는 staggered grid와 CUPID가 사용하는 collocated grid의 차이로 인하여, 모델의 직접 대입은 CUPID 셀 중앙에서의 횡방향 운동량 상쇄를 유발할 수 있다. 따라서 이를 보상하기 위하여 다음과 같은 두 가지 수정이 진행되었다. 먼저, 모델이 운동량 방정식만이 아닌 질량, 에너지 방정식에도 도입되었다. 또한 혼합날개로 인해 추가적으로 발생하는 난류혼합을 고려하기 위하여, 난류혼합

계수 β를 $\beta_{default} + \beta'$으로 대체하였다. β'은 CTF와의 결과 비교로부터 결정되었다. 추가로 가이드튜브 근처에서 혼합날개의 효과가 불균일하게 달라지는 것을 고려하였으며, 지지격자로 인해 발생하는 압력강하를 확인하고 이를 적용하였다.

이후 핵연료봉 1차원 열전도모델을 개선하였다. 부수로가 물리적으로 타당한 개수의 연료봉과 접하도록 하였으며 핵연료봉을 사등분하였다. 사등분 된 핵연료봉은 온도 및 속도가 각기 다른 부수로와 마주하며 이로 인해 단일 핵연료봉 클래딩 표면 온도가 달라질 수 있다. 이때 사등분 핵연료봉 내부에서도 열전도가 발생하므로, 핵연료봉 중앙에 가까워짐에 따라 온도차가 점차 감소한다. 이후 Biasi 상관식과 CE-1 상관식이 CHF 모델로서 추가되어 DNBR 계산에 사용되었다.

모델의 대입과 개선이 진행된 뒤, APR1400 단일어셈블리에 대한 모델의 검증이 진행되었다. 시뮬레이션을 위해 어셈블리 23으로부터 출력을 입력하였으며, 이는 중성자 수송 코드인 nTRACER 계산 결과로부터 입력되었다. 이후 지지격자-유도 횡류 모델과 핵연료봉 열전도모델의 검증 및 CTF와의 코드 대 코드 비교가 진행되었다.

이후 검증된 모델을 이용하여 APR1400 전노심 계산이 수행되었다. 지지격자-유도 횡류 모델로 인한 전노심 냉각재 온도 분포 변화, 워터갭에서의 높은 수력직경으로 인해 빨라지는 냉각재 속도가 확인되었다. 다음으로는 핵연료봉 열전도 모델이 적용되어, 어셈블리 23에 대해 수행한 단일어셈블리 계산 결과와 전노심 계산 결과를 비교하였다. 이는 CUPID를 이용한 부수로스케일 전노심 해석의 기반으로 사용될 수 있다.

주요어: 부수로 스케일 열수력 해석, 노심 열수력 해석, 혼합 날개, 핵연료봉 열전도, CUPID, APR1400

학번: 2016-26072